STATUS OF THESIS

Title of thesis | Surface Characteristics and Performance of Stainless Steel AISI 316L of Low Temperature Hybrid Thermochemical Treatment

I, ASKAR TRIWIYANTO BRONTO AGUNG

hereby allow my thesis to be placed at the Information Resource Center (IRC) of Universiti Teknologi PETRONAS (UTP) with the following conditions:

1. The thesis becomes the property of UTP
2. The IRC of UTP may make copies of the thesis for academic purposes only.
3. This thesis is classified as

☐ Confidential

☑ Non-confidential

If this thesis is confidential, please state the reason:

_____
_____
_____

The contents of the thesis will remain confidential for _____ years.

Remarks on disclosure:

_____
_____
_____

Endorsed by

_____ _____

Signature of Author | Signature of Supervisor

Permanent address: Komplek Timah Kelapa Dua Blok CC No 53, Cimanggis, Depok, Jawa Barat, Indonesia 16951

Name of Supervisor
Assoc. Prof. Dr. Patthi Hussain

Date : 22 May 2014 | Date : 22 May 2014

UNIVERSITI TEKNOLOGI PETRONAS

SURFACE CHARACTERISTICS AND PERFORMANCE OF STAINLESS STEEL AISI 316L OF LOW TEMPERATURE HYBRID THERMOCHEMICAL TREATMENT

by

ASKAR TRIWIYANTO BRONTO AGUNG

The undersigned certify that they have read, and recommend to the Centre for Postgraduate Studies for acceptance this thesis for the fulfillment of the requirements for the degree stated.

Signature: _____

Main Supervisor: Associate Professor Dr. Patthi Hussain

Signature: _____

Co-Supervisor: Associate Professor Dr. Mokhtar Che Ismail

Signature: _____

Head of Department: Associate Professor Ir. Dr. Masri Baharom

Date: _____

SURFACE CHARACTERISTICS AND PERFORMANCE OF STAINLESS STEEL AISI 316L OF LOW TEMPERATURE HYBRID THERMOCHEMICAL TREATMENT

by

ASKAR TRIWIYANTO BRONTO AGUNG

A Thesis

Submitted to the Postgraduate Studies Programme

as a Requirement for the Degree of

DOCTOR OF PHILOSOPHY

MECHANICAL ENGINEERING

UNIVERSITI TEKNOLOGI PETRONAS

BANDAR SERI ISKANDAR,

PERAK

SEPTEMBER 2014

DECLARATION OF THESIS

Title of thesis | Surface Characteristics and Performance of Stainless Steel AISI 316L of Low Temperature Hybrid Thermochemical Treatment

I, ASKAR TRIWIYANTO BRONTO AGUNG

hereby declare that the thesis is based on my original work except for quotations and citations which have been duly acknowledged. I also declare that it has not been previously or concurrently submitted for any other degree at UTP or other institutions.

Witnessed by

_____ _____

Signature of Author | Signature of Supervisor

Permanent address: Komplek Timah Kelapa Dua Blok CC No.53, Cimanggis, Depok, Jawa Barat, Indonesia, 16951

Name of Supervisor
Assoc. Prof. Dr. Patthi Hussain

Date : 22-05-2014 | Date : 22-05-2014

D E D I C A T I O N

To

Dra. Hj. Hakimah M Hasan,

Dra. Hj. Rusmaningsih, Apt.

&

My Partner in this Long Journey

Silvia Anggraeni, MSc

ACKNOWLEDGEMENT

I would like to deeply thank my supervisor Assoc. Prof. Dr Patthi Hussain for his unconditional support, guidance and understanding, continuous inspiration throughout my work. He encouraged me to investigate the topic of this work which I found it very interesting. His guidance throughout my study thought me to become an independent researcher, which may be of more value. I would like to thank also my co-supervisor Assoc. Prof. Dr. Mokhtar Che Ismail for his support and Prof Dr. Norani Bt. Muti for allowing us to use NanoLab facilities during my research work.

Special thanks go to Mechanical Engineering Materials laboratory technologists Mr. Anuar, Mr. Idrus, Mr. Mahfuz, Mr. Irwan, Mr. Paris, Mr. Faisal and Mr Rosli from NanoLab, for their help in executing my experiments. I also thank Universiti Teknologi PETRONAS for the financial support during my whole study through the Graduate Assistantship (GA) scheme.

I am indebted to my friends in UTP especially Dr Syahrir Ridha, Dr Munir Lubis, Ust Drs H. Dawi Cahyono, Ust Hj Rahmat Abu Seman and all PPI UTP member for their continuous support and the brainstorming discussions which I strongly believe that what I have learned from them during the study period is worthy to articulate the true meaning of this long journey.

Finally, my greatest thanks go to my parents and my lovely family Silvia-Nabila-Taufiq who shaped me with their never ending patience.

Askar Triwiyanto

May, 2014.

ABSTRACT

Austenitic stainless steels are the most popular materials in the stainless steel due to their excellent corrosion resistance and good forming characteristics. Nevertheless, this type of materials has low hardness as well as poor wear resistance due to the inherent austenitic structure. Earlier attempts to increase the surface hardness and wear resistance of austenitic stainless steels by surface treatments have led to the deterioration in corrosion resistance arising from the depletion in chromium in the hardened layer. The development of low temperature surface treatment carried out at temperatures lower than 500°C has been successfully conducted by innovative techniques including plasma nitriding, ion beam nitriding and ion implantation.

This work describes the resulting layers from different thermochemical treatments are carried out at 400^{o}C to 500^{o}C in a conventional tube furnace which involving the simultaneous incorporation of nitrogen and carbon. The characterization of resulting layers would concern on phase constituents, microstructure, composition and hardness of the expanded austenite/S-phase. Based on the characterization data, the structure of the hybrid layer depends on the temperature which increases up to 500°C and gives formation of CrN which confirms the breakdown of its corrosion resistance. The transfer mechanism of elements on the surface of the 316L steel are controlled by high chemical potential of nitrogen and/or carbon which constitute the driving force for interstitial thermochemical diffusion. Furthermore, the atoms occupy the interstitial sites of the fcc lattice in the surface region. This diffusion generates crystal lattices expansion which contributes to the increased hardness level up to 1400Hv.

As conclusion, this analysis indicates that the identified optimum parameter for generating expanded austenite on 316L in this investigations are achieved at 450^{o}C, where the high level hardness and wear resistance were achieved without impairing its corrosion resistance. Thus, the hybrid treatment will open wider application to the austenitic stainless steel users such as marine environment and biomaterial, because of the significant improvement in surface properties.

ABSTRAK

Keluli tahan karat austenit adalah bahan yang paling popular dalam kumpulan keluli tahan karat kerana rintangan kakisan yang sangat baik dan ciri-ciri membentuk yang baik. Namun begitu, bahan-bahan jenis ini mempunyai kekerasan yang rendah dan kekangan dalam rintangan haus disebabkan oleh struktur austenit yang semulajadi. Usaha awal untuk meningkatkan kekerasan permukaan dan rintangan haus daripada keluli tahan karat austenit melalui rawatan permukaan membawa kepada kemerosotan dalam ketahanan kakisan yang wujud daripada kekurangan kromium dalam lapisan keras. Pembangunan rawatan permukaan bersuhu rendah yang dilakukan pada suhu yang lebih rendah daripada 500°C tanpa merosakkan ketahanan kakisan yang telah dijalankan dengan jayanya oleh teknik inovatif, termasuk nitriding plasma, nitriding sinaran ion dan implantasi ion.

Kajian ini menerangkan lapisan yang wujud pada permukaan keluli 316L hasil rawatan termokimia yang berbeza dengan dijalankan pada suhu 400°C kepada 500°C dalam relau tiub konvensional dengan menggabungkan nitriding-carburizing atau proses hibrid yang melibatkan penubuhan nitrogen dan karbon secara serentak. Pencirian lapisan menunjukkan kepada struktur, komposisi, kekerasan dan rintangan kakisan dari fasa perluasan austenit/S-phase. Berdasarkan data pencirian, pembangunan struktur lapisan hibrid bergantung kepada suhu pemprosesan : peningkatan suhu kepada 500°C mengakibatkan pembentukan sejumlah besar CrN di bahagian atas lapisan yang juga menyebabkan kemerosotan dalam ketahanan kakisan. Mekanisme pemindahan unsur-unsur pada permukaan keluli ini dikawal oleh keupayaan kimia yang tinggi dari nitrogen dan/atau karbon yang menjadi daya penggerak bagi resapan celahan termokimia kemudian menjana pengembangan kekisi kristal. Pengembangan kekisi kristal ini menyumbang kepada kekerasan yang meningkat sehingga 1400Hv samada rintangan haus yang lebih tinggi.

Kesimpulan utama dari hasil kerja-kerja ini menunjukkan bahawa parameter optimum yang dikenal pasti bagi menjana perluasan austenit pada keluli 316L dalam penyiasatan ini dicapai pada 450^{o}C, dimana kekerasan tinggi serta rintangan haus telah dicapai tanpa merosakkan ketahanan kakisan. Oleh itu, rawatan hibrid suhu rendah ini akan membuka aplikasi yang lebih luas kepada pengguna keluli tahan karat austenit seperti aplikasi persekitaran marin dan biobahan, karena peningkatan sifat permukaan yang nyata.

TABLE OF CONTENT

LIST OF FIGURES

LIST OF TABLES

LIST OF ABBREVIATIONS

AISI	American Institute of Steel and Iron
ASTM	American Society for Testing Material
EIS	Electrochemical Impedance Spectroscopy
FESEM	Field Emission Scanning Electron Microscopy
EDX	Energy Dispersive X-rays analysis
EA	Expanded Austenite
HV	Hardness Vickers number
LPR	Linear Polarization technique
SE	Surface Engineering
SCE	Standard Calomel Electrode
USPM	Universal Scanning Probe Microscopy
CH_4	Methane gas
NH_3	Ammonia gas
N_2	Nitrogen gas
XPS	X-rays Photoelectron Spectroscopy
XRD	X-Ray Diffraction

CHAPTER 1

INTRODUCTION

1.1 Overview

This work focuses on exploiting science and technology of nanostructured materials for future generation. The works involved syntheses of various novel hybrid surface treatments, development of experimental techniques for characterization of nano phase, discovery of new phenomena, and searching for new applications. This works is not only to achieve excellence in academic world but also to provide some solutions to technological applications in the real world.

This investigation proposed the low temperature thermochemical treatments in conventional tube furnace of hybrid treating which introduces nitrogen and carbon simultaneously with the aim to improve surface properties of AISI 316L. The outcome of the work showed the formation expanded austenite structured which is supersaturated with nitrogen and carbon. This structure is responsible to the higher hardness and has better wear property without impairing its corrosion resistance. Characterization of this expanded austenite layers were be performed including XRD analysis, SEM and USPM. All these characterizations were used to reveal the characters of the produced thin layers. Elemental profile of nitrogen and carbon across the hybrid treated layer were obtained by EDS-SEM.

The improvement of mechanical properties such as hardness and wear property were measured by micro hardness, wear tests and nanomechanical testings. The corrosion resistance performance was measured by anodic Polarization test and by using USPM to confirm the corrosion behavior which is related to the nanostructure of treated layer. At the end of the chapter, organization and content of each chapter is explained to help the readers to go through the dissertation more easily.

1.2 Background

Austenitic stainless steels are the most widely used in chemical and food processing industries. This type of steel has excellent corrosion resistance and forming characteristics. However, this material has relatively low in hardness as well as poor wear resistance due to its inherent austenitic structure [1].

Earlier works in surface engineering for increasing the surface hardness and the wear resistance of the austenitic stainless steels, such as conventional nitriding and nitrocarburizing, have led to the deterioration in the corrosion resistance arising from depletion of chromium in the hardened layer. Attempts have been made to harden the surface of these materials without compromising their good corrosion resistance. These works have encouraged the development of the low temperature nitriding and carburizing processes which are carried out at temperatures lower than 500°C. So far, low temperature nitriding and carburizing of austenitic stainless steels have been successfully conducted by innovative techniques, including plasma nitriding which is conducted by Ichii, et. al [2] and Lewis, et. al [3], for the use of ion beam nitriding and ion implantation respectively [4, 5]. However, only few investigations have been made commercially by using conventional processes such as gaseous and fluidized bed processes. Previous work has shown that low temperature nitriding of austenitic stainless steel is possible to be conducted by using a fluidized bed furnace [6].

Other work by Gemma et. al in 2001 [7] has proven the feasibility and industrially acceptance for performing low-temperature nitriding and carburizing of stainless steels. The precondition before performing low-temperature nitriding and carburizing involves the component surface activated before the gaseous process by special chemical treatments to remove the oxide film which acts as a barrier for diffusion process.

The low temperature nitriding is suitably performed at temperature below 500ºC to dissolve a large amount of nitrogen in the nitrided layer which is able to reach 20 μm thick of an expanded austenite (γ_N) structure and free from nitride precipitates. Such a low temperature nitrided layer possesses good corrosion resistance and high hardness but quite brittle. Moreover, it has relatively low load bearing capacity due to its small thickness and the abrupt hardness drop at the layer-core interface [8].

On 1999, Sun et.al has found another technical problem associated with the nitriding process which is the non-uniformity of layer thickness across the treated surface [9].

In further effort to improve the quality of the surface harden for industrial applications, it has been found that treatment gas composition has a significant effect on the structural characteristics of the nitrided layer using plasma processing technique. A small amount of carbon-containing gas such as methane (CH_4) to the treatment atmosphere can alter the structural development in the alloyed zone and offer several beneficial effects to the nitriding process [10]. Based on this discovery, it is possible to attempt a new hybrid process, which involves the simultaneous incorporation of both nitrogen and carbon into the alloyed zone to form a dual-layer structure. As a result, the surface hardness was increased up to 1550 VHN, which is considerably higher (around six times) than the untreated austenitic stainless. The process also improved a corrosion resistance of the alloy, as achieved by several investigators [11]. Indeed, nitriding and nitrocarburizing are now commonly performed in conventional and fluidized bed furnaces for surface hardening of engineering steel components.

However, very few efforts have been made to produce expanded austenite layers on austenitic stainless steels in a conventional tube furnace by employing the low-temperature techniques. Recent study by Haruman et.al, has demonstrated that a nitrogen expanded austenite layer can be formed on 316L austenitic stainless steel in a fluidized bed furnace by low-temperature nitriding [6].

Extensive research of surface thermochemical treatment has been conducted in the range of temperature where 400^{o}C to 500^{o}C is possible to produce expanded austenite layers which is responsible to highly demanded better hardness level without sacrifying its corrosion resistance. Furthermore, with regards to thermodynamic conditions, expanded austenite phase is metastable and it will decompose at 450^{o}C (AISI 304) and 460^{o}C (AISI 316) [11].

Based on the above evidence, the proposed research aims to explore the possibility of implementing the hybrid process of low temperature nitriding-carburizing in the temperature of 400^{o}C, 450^{o}C and 500^{o}C with its special characteristics of resulting

layers, especially according to nano mechanical properties performance of surface harden layers for potentially commercial application by using conventional gaseous furnace type. It is expected that a successful investigation may extend the application of austenitic stainless steels for various combined wear-corrosion environments, and may provide new innovative surface heat treatment for stainless steel materials.

1.3 Problem statement

The common practice of surface treatments by using carbon and/or nitrogen source gases is usually performed with temperature around 500^{o}C (932^{o}F). However, stainless steels raise two problems: first, the native passive layer may cause problem to nitrogen and carbon atoms for penetrating through thermal activated diffusion processes. Second, chromium tends to reacts with nitrogen and carbon then forms nitrides/carbides which will cause the breakdown of corrosion resistance [12].

Austenitic stainless steels exhibit a native surface oxide layer that protects the substrate-metal matrix from corrosion. It is difficult to harden the surface by gaseous thermochemical treatment as the native passive layer which is impenetrable by nitrogen and carbon atoms. The oxide layer is believed to act as a barrier for diffusion nitrogen transport. Therefore, in process of optimization toward efficient nitriding by a pre-cleaning procedure, is supposed to remove the oxide layer, which is generally recommended [13].

Moreover, traditional gaseous thermochemical treatment is associated with a loss of corrosion resistance where nitrogen and carbon react with chromium to form carbides/nitrides. The reaction arises a problem due to the sensitization effect caused by the formation of chromium nitrides when these materials are treated at a nitriding temperature above 500°C [14], thus redrawing chromium from solid solution. The precipitation of chromium carbides/nitrides triggers hardening of the nitrided case, but also lead to depletion of chromium content in the austenitic matrix, then significantly reduces the corrosion resistance of the carburized/nitrided layers. On the other hand, the improvement on corrosion resistance is related to the presence of γ_N −nitrogen expanded austenite [8]. As a consequence, surface hardening of stainless steel by thermochemical treatment has been considered as a bad practice or a compromise

between corrosion properties and tribological properties, as surface engineering invariably impairs the corrosion resistance. In terms of carburizing, hardness is increased only by giving up the corrosion resistance property [14].

The most popular technology used to achieve the aforementioned low temperature thermochemical treatments of stainless steels is plasma technology, namely plasma nitriding [15, 16], plasma carburizing [17, 18] and plasma hybrid treatments [19, 20]. Early investigations in the mid of 1980's suggested that applying low temperature plasma nitriding would suppress the formation of chromium nitrides and produce a thin nitrided layer with high hardness and acceptable corrosion resistance [2]. On the other hand, the method of surface heat treatment using plasma technology is hardly found in such mass production industries due to cost consideration and high investment facility. The necessity of an alternative method is an essential thing, such as the use of conventional gaseous processes like gas nitriding [7] and gas carburizing [21]. Therefore, it is important to investigate the use of conventional gas treatments which incorporates treatment parameters on austenitic stainless steel without sacrificing its corrosion resistance.

Previous work which conducted by Sun et al. (1999) has shown that individual low temperature nitriding of austenitic stainless steel is possible to produce expanded austenite layer, although possesses good corrosion resistance and high hardness, is quite brittle and has relatively low load bearing capacity due to its small thickness and the abrupt hardness drop at the layer-core interface [8]. Another technical problem associated with the nitriding process is the non-uniformity of layer thickness across the treated surface [9]. Meanwhile, the low temperature carburizing also forms an expanded austenite like layer at the surface of austenitic stainless steel. These carburized layers have a gentle drop of hardness but have a lower surface hardness than that of nitrogen expanded austenite [8].

More recently, a new hybrid process has also been developed, which involving the simultaneous incorporation of nitrogen and carbon into the austenite lattice to form a dual layer structure which comprising a nitrogen expanded austenite layer on top of a carbon expanded austenite layer [19, 20]. Hence the case hardening process of combination carburizing-nitriding is chosen for this study.

The purpose of this work investigates the feasibility of conventional tube furnace for hybrid treating of nitriding-carburizing of austenitic stainless steels at low temperatures to form a precipitation-free layer with improved properties.

1.4 Objective

The main objective of the research develops a novel hybrid surface harden layer on AISI 316L using conventional tube furnace at low temperature thermochemical treatments:

- To establish the optimal treatment parameters of low temperature hybrid thermochemical to produce the hardened expanded austenite layer on AISI 316L without impairing its corrosion resistance.
- To investigate the effect of treatment temperature in order to characterize the expanded austenite layers formed during the optimized hybrid thermochemical treatments in terms of phase constituents, microstructure, composition and hardness, thus advancing the scientific understanding of this layer.
- To evaluate the wear and corrosion performance of the hybrid treated austenitic stainless steel AISI 316L.

So far, the surface and near-surface mechanical properties of thin films or coatings can be related to the final performance of materials. Nearly all the researches to-date are directed to explore the nanocharacteristics of the layers resulting from low temperature hybrid treatments in order to open the opportunity of wider application to the austenitic stainless steel users because of significant improvement in surface hardness and tribological properties which obtained by the nanoindentation measurement and surface morphology characterizations that were performed on all treated and substrate materials.

1.5 Scope of Thesis

This research is conducted through three stages: Firstly, the development of hybrid process of low temperature nitriding-carburizing in order to improve surface properties of the austenitic stainless steel which is derived from the analysis of literature review. Secondly, the systematic characterization of resulting layers are performed for the purpose of evaluating the specimens that include X-ray diffraction analysis, micro structural examination by optical and electron microscopy, as well as scanning probe microscopy for nano feature of surface topography, elemental analysis by x-ray spectroscopy. Together with these characterizations, nanomechanical and wear tests are carried out to the selection of specimens to correlate with the results from the above characterization methods. Thirdly, polarization test is conducted to investigate the behavior of hybrid layers in corrosive environment. Lastly, results analysis and interpretation of the resulting layers are carried out to enhance the understanding of hybrid processing, the carbon and nitrogen expanded austenite layers and its relationship to the hardness and wear properties.

1.6 Thesis Organization

This thesis consists of five chapters. Chapter one describes the background, problem statement, research objective, scope of study as well as thesis organization. Chapter two consists of literature review. This chapter will start with introduction then followed by classification of stainless steels and current applications of austenitic stainless steel, sensitization phenomena, surface engineering design, nitriding in gaseous atmosphere, diffusion model of nitriding, thermochemical surface treatment of austenitic stainless steel to produce expanded austenite and reasons for selecting the combination of nitriding-carburizing (hybrid) process for the study. Chapter three illustrates on the methodology where research method, materials preparation, experimental procedure, characterization techniques such as optical microscopy, field emission scanning electron microscope (FESEM), scanning probe microscope (SPM), energy dispersive X-ray spectroscopy (EDS), X-ray diffraction, microhardness measurement, nanoindentation, wear testing and corrosion test. Results of the

experiment and its analysis are discussed in chapter four. In this chapter, the results on microsructure imaging, XRD, microhardness and nanoindentation test results, wear, and corrosion properties are presented. Finally, in chapter five, conclusions and recommendations as result of analysis are presented. This chapter summarizes experiment's finding, goals achieved and recommendation for future work which might be possible for development.

CHAPTER 2

LITRATURE REVIEW

2.1 Overview

This chapter contains a review on the theory and previous works that are relevant with this research. The first section deals with the materials used in the development of the composite. The second section presents the basic understanding of the thermodynamic and kinetic phenomena of the diffusion process in pressure-less sintering. Within this section it is also discussed previous works of pressure-less sintered composite of related materials. In the third section, the mechanical properties and toughening methods in relation with the microstructural design, has been reviewed. In the last section, the need for thermal shock resistance of the material produced is discussed since it is related to the objectives of the research. Basically, this chapter attempts to examine the previous works and identifies the issues which are relevant to this work.

2.1.1 Stainless Steels

The discovery of stainless steel dates back to a period just after the turn of the century when French, German, English and later US metallurgists began publishing the results of their studies on low carbon, chromium containing ferrous alloys. The industrial usefulness of stainless steel became evident between 1910 and 1915 when Harry Brearley (England) developed martensitic stainless steels; Fredrick Becket and Christian Dantisizen (United States) developed ferritic stainless steels; and Edward Maurer and Benno Straus (Germany) developed austenitic stainless steel [22, 23].

Stainless steel is a widely used material where corrosion resistance is needed. In 2010, the production of stainless steel is 30.7 million tons worldwide, which is more

than carbon steel. And among that, 57.7% is 300 series austenitic stainless steels (Global stainless steel output figure for 2010, ISSF 2011).

According to metallurgical aspects, the stainless steels are iron-based alloys that contain a minimum of approximately 11% Cr. The amount of Cr is needed to prevent the formation of rust in unpolluted atmospheres. The material must be a ferrous alloy and it must contain more than 50% iron [4]. They achieve their stainless characteristics through the formation of an invisible and adherent chromium-rich oxide surface film. This oxide forms and heals itself in the presence of oxygen. Other alloying elements such as nickel, molybdenum, carbon, titanium, aluminum, silicon, niobium, nitrogen, sulphur and selenium are added to improve particular characteristics [23].

2.1.2 Classification of Stainless Steels

Stainless Steels can be divided into five groups. Four are based on the characteristic crystallographic structure/microstructure of the alloys in the family: ferritic, martensitic, austenitic or duplex (austenitic and ferritic). The fifth group the precipitation-hardenable alloys, is based on the type of heat treatment used, rather than microstructure. Figure 2.1 is shown Fe-Cr phase diagram.

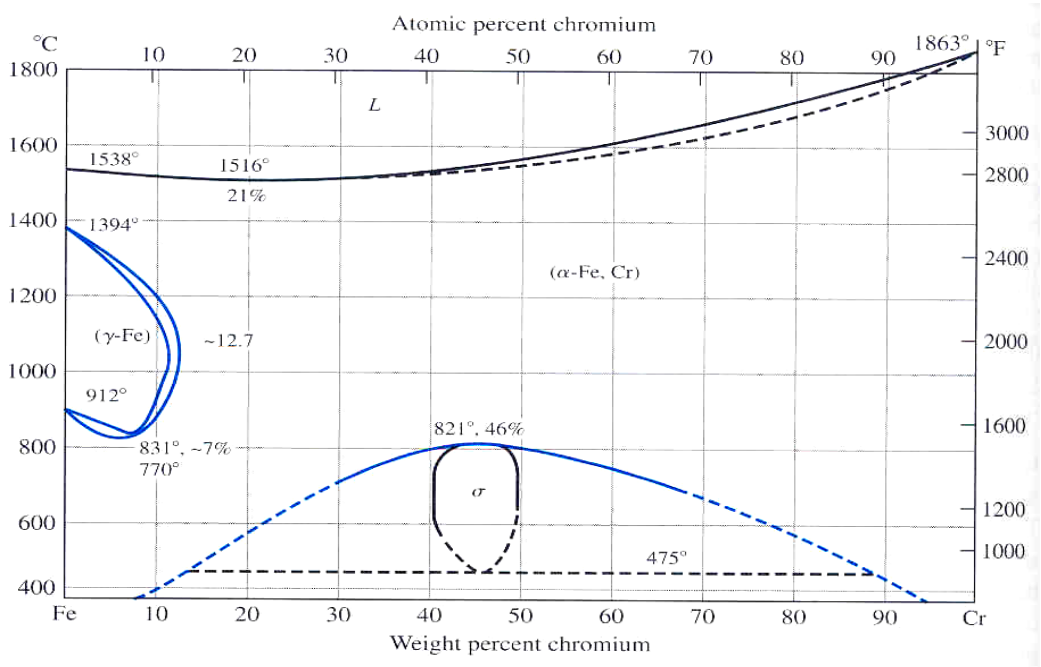

Figure 2.1. Fe – Cr Phase Diagram [25].

The iron-chromium phase diagram is the primary diagram to describe stainless steels, since chromium is the primary alloying element. Chromium is the major alloying element as shown in Figure 2.1 that imparts to stainless steels. Its corrosion resistance is defined by combining with oxygen to form a thin, invisible chromium-oxide protective film on the surface. Since the passive film is an important factor, there are precautions which must be observed in designing stainless steel equipment, in manufacturing the equipment, and in operation and use of the equipment, to avoid destroying or disturbing the protective film. Figure 2.2 shows that various alloying elements are added to the basic iron-chromium-carbon and iron-chromium-nickel systems to control microstructure and properties.

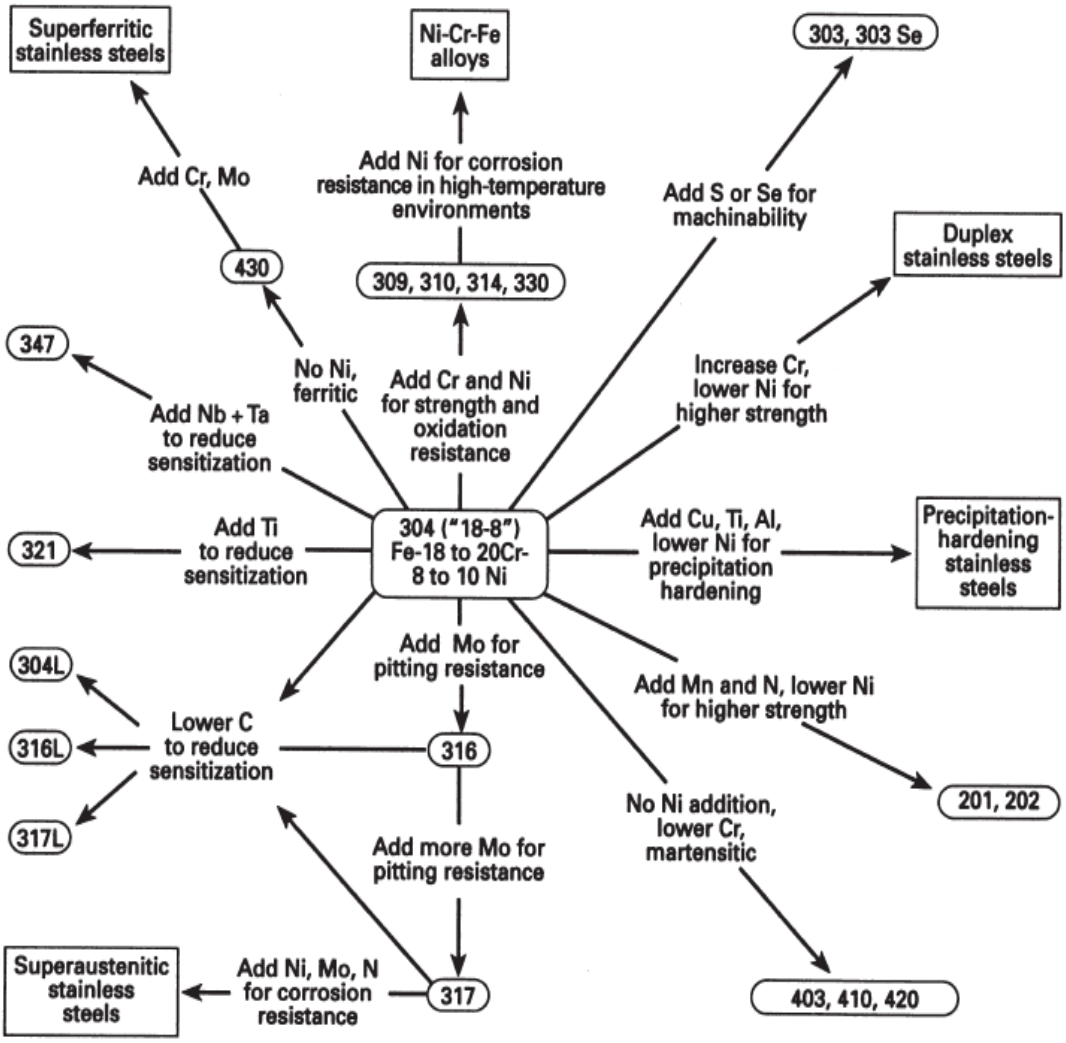

Figure 2.2. Family of Stainless Steel Relationship for Common Martensitic, Austenitic and Ferritic [25].

There are over 150 grades of stainless steels of which austenitic stainless steels (type 304, type 316, 18/8, etc.) are the most widely used. For example, the elements included alloying, are manganese for 200 series, molybdenum for pitting resistance in AISI 316, niobium to reduce sensitization in AISI 347, titanium to reduce sensitization in AISI 321 and nitrogen.

In addition, Figure 2.3 shows the Schaeffler diagram roughly which illustrates the structure obtained after rapid cooling to room temperature from 1050°C. The Schaeffler diagram is an approximation, not a phase diagram and is expressed in terms of weight percent of chromium and nickel due to their respective roles as a ferritic stabilizer and an austenitic stabilizer. Relationship between the Schaeffler diagram to steel chemistry show that the temperature treatment also influences phase balance and phase prediction. Furthermore, in the case of thermochemical treatment, precipitation of carbides/carbonitrides may alter steel chemistry [27].

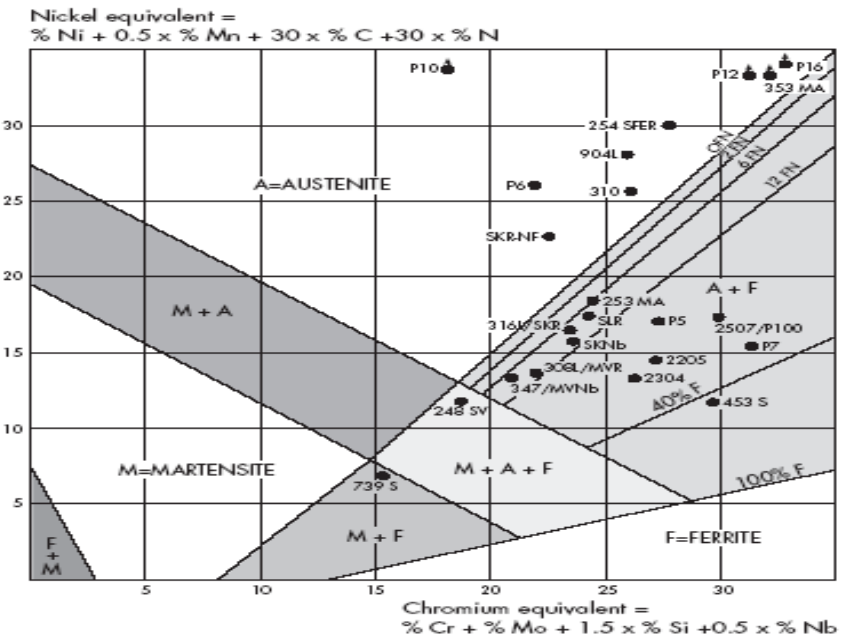

Figure 2.3. Schaeffler Constitution Diagram for Stainless Steels [26].

2.1.3 Austenitic grade of stainless steel

This grade of steel contains at least 16% chromium and 6% nickel (the basic grade 304 is referred to as 18/8) and range through to the high alloy or "super-austenitic" such as 904L and 6% molybdenum grade, and also the higher-alloy AISI 310S and ASTM N08904. The addition of nickel as an alloying element is to maintain the

austenitic structure of this steel. Austenitic steels are characterized by their high content of austenite-formers, especially nickel. They are also alloyed with chromium, molybdenum and sometimes with copper, titanium, niobium and nitrogen. Alloying with nitrogen raises the yield strength of the steels. Austenitic steels cannot be hardened by heat treatment. They are normally supplied in the quench annealed state, which means that they are soft and highly formable. Their hardness and strength are increased by cold working. Certain steels grades are supplied in the cold-stretched or hard-rolled condition. These groups of steels are also suitable for cryogenic applications because the effect of the nickel content in making the steel austenitic avoids the problems of brittleness at low temperatures, which is a characteristic of other types of steel.

In most of the steels shown in Table I of Appendix by Padilha et al. (2007) reported that the maximum silicon content is 1 wt% [27]. However, higher Si contents between 1 and 3 wt% can improve oxidation or scaling resistance. Even higher Si contents up to 5 wt% are used in certain cases to improve the corrosion resistance in nitric acid. The term super-austenitic relates to austenitic stainless steels containing high amounts of chromium, nickel, molybdenum and nitrogen, resulting in an iron content close to or less than 50 wt%. One of the most well-known super-austenitic stainless steels is the UNS S32654 (also known as 654 SMO®): Fe-0.02C-3Mn-24Cr-7.3Mo-22Ni-0.5Cu-0.5N wt%. Other alloying elements such as copper, boron or sulfur are sometime added to the austenitic stainless steels and will be mentioned during this review. Using low carbon content (such as AISI 304L, 316L and 317L) or/and titanium or niobium stabilized alloys (such as AISI 321 and 347) it is possible to minimize intergranular attack in austenitic stainless steels.

2.1.4 Metallurgy of Austenitic Stainless Steel

2.1.4.1 Physical Metallurgy

Austenitic stainless steels contain large amounts of chromium and iron, therefore the iron chromium phase diagram provides the basis for understanding its basic metallurgy. As can be seen in Figure 2.1, the allotropic forms of iron constitute the iron end of the diagram. With increasing chromium content, the ferrite field expands and the austenite (γ) field contracts, thus providing the so-called γ-loop since

chromium is a ferrite stabilizing element [28]. Figure 2.4 shows the iron-chromium-nickel ternary alloy system. The figure illustrates how temperature affects solubility of three elements at 750°C [29].

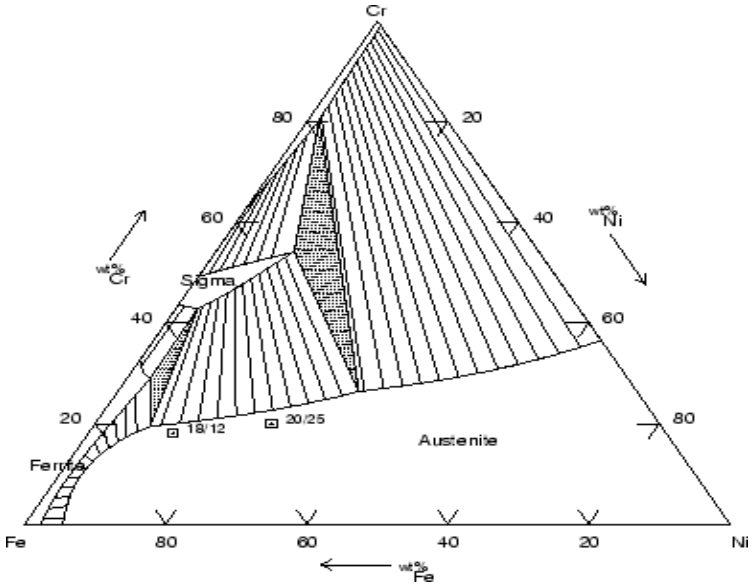

Figure 2.4. Iron-Chromium-Nickel System at 750^{o}C [29].

Next to chromium, nickel is the alloying element that mostly influences alloy design. The prototype ferritizing element is chromium while the prototype austenising element is nickel. When comparing the ternary diagram with the iron-chromium binary diagram, it can be clearly seen that nickel addition extends the austenite phase field. The phase diagram also indicates that as the chromium content increases above 18%. It also becomes necessary to raise the nickel content otherwise increasing amounts of ferrite will form [25]. Carbon is considered as a strong austenite former, while manganese does not seem to promote transformation of ferrite to austenite but promotes solubility of nitrogen in steel. Nitrogen also enhances the formation of austenite and its influence on phase equilibria in the Fe-Ni-Cr phase diagram is shown in Figure 2.5 [30].

In reality, the commercial alloys also contain a certain amount of other alloying elements which might somewhat alter the phase balance, but by large the structure is determined by the three primary constituents: iron, chromium and nickel. In order to broadly describe the effect of composition on microstructure in a wide range of stainless steels, the concept of chromium and nickel equivalent was developed to

normalize the effect of these alloying elements on the microstructure evolution relative to the effects of chromium and nickel.

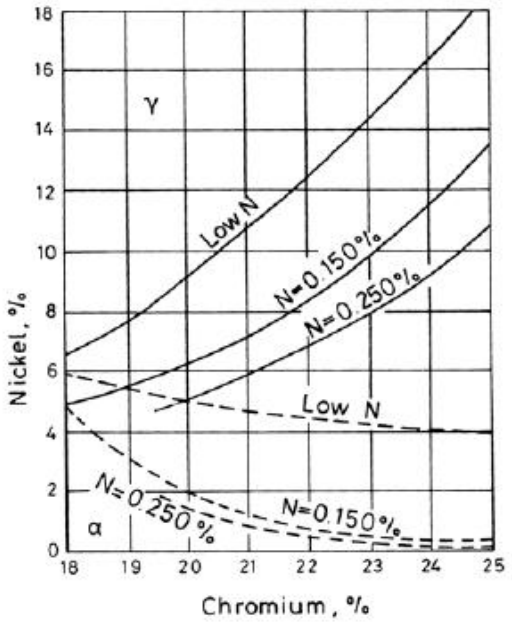

Figure 2.5. Effect of Nitrogen on Austenite Loop [30].

The Schaeffler diagram shown in Figure 2.3 is a plot of chromium and nickel equivalents on opposing axis to provide a graphic depiction on the relationship between composition and microstructure for stainless steel. Molybdenum, silicon and niobium are considered as ferrite formers and therefore they are included in the chromium equivalent axis [26]. It is for this reason that both carbon and manganese are found in the nickel equivalent axis [28]. The martensite may form in austenitic stainless steel during cooling below room temperature (i.e. thermally) or in response to cold work (i.e. mechanically). Besides extending the γ-phase field nickel also lowers the martensite start (M_s) after cooling from solution annealing. In fact all the alloying elements commonly found in austenitic stainless steels lower the M_s, including chromium and molybdenum which at high temperatures promote the ferrite formation. Strain-induced martensite formation is a unique feature in austenitic stainless steels. This forms at higher temperatures than does martensite, which forms on cooling [25].

2.1.4.2 Inclusions and Precipitates

Lack of steel cleanliness and improper heat treatment can produce deleterious changes in the microstructure of austenitic stainless steels. These inclusions and precipitates also increase the susceptibility to localized corrosion and embrittlement. Figure 2.6 shows curves which separate the area to the left, where sensitization is negligible, from that to the right of the curve, where sensitization is present.

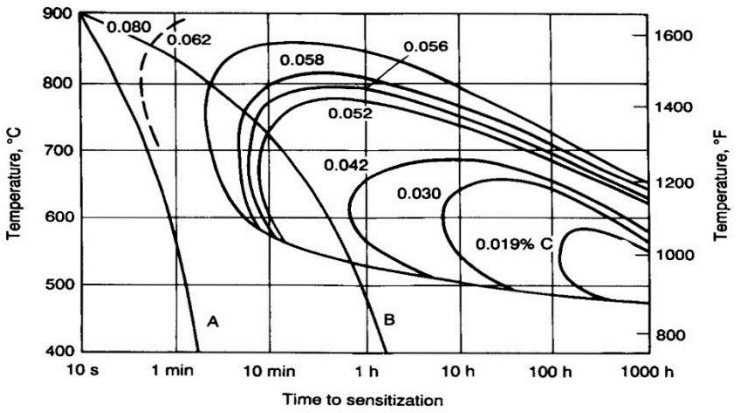

Figure 2.6. Time – Temperature Curves Showing Effect of Carbon Content on Carbide Precipitation [31].

a. Carbide Precipitation

Sensitization or carbide precipitation at grain boundaries can occur when austenitic stainless steels are heated for a period of time in the range of about 425°C to 870°C [25]. Time-temperature sensitization curves, as shown in Figure 2.6, provide a guidance to avoiding sensitization and illustrate the carbon content on this phenomenon [28]. In the absence of stabilizing elements, $M_{23}C_6$ is the predominant carbide formed in austenitic stainless steels. The $M_{23}C_6$ is mainly composed of chromium carbide, so the designation $Cr_{23}C_6$ is used frequently [32]. However, since other elements can particularly substitute for chromium, the formula may be written as: $(Cr,Fe,Mo)_{23}C_6$, $(Cr,Fe)_{23}C_6$ [26], $(Fe,Cr)_2Mo_2C_6$ [33]. Austenitic Stainless steels which are alloyed with titanium and/or niobium resist better carbide precipitation and are called stabilized steels. These elements have an affinity for carbon and form MC type carbides readily; effectively reducing the matrix carbon content and thus protecting against the deleterious $M_{23}C_6$ precipitation [34].

b. Nitride Precipitation

Nitrogen in solid solution is the most beneficial alloying element in promoting high strength of austenitic stainless steel without affecting their good ductility and toughness properties as long as the solubility of nitrogen in γ is not exceeded (<0.9wt%N). If the solubility is exceeded, Cr_2N precipitates at the grain boundaries of the austenitic stainless steel [35].

c. Sulphides

Several types of sulphides have been observed in austenitic grades, the most common being MnS. However if the manganese content is low, chromium will replace some of the manganese in the sulphide [36, 37].

d. Other Phases

Z-Phase is a niobium rich nitride with a typical composition of $Cr_2Nb_2N_2$. Primary precipitation are frequently present as agglomerates and can be found at grain boundaries and at the triple point grain boundary of high-N stainless steel [38, 39].

Sigma phase (σ) formed in austenitic stainless steels is a hard and brittle intermetallic phase which is rich in chromium and molybdenum as described in Table II of Appendix. Sigma phase precipitates on grain boundary triple points and then grain boundaries after a long time at high temperature on incoherent twins and intergranular inclusions [40].

2.2 Corrosion of Austenitic Stainless Steel

The corrosion protection for austenitic stainless steel is in contrasts to carbon steels, alloy steels and other metals [41]. Austenitic stainless steels like other related chromium bearing alloys, rely mainly on the phenomena of passivity. Passivity is a result of a transparant and thin passive film that forms on the surface of the austenitic stainless steel.

Chromium is the one element essential in forming the passive film. This passive film has the property of ‘self-repair’ and will spontaneously re-form if the surface is broken or damaged mechanically, provided that there is a source of oxygen present.

This passive film acts as a barrier and separates the metal from the surrounding atmosphere and therefore the integrity of this film is crucial in protecting the austenitic stainless steel against corrosion. If passivity is destroyed under conditions that do not permit restoration of the passive film, then the austenitic stainless steel will corrode much like a carbon or low alloy steel would do [11]. In reality the total loss of the passive film is not a common occurrence but localized breakdown of the film. This breakdown of the film leads to localized corrosion which is great concern in austenitic stainless steel.

The forms of corrosive attack that most affect austenitic stainless steels which include general (uniform corrosion), galvanic corrosion, pitting corrosion, crevice corrosion, intergranular corrosion, stress-corrosion cracking and wear-corrosion [26].

2.2.1 General Corrosion

General corrosion refers to corrosion dominated by uniform thinning that proceeds without appreciable localized attack. Passive materials like austenitic stainless steels are generally subject to localized attack however under specific conditions - high temperature corrosive environments - they are also susceptible to general corrosion [25].

2.2.2 Galvanic Corrosion

Galvanic corrosion results when two dissimilar metals are in electrical contact in a corrosive medium. Galvanic corrosion behavior of austenitic stainless steel is difficult to predict because of the influence of passivity. In fact austenitic stainless steels occupy two positions in the galvanic series, representing the active and passive states; close to steel when active and in a more noble state when passive [34]

2.2.3 Pitting Corrosion

Pitting corrosion is a type of localized corrosion in which microscopic holes or cavities form on the surface of metals. This attack occurs either due to direct corrosion of heterogeneities present on the surface, local discontinuity of the passive film or due to the localized damage of the protective passive film. Under certain environmental conditions, particularly in the presence of aggressive ions such as halides, the protective passive film of austenitic stainless steel is damaged at weak

sites either by adsorption and penetration or by penetration and migration of aggressive ions. The preferential sites of attack are in the proximity of surface defects which are in the form of: inclusions, second phase precipitates, grain boundaries, slip steps and segregated interfaces [37]. It is for this reason why steel cleanliness in austenitic stainless steel is given so much importance. Figure 2.7 shows a schematic diagram of a pit forming in the presence of halide ions.

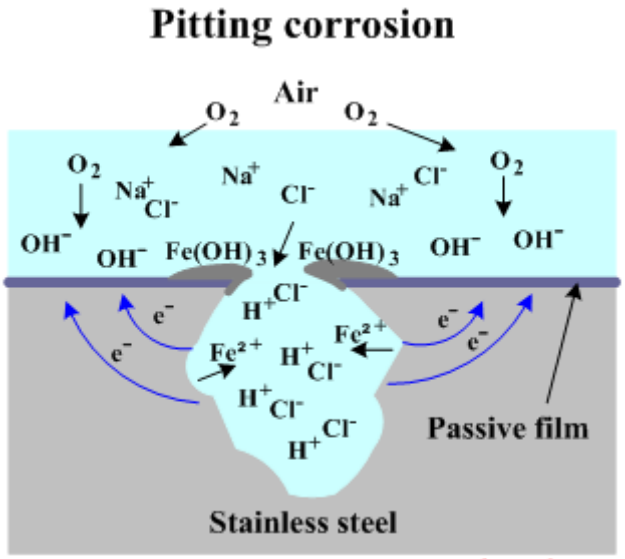

Figure 2.7. Schematic of Various Events During the Growth of Pits [42].

Pit initiation originates when aggressive chloride anions react with the metal atoms at the film-substrate interface to form metal chlorides. These, consecutively, hydrolyze according to the reaction in equation 2.1 to give metal hydroxide, but at the cost of increasing acidity at the reaction site [43].

$$M^{+}Cl^{-} + H_2O \rightarrow MOH + H^{+}Cl^{-}. \quad (2.1)$$

There is a decrease in pH at these pitting sites and this enriches further the metal dissolution according to the reaction in equation 2.2 [37]. The rapid dissolution of metal within the pit produces surplus of positive charges in this area, causing migration of more chloride ions into the pit. Both hydrogen and chloride ions act together to stimulate the dissolution even further and the entire process accelerates

with time. Also because the solubility of oxygen is nearly zero in concentrated solutions, no reduction of oxygen occurs within a pit [41].

$$Fe \rightarrow Fe^{2+} + 2^{-}. \quad (2.2)$$

The electrons released during dissolution are consumed by the cathodic reaction occurring on the passive film present further away from the pitting sites. There are two types of reduction reactions that occur at the cathode: hydrogen evolution (equation 2.3) and reduction of oxygen (equation 2.4 and 2.5) [29].

$$2H^{+} + 2e^{-} \rightarrow H_2. \quad (2.3)$$

$$2H^{+} + \tfrac{1}{2} O_2 + 2e^{-} \rightarrow H_2O. \quad (2.4)$$

$$H_2O + \tfrac{1}{2} O_2 + 2e^{-} \rightarrow 2OH^{-}. \quad (2.5)$$

Cathodic reduction of oxygen on the surface areas nearby to the pit tends to suppress corrosion on these surfaces and therefore isolated pits cathodically protect the surrounding metal surface [37]. When all of this occurs, it is said that the pit has reached a stable stage, making the environment inside the pit more aggressive, and therefore penetrates the metal at an ever-increasing rate by an autocatalytic process [41].

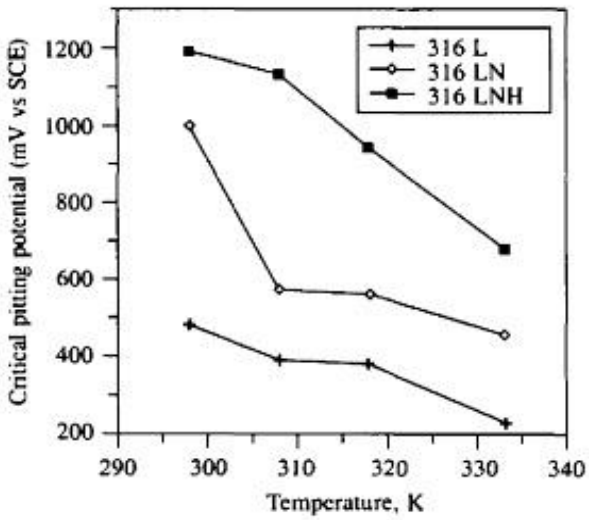

Figure 2.8. Influence of Nitrogen Addition on Pitting Corrosion Resistance [44].

In fact, as it can be seen from Figure 2.8, the addition of nitrogen significantly improves the pitting corrosion resistance in acidic and neutral chloride media up to a temperature of 65°C (338K).

The chemical composition of the austenitic stainless steel plays a major role in affecting the pitting resistance. Chromium, molybdenum and to a lesser extent nickel are the main alloying elements required to improve the pitting resistance but nitrogen is also deliberated as an important alloying addition as it promotes passivity and widens the passive range in which pitting is less probable. Pitting resistance of austenitic stainless steel is primary a function of the Cr, Mo and N levels. The pitting resistance equivalent (PRE) of an alloy, which also can be used for alloy ranking, according to [29, 37, 41] is generally defined as:

$$\text{PRE} = \%\text{Cr} + 3.3(\%\text{Mo}) + x(\%\text{N}) \quad \text{where } x = 13,\ldots,30. \tag{2.6}$$

The reason why nitrogen improves the pitting resistance of the alloy is not fully understood and the following mechanisms have been suggested to explain how nitrogen operates [43, 45]:

(1) Nitrogen in solid solution dissolves and produces NH_4^+, raising the pH and depressing oxidation inside a pit.
(2) Concentrated nitrogen at the passive film-alloy surface stabilizes the film, and prevents attack of the anions (Cl^-).
(3) Nitrate ions are produced and these improve the resistance to pitting corrosion.
(4) Nitrogen addition stabilizes the austenite phase.
(5) Nitrogen blocks the kink, and controls the increase of electric current for pit production.

2.2.4 Crevice Corrosion

Crevice corrosion is a form of localized attack that affects both active and passive metals nevertheless the attack is often more severe for passive alloys, particularly those in the stainless steel group. This type of attack occurs at circumscribed regions, in sealed areas, in shielded areas, at narrow openings or gaps (spaces) between metal-to-metal or non-metal to-metal components. In practice, it is very difficult to avoid all crevices and these can be produced by design or by coincidence. Crevices caused by design, occur at gaskets, flanges, rubber O-rings and anywhere which has close fitting surfaces [25]. Crevices caused by coincidence, occur in sealed regions that are formed

under tubercles, deposits, and below accumulation or biological materials. Similarly, accidental crevices such as cracks, seams or any other metallurgical defect could serve as sites for corrosion [41].

This type of attack results from a concentration cell formed between the electrolyte inside the crevice, which is oxygen famished, and the electrolyte outside the crevice, where oxygen is more plentiful. Thus, making the metal within the crevice is an anode, and the exterior metal as a cathode.

Based on the understanding of the influence of various factors a cohesive crevice corrosion mechanism (Figure 2.9) has been projected [46] and is described below:

Initially the cathodic reduction ($H_2O + ½O_2 + 2e^- \rightarrow 2OH^-$) and the anodic dissolution ($M \rightarrow M^+ + e^-$) processes, occur homogeneously over the entire metal surface, including crevice exterior.

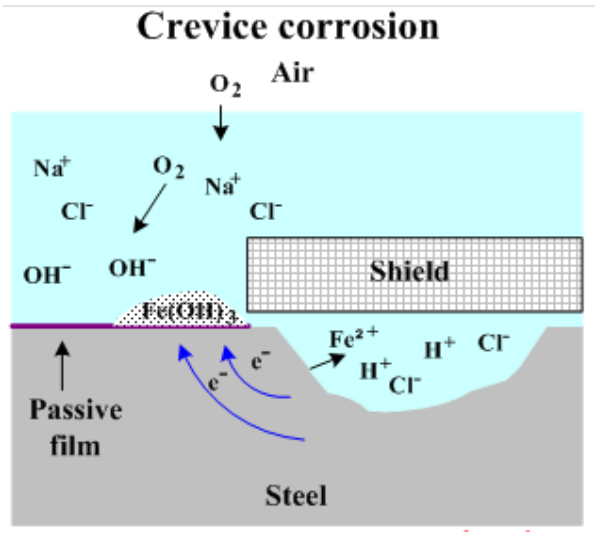

Figure 2.9. Schematic of Various Events during Crevice Corrosion [42].

The oxygen in the shielded crevice area is consumed after some cultivation period, but the decrease in cathodic reaction rate is negligible because of the small area involved. Subsequently, the corrosion of the metal inside and outside the crevice continue at the same rate. With the dissolution of the cathodic hydroxide producing reactions however, the migration of negative ions (e.g. chlorides) into the crevice is required to maintain charge balance. The resulting metal chloride hydrolyses to insoluble metal hydroxides and hydrochloric acid, which results in the advanced

acidification of the crevice ($M + Cl^- + H_2O \rightarrow MOH + H^+ Cl^-$). Both the chloride ions and low pH accelerate crevice corrosion in a manner similar to autocatalytic pitting while reduction reaction cathodically protects the exterior surface.

Pitting and crevice corrosion act in the same way and both the corrosion initiation sites within a crevice and the alloying elements that resist crevice corrosion are similar to that of pitting. Apart from material related factors, the origination of crevice corrosion can also be influenced by non-material related factors. Factors such as; crevice type, crevice geometry, number of crevices, exterior to interior crevice area ratio, bulk solution composition (chloride and oxygen content, pH and pollutants), bulk solution environment (temperature, agitation, volume) and mass transport inside and outside of the crevice; influences significantly crevice attack [46].

2.2.5 Intergranular Corrosion

Intergranular corrosion is defined as the selective dissolution of grain boundaries, or closely contiguous regions, without noticeable attack of the grains themselves. This dissolution is caused by a potential difference between the grain-boundary region and any precipitates, intermetallic phases, or impurities that form at the grain boundaries [23].

Intergranular corrosion in austenitic stainless steels is generally the result of sensitization. This condition occurs when a thermal cycle leads to grain-boundary precipitation of carbide, nitride, or intermetallic phases without providing sufficient time for chromium diffusion to fill the locally depleted region [41]. The diffusion rate of chromium in austenite is slow at the precipitation temperatures; therefore the depleted zone persists. When the chromium level in the depleted area falls below that required for passivation the austenitic stainless steel develops susceptibility to intergranular corrosion [33].

The detected damages are then not only the attack and dissolution of grain boundary areas but also result in successive severe falling out of whole grains inducing macroscopic damages as shown in Figure 2.10. This is because the depleted zones have higher corrosion rates than the matrix in many environments leading to a favored dissolution at the grain boundary [48].

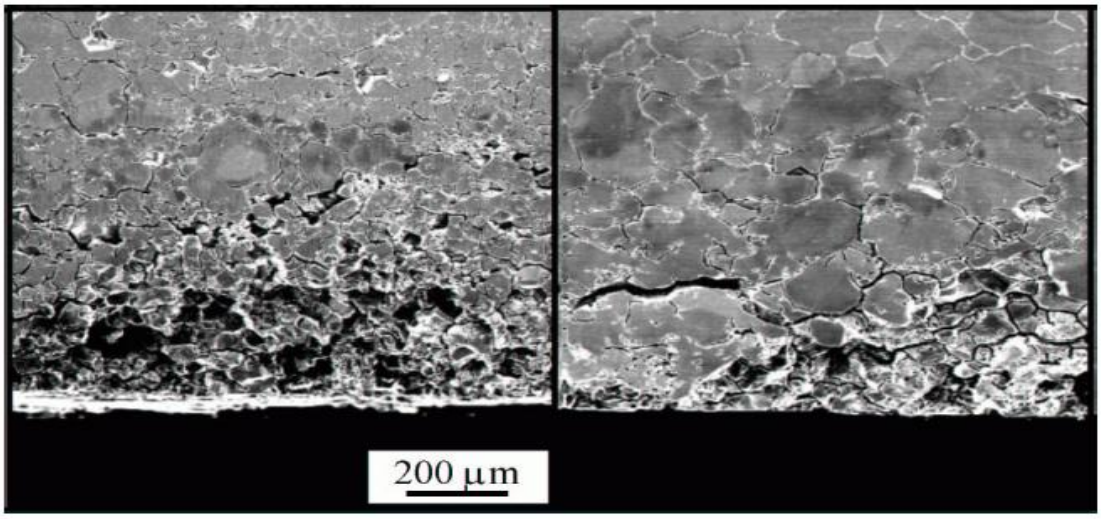

Figure 2.10. Micrograph with Grain Dropping due to Intergranular Corrosion [48].

2.2.6 Stress-Corrosion Cracking

Stress Corrosion cracking (SCC) is a corrosion mechanism in which the combination of alloy susceptibility, tensile stress above a threshold value, and a particular environment leads to cracking. The overall SCC process can be divided into two stages: the initiation process and the propagation process. During the initiation process, development of a sealed cell with its acidification and concentration of anionic species takes places. In fact, many SCC failures have been reported to initiate from pits [49].

2.3 Wear of Austenitic Stainless Steel

Wear, as defined by ASTM [50], is the damage to a solid surface: usually comprising progressive loss of material, due to relative motion between surface and a contacting substance or matters.

Austenitic stainless steels are used in various applications due to their excellent corrosion resistance and good forming characteristics. Nevertheless, this type of materials has low hardness as well as poor wear resistance due to the inherent austenitic structure. The low hardness and poor wear resistance of austenitic stainless steels are their major limitations for tribological applications [25].

The types of wear mechanism defined below include abrasive, adhesive, oxidative, fatigue, corrosive and fretting. Austenitic stainless steels are subjective to any of these types of wear mechanisms.

2.3.1 Abrasive Wear

As defined by ASTM [51], abrasive wear occurs as a result of hard particles or hard swellings forced against and moving along a solid surface. Generally, a material is seriously abraded or scratched only by a particle harder than itself [25]. Abrasion is typically deliberated according to types of contact. Types of contact include two-body and three-body wears. The former occurs when attached abrasives slide along a surface, and the latter, when an abrasive is caught between one surface and another.

Abrasive wear is shown in the forms of scratches or grooves. Scratching is the mechanical removal or displacement (or both) of material from a surface by the action of abrasive particles or swellings and sliding across surfaces. Wear in the form of grooves is divided into two: plowing or scoring. Plowing is the formation of grooves by plastic deformation of the softer of two surfaces in relative motion while scoring, which is a severe kind of wear, is reflected by the formation of extensive grooves or scratches in the direction of sliding.

For austenitic stainless steels, abrasion resistance is highly dependable on two metallurgical variables: hardness and carbon content. Austenitic stainless steels with high carbon content and/or a high work-hardening rate, favors better abrasion wear resistance.

2.3.2 Oxidative Wear

This form of wear is considered as mild wear and is abided by most moving components. Oxide particles are loosened and move about within the contact region, they loosen more particles, some of which leave the system as wear debris, but the oxides do not abrade the substrate in most systems. Wear by loosening of and loss of oxide should not be identified as abrasive wear [52].

2.3.3 Fatigue Wear

This type of wear occurs when a surface is stressed in a cyclic manner. The fatigue wear rate of stainless steels is affected by surface conditions such as finish, residual stress, hardness and microstructure. Surface treatments such as: nitriding, carburizing and shot peening, which increases the surface hardness and improve residual stress distribution, were act in preventing this type of wear [25].

2.3.4 Corrosion-wear

Corrosion-wear or tribo-corrosion is a material deterioration or transformation resulting from simultaneous action between mechanical wear processes and electrochemical corrosion processes and lead to material loss [53]. The consequences of coupling wear and corrosion are complex. Corrosion-wear is often related to the synergy resulting from the combination of mechanical and environmental effects. According to Watson et al. [54] the total volumetric corrosion wear rate (CW) can be regarded as the sum of all the surface damage due to the volumetric corrosion (C), the volumetric mechanical wear rate (W) and the volumetric rate of degradation due to the corrosion-wear synergy (S):

$$CW = C + W + S. \tag{2.7}$$

The synergy (S) [44, 57] can be regarded as the sum of the corrosion-enhanced wear (W_c) and the wear-enhanced corrosion (C_w):

$$S = W_c + C_w. \tag{2.8}$$

Possible wear-enhanced corrosion (C_w) mechanisms include [50]:

(i) Stripping of the protective corrosion film creating fresh reactive corrosion sites.

(ii) Local acidification at wear sites, prohibiting film formation and accelerating corrosion rates.

(iii) Anodic wear scars that can cathodically polarize the surrounding unworn surfaces and destabilizing passive film in these regions enhancing corrosion.

(iv) Roughening of the specimen surface increasing the corrosion rate.

(v) Increased mass transport by high turbulence.

Possible corrosion-enhanced wear (W_c) mechanisms include:

(i) Removal of work hardened surfaces by corrosion processes and exposing the underlying base metal to wear mechanisms

(ii) Preferential corrosive attack at grain boundaries resulting in grain loosening and eventual removal

(iii) Lowering the fatigue strength of a metal by corrosion

(iv) Increase in the number of stress concentration defects resulting from micro-pitting.

(v) Detachment of plastically deformed flakes on the metal surface due to stress corrosion cracking.

However, in some instances negative synergy can also occur, called antagonistic effect. Possible opposed effects which reduce corrosion rates ($-C_W$) are rapid corrosion film growth; scaling; the formation of a passive film; or thermally affected films. Whilst the reduction in wear rates can result from: the presence of a soft or loosely adherent corrosion film reducing contact stresses; or blunting of the crack tips by lateral dissolution and thus retarding the speed of crack propagation [50].

The synergy component in corrosion-wear is further complicated for surface engineered stainless steels where subsurface corrosion can occur at the interface with the substrate or inter layers. Dearnley and Aldrich-Smith [51] have suggested three major wear corrosion mechanisms that affect 316L stainless steels when they are protected by hard cathodic surface coatings like expanded austenite and CrN:

Type I: The removal of the coating passive film during sliding contact and its subsequent regeneration.

Type II: Galvanic attack of the substrate – leading to blistering and fracture followed by the removal of coating fragments during sliding contact.

Type III: Galvanic attack of the counterface material which causes to be rough – this leads to mechanical damage (abrasion) of the coating during subsequent sliding contact.

Although these 3 mechanisms proposed by Dearnley and Aldrich-Smith are related to coatings, mechanisms (I) and (III) apply for uncoated stainless steels involved in corrosion-wear.

Type I corrosion-wear occurs because stainless steels rely on a 1−10nm thick surface passive film for the protection from aggressive and corrosive environments. This passive film forms instantaneously when oxygen is available in the environment but abrasion can lead to a complete removal of this film exposing the substrate to the aggressive environment. Unless re-passivation occurs faster dissolution will occur

within the worn site. If the rate at which the stripping of this passive film is higher than its regeneration, the nascent bulk material is exposed longer to the corrosion environment and high dissolution rates may result. Therefore the corrosion-wear performance of stainless steel depends on the ability and rapidity of the passive film to self-heal [41].

Type III corrosion-wear can occur in counterforce materials which are composite (WC in cobalt binder) or are stainless steels that contain precipitates. For example, the presence of carbides in sensitized stainless steel establish a micro-corrosion cell as the carbide is likely to be cathodic with respect to the surrounding metal matrix. This can result in preferential anodic dissolution of the metal matrix close or at the matrix/carbide interface and thus accelerate carbide removal from the surface which ultimately roughens the surface [50].

2.3.5 Fretting Wear

Fretting wear occurs when material is removed from contacting surfaces when motion between the surfaces is restricted to very small amplitude oscillations (often, the relative movement is hardly visible) [57]. Although fretting wear can be regarded formally as reciprocating sliding wear with very small displacements, there are enough alterations in both wear rates and mechanism to merit the use of a distinct term. However, sliding wear usually results from slow movement of the surfaces, fretting often arises in components those are considered fixed and are not expected to wear, but which nevertheless experience a small oscillatory relative movement. These small displacements often initiate from vibration.

In the same way to sliding wear, fretting wear can also occur in corrosive environments and when this occur the term fretting corrosion-wear, fretting corrosion or mechanically assisted crevice corrosion (MACC) [58] is used. The micro-motion in corrosive environments creates the ideal site for the generation of fretting corrosion products. This motion results in increased rates of corrosion produced by the repeated fracture and reformation of oxide layers (re-passivation), which form over stainless steels [41].

For sphere-plane contact, under a normal load, the contact zone generated is circular and the contact pressure reaches maximum at the centre of the contact circle,

and falls to zero at the edges. Figure 2.11 (a and b) illustrates this pressure distribution, and also shows a plan view of the area of contact respectively.

If a small cyclic tangential force is superimposed on the normal force, some displacement may occur between the surfaces around the edges of the contact zone, where the normal pressure is lowest and the frictional stress opposing movement is therefore least (Figure 2-10c). The contact zone can then be divided into two regions: a central area where there is no relative tangential movement and an annular zone in which micro-slip occurs [55]. As the cyclic tangential force is increased, the central area with no slip occurs shrinks until ultimately slip occurs over the whole contact area (Figure 2.11d). The tangential force can be interpreted into a comparable macroscopic tangential displacement, which is convenient measure of fretting.

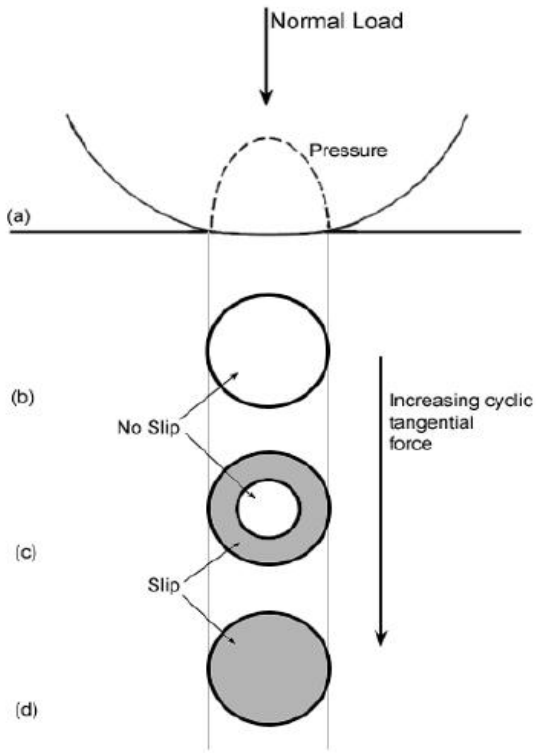

Figure 2.11.

(a) Distribution of Elastic Normal Stress beneath a Sphere.

(b) to (d) Plan Views of Area Contact with Increasing Cyclic Tangential Force [55].

The regimes of the normal load and displacement amplitude corresponding to stick, mixed stick-slip and gross-slip are plotted in Figure 2.12. At a fixed normal

load, increasing the amplitude of the cyclic tangential displacement (or load) leads to an increase in the extent of slip; a similar effect results from increasing the normal load at fixed amplitude.

These three different regimes are easily identified in the tangential load displacement plots (F_t-D) where gross slip is characterized by an open parallelogram shaped F_t-D plot; stick by a closed shaped F_t-D plot; and mixed stick-slip by an elliptical F_t-D plot [55].

Fretting damage occurs in the micro-slip region. In the relative slip fretting process the applied normal load causes adhesion of asperities and as the contact areas slip, wear debris is produced which accumulate in the adjoining valley. These fine metal particles removed by adhesive wear oxidize and work-harden between the fretting surfaces. These hard particles then act like abrasives and increase the rate of material removal [57].

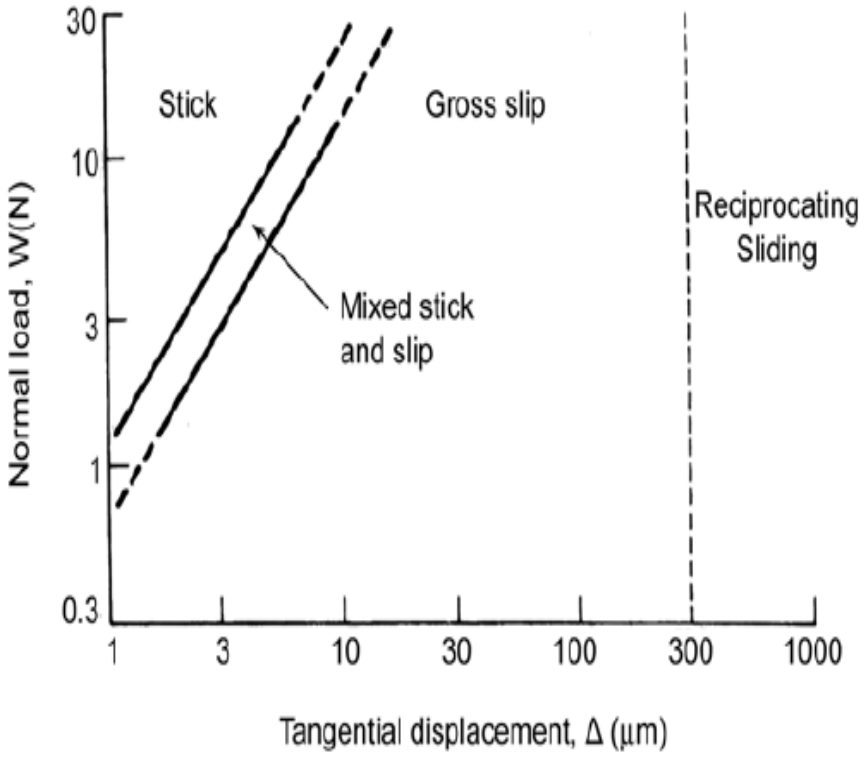

Figure 2.12. Fretting Regimes between Stainless Steel Surfaces [55].

2.4 Enlarging applications of austenitic stainless steel

Austenitic stainless steel are critical in the modern economies with applications ranging from food processing and cryogenic machinery to medical implants and aerospace instrumentation. Tough, resistant low-temperature embrittlement and many forms of corrosion, these steel are, nevertheless, prone to scratching and galling in service. In relation with the functional properties of a part, such as fatigue and static strength, or wear and corrosion resistance, are the basis of specifying the proper process and steel as illustrated in Figure 2.13.

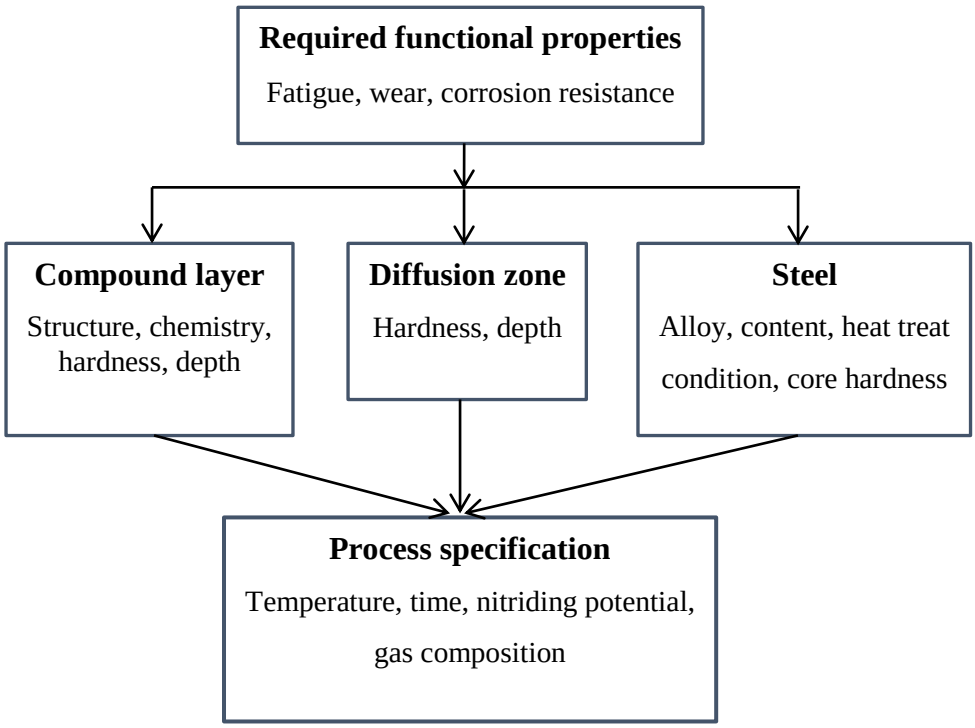

Figure 2.13. Steps to Process Specification [58].

The functional part properties that essentially depend on the compound layer are wear resistance, tribological properties, corrosion resistance and general surface appearance. Both abrasive and adhesive wear resistance increase with hardness and with minimized porosity of the compound layer. Porosity can be positive in lubricated machinery parts as the pores act as lubricant reservoirs. The compound layer depth has to be deep enough not to be worn away. The diffusion layer (depth, hardness and

residual stress) determines surface fatigue resistance and resistance to surface contact loads.

The efforts have been made in the past decades to modify the surfaces of these materials to improve their surface hardness, wear resistance as well as corrosion resistance which are shown in Figure 2.14. Starting from the mid of 1980's, investigations have been performed to improve surface hardness of ASS and thus enlarging their possibility of wider application, but led significant loss of its corrosion resistance. This tendency is occur due to the sensitivity effect. Sensitization is a common problem in austenitic steel where precipitation of chromium carbides ($Cr_{23}C_6$) occurs at the grain boundaries at elevated temperatures, typically between 450^{o}C to 850^{o}C.

Figure 2.14. Application of Austenitic Stainless Steel [59].

As it is illustrated in Figure 2.14, the medium will determine the way in which the diffusing elements are delivered to the metal surface. A number of different media are available (solid, liquid, gas and plasma), and a detailed account of the media used for carburizing/nitriding will be given in a following section.

Diffusion reaction in forming chromium nitride/carbide leads to the depletion of Cr in the austenitic solid solution and consequently unable to produce Cr_2O_3 passive layer to make stainless feature. As a result, it reduces the corrosion resistance property of the stainless steel. This phenomenon causes reduction in ductility, toughness and aqueous corrosion resistance [60]. Bell et al. (1999) suggested that a low temperature nitriding can eliminate the formation of chromium nitrides but at the expense of strengthening effects made by CrN precipitates. Alternatively, the strengthening effect will be replaced by supersaturation of interstitial species in austenite matrix which leads to the hardening of the surface region several tens micro meter thick. This precipitation-free nitride layer not only exhibits high hardness but also possesses good corrosion resistance due to the availability of retaining chromium in solid solution for corrosion protection [61].

2.4.1 Ion, Liquid (Salt) and Gas Processes – Differences in Effectiveness

There are a number of commercial processes which can be used to diffuse nitrogen and carbon into the surface of stainless steels. Examples of the different processes and names of processes available include plasma nitriding, plasma carburizing, gas carburizing and nitriding, microwave nitriding, radio-frequency nitriding, ion implantation, plasma immersion ion implantation, low-pressure arc discharge, reactive magnetron sputtering, salt bath nitrocarburizing and glow-discharge nitriding.

The advantages and disadvantages of these techniques are typically related to process time, process temperature, effectiveness of diffusion and case depth. In order to conventionally gas nitride a stainless steel, the surface must be activated in order to remove the adherent chromium oxide film to permit the diffusion of hydrogen [62]. Conversely, plasma nitriding with a sputtering surface activation

permits faster nitride diffusion when compared with gaseous nitriding. For example, the passive layer removal can be facilitated by sputtering with hydrogen in the same vessel immediately prior to introducing the nitrogen-rich process atmosphere [63]. Glow discharge nitriding processes have also found increased application as the diffusion rates of nitrogen are sufficiently high to allow lower process temperatures and shorter treatment times [64]. Characteristics of resulting layer from different nitriding methods can be seen in Table 2.1.

Table 2.1: Typical Characteristics of Nitriding [65].

Process Nitriding	Name of case	Process temperature °C	Case hardness, typical case depth	Hardness, HRC	Typical base metals	Process characteristics
Gas	Diffused nitrogen, nitrogen compounds	480-590	125µm - 0.75mm	50-70	Alloy steels, nitriding steels, stainless steels	Hardest case from nitriding steels, quenching not required, low distortion, process is low, is usually a batch process
Salt	Diffused nitrogen, nitrogen compounds	510-565	2.5µm-0.0.75mm	50-70	Most ferrous metals, including cast iron	Usually used for thin hard cases <25µm<1mm. No white layer, most are proprietary processes
Ion	Diffused nitrogen, nitrogen compounds	340-565	75µm-0.75 mm	50-70	Alloy steels, nitriding steels, stainless steels	Faster than gas nitriding. No white layer, high equipment costs, close case control

2.4.2 Thermochemical and Diffusion Mechanism

Thermochemical treatments, sometimes referred to as case hardening or cementation, are based on the modification of the chemical composition of the substrate material. These treatments can be succeeded by a change in the structure through heat treatment. The formal definition available in BS EN 10052:1994 [66] reads as follows:

a). Thermochemical treatment

Heat treatment carried out in a medium suitably chosen to produce a change in the chemical composition of the base metal by exchange with the medium.

b). Diffusion treatment

Heat treatment or operation intended to cause the diffusion towards the interior of the ferrous product of elements previously introduced into the surface (for example, following carburizing, boriding or nitriding).

The two major low temperature thermochemical processes developed for austenitic stainless steels are nitriding and carburizing [67, 68]. The former is normally carried out at temperatures below 450ºC and the later below 500ºC. The purpose of using low temperatures is to suppress the formation of chromium nitrides and carbides in the alloyed layers, such that chromium is retained in solid solution for corrosion protection [69]. Hardening of the nitrided layer and the carburized layer is due to the incorporation of nitrogen and carbon respectively in the austenite lattice, forming a structure termed expanded austenite, which is supersaturated with nitrogen and carbon respectively. More recently, a hybrid process has also been developed, which combines the nitriding and carburizing actions in a single process cycle by introducing nitrogen and carbon simultaneously into the austenite lattice to form a hardened zone comprising a nitrogen expanded austenite layer on top of a carbon expanded austenite layer [70-72]. There exist some synergetic effects between nitrogen and carbon: under similar processing conditions, the hybrid treated layer is thicker, harder and possesses better corrosion resistance than the individual nitrided layer and carburized layer.

From these definitions it becomes clear that two main factors will govern the process, namely: the exchange or absorption reaction with the medium, and the diffusion in the metal [66].

Kinetics of nitriding/nitrocarburizing have been the subject of a large number of investigations [73-77]. Considering practical application, model description for the kinetics (i.e. time and temperature dependence) of precipitation fronts is needed. For this purpose it is essential to recognize the controlling parameters and the affecting variables.

Once in the metal, the transport of the absorbed substance takes place by diffusion, and follows Fick's laws:

$$J = -D\left[\frac{dC}{dx}\right]. \quad (2.9)$$

$$J = -D\left[\frac{\partial C}{\partial x}\right]. \quad (2.10)$$

$$\frac{\partial y}{\partial x} = \left(\frac{\partial^2 C}{\partial x^2}\right)\Big/ \partial x^2. \quad (2.11)$$

where J is the flux of diffusing substance, D is the diffusion coefficient, and $\partial C / \partial x$ is the concentration gradient [75].

Therefore, the transport of the substance in solution is driven by its concentration gradient and the diffusion coefficient which, at the same time, depends on the temperature, the chemical composition and phase structure of the substrate. For a given alloy, kept at constant temperature in a medium with a consistent concentration of the substance of interest, the case depth will only depend on the time, according to Harris equation [78]:

$$x = a(Dt)^{1/2} = Kt^{1/2}. \quad (2.12)$$

where x is the case depth, a is a constant, D is the element diffusivity, t is the treatment time and K is a factor determined by a and D.

Higher treatment temperatures yield the same case depth in shorter time, although there are technical limitations related with life of the furnaces, and metallurgical considerations regarding the side effects of keeping the substrate material at high temperatures [79]. Consequently, diffusion treatments are slower when compared to other surface deposition techniques [80], and treatments as long as 72 hours are common practice in industry.

The diffusional flux of nitrogen and carbon from the gas to the steel surface is proportional to the concentration differences between the gas and the surface :

$$dm_N / dt_{(surface)} = k_1 [\, c_{N(gas)} - c_{N(surf)}]. \quad (2.13)$$

$$dm_C / dt_{(surface)} = k_2 [c_{C(gas)} - c_{C(surf)}]. \quad (2.14)$$

where m denotes mass, t time, c concentration per volume unit and k_1 and k_2 are reaction rate coefficients.

In nitrocarburizing as illustrated in Figure 2.15, it is additionally necessary to have a carbonaceous gas transferring carbon to the steel surface.

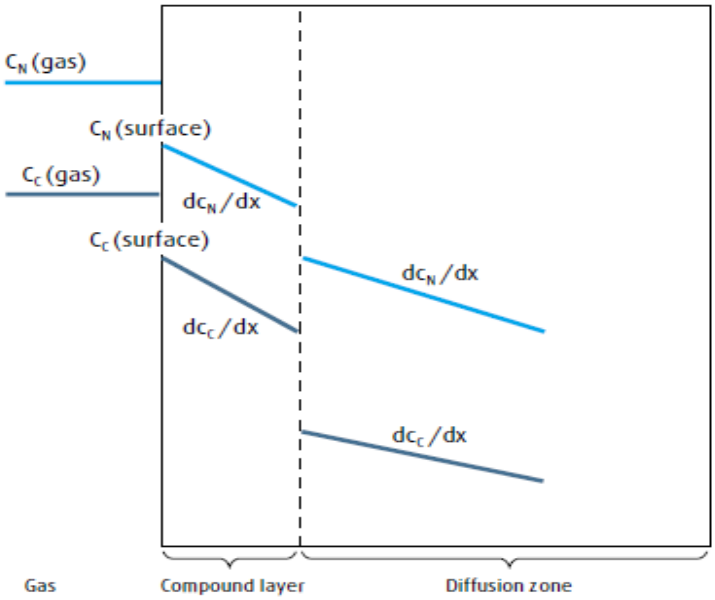

Figure 2.15. Concentrations and Concentration Gradients of Nitrogen-Carbon [58].

The transfer of nitrogen and carbon from the surface further into the steel is controlled by diffusion. Diffusion rates follow Fick's first law, which for the compound layer and diffusion zone are respectively [59]:

$$dm/dt_{(comp\ layer)} = -D_{Comp}\, dc/dx. \tag{2.15}$$

$$dm/dt_{(diff\ zone)} = -D_{Diff}\, dc/dx. \tag{2.16}$$

Balance of mass requires that all three mass transfer rates are equal:

$$dm/dt_{(surface)} = dm/dt_{(comp\ layer)} = dm/dt_{(diff\ zone)}. \tag{2.17}$$

The slowest of the three stages controls the nitrogen and carbon transfer rates. For a compound layer consisting of alternating ε-γ'-ε layers, the rate will be determined by the phase with the slowest diffusion properties. In this focus, the main reaction that controls the reaction rate of nitrogen and carbon are:

$$2NH_3 \rightarrow 2N + 3H_2. \tag{2.18}$$

$$CH_4 \rightarrow C + 2H_2. \tag{2.19}$$

$$a_c = K_1 \frac{p_{CH_4}}{p_C}; a_N = K_2 \frac{p_{NH_3}}{p_{H_2}^{3/2}} . \tag{2.20}$$

$$C_p = K_1 \frac{[CH_4]C_p}{K[C]}; N_p = \frac{p_{NH_3}}{p_{H_2}^{3/2}} . \tag{2.21}$$

$$C_p = K_1 \frac{[CH_4]C_p}{K[C]}; N_p = \frac{p_{NH_3}}{p_{H_2}^{3/2}} . \tag{2.22}$$

On the other hand, thermochemical treatments produce smooth case-core interfaces, which are beneficial for not only the wear and fatigue performance, but also the load bearing capacity [81]. During nitriding, ammonia (NH_3) in the furnace atmosphere decomposes into hydrogen and nitrogen at the surface, enabling nitrogen atoms to be adsorbed at the steel surface and to diffuse further into the steel.

In order to optimize treatments parameter, the nitrogen/carbon flux control is important issues. The flux values measured from the weight differences before and after treatments. Weight differences indicated the weight gain for each treated sample after the treatment processes. Equation 15 is used in which; *J*- flux, *A*-surface area and *t*-diffusion time, $\Delta M/A$ is the weight gain per unit area of the treated part [82].

$$J = \frac{weight\ gain}{A.t} \tag{2.23}$$

The flux calculation is, $\int_0^{x_\infty} C(x,t)dx = \int_{t_0}^{t_f} J_C dt = \frac{\Delta M}{A}$. (2.24)

The diffusion is,

$$\frac{d}{dt}\int_{C'}^{C_0} xdC - J_C(x_0) = 0; J_C(x_0) = -D(x_0).\frac{dC}{dx}(x_0,t) . \tag{2.25}$$

2.4.3 Possible Configurations of Nitriding and Carburizing

The mechanisms of nitriding and carburizing involve the transfer of the diffusing species to the surface, the establishment of a diffusing species activity gradient which

drives the diffusion process, and the diffusion for itself, may be accompanied by the formation of nitrides or carbides (on the surface or in the core). The diffusion of interstitial species into a metal can only proceed if it exists a chemical potential (or activity) gradient of those species between the surface and the core of the material.

The first step of a thermochemical treatment therefore leads to enrichment of the treated substrate surface with active species. This process makes it necessary to decompose or activate (thermally or in plasma) the gaseous atmosphere and to bring the active species to the surface, so that they can be initially absorbed and afterwards diffuse into the substrate. Table 2.2 (a) and (b) summarize the possible nitriding and carburizing configuration as described by Hertz, et al. [83].

Table 2.2: Possible Configurations of (a) Nitriding (b) Carburizing.

Substrate	N solubility	Potential nitride	Compound layer + diffusion layer + precipitation	Compound layer + diffusion layer	Diffusion layer + precipitation	Diffusion layer only
Engineering Steels	A little in α more in γ	$\alpha Fe_{2-3}N$ γ'-Fe_4N CrN with alloys elements	Yes	Yes	Yes	Yes
Engineering Steels	A little in α more in γ	$\alpha Fe_{2-3}N$ γ'-Fe_4N CrN with alloys elements	Yes but with reduced corrosion resistance	Yes	Not of industrial interest	Yes

(a)

Substrate	N solubility	Potential carbide	Compound layer + diffusion layer + precipitation	Compound layer + diffusion layer	Diffusion layer + precipitation	Diffusion layer only
Engineering Steels	A little in α more in γ	Fe_3C, CrC with alloys elements	Yes	Yes	Yes	Yes
Engineering Steels	A little in α more in γ	Fe_3C CrC with alloys elements	Yes but with reduced corrosion resistance	Yes	Not of industrial interest	Yes

(b)

The diffusion of the nitrogen and/or carbon elements successively leads to the following steps: (i) the formation of a diffusion layer enriched with the diffusing elements and if the solubility of the latter in the substrate is sufficient then this

diffusion layer can be out of equilibrium at low temperatures (ii) at higher temperatures the follow steps occur. The surface formation of nitride, carbide or carbonitride layers of the main element of the substrate and (iii) the subsurface precipitation of nitrides, carbides or carbonitrides of alloying elements in the substrate (e.g. Fe, Ti, Al, Cr, Mo, V). In addition to the law of thermodynamics, the formation of the various expanded austenite is also govern by the nitrogen and carbon surface activities, and therefore are related to the temperature of the process used (gaseous or plasma), and to the composition of the gas.

To reduce further the potential of distortion and to avoid structural modifications of the substrate, and without repeating the quench and tempering treatments, these carburizing and nitriding treatments have evolved, in the past few years, towards lower temperature processes ($350^{o}C$ – $450^{o}C$ for austenitic stainless steels). This reduction in the treatment temperatures had to include specific treatments for removing oxide layers, which act as a barrier to the diffusion of nitrogen and carbon [25].

2.5 Expanded Austenite from Thermochemical Surface Treatment

As it has been known that the chemical composition of austenitic stainless steel makes them fully austenitic up to room temperature, and thus no phase transformation hardening takes place upon quenching. Consequently, surface treatments are an interesting alternative way to increase the surface hardness and improve the wear resistance. However, surface treatment of this steel has traditionally been considered bad practice [84], as it poses two main problems: the passive oxide film and the precipitation of chromium carbides [69]. The passive chromium oxide film on austenitic stainless steel is stable under a wide range of conditions and isolates the substrate from the environment. This effect has been of interest for austenitic stainless steel components exposed to carburizing gas mixtures, either in service [85] or for surface engineering purposes [86]. In the latter case, the oxide layer impairs diffusion of the hardening elements and, consequently, needs to be removed by applying some sort of surface activation process prior to the surface engineering treatment [87].

Furthermore, traditional surface engineering treatments are conducted at high temperature, around $500^{o}C$ – $600^{o}C$ in the case of nitriding, and $900^{o}C$ – $1000^{o}C$ for carburizing [88]. At these temperatures, and with increasing availability of nitrogen

and carbon from the hardening medium, profuse precipitation of chromium nitrides and carbides occurs, leading to a marked deterioration of the corrosion resistance of Austenitic stainless steel. However, low temperature thermochemical diffusion treatments with nitrogen and/or carbon have been reported to increase the surface hardness without affecting or even improving the corrosion resistance [81].

The most popular technology used to achieve the aforementioned low temperature thermochemical treatments of stainless steels is plasma technology, namely plasma nitriding [89, 90], plasma carburizing [17, 18] and plasma hybrid treatments [19, 20]. Due to the formation of a native oxide film stainless steel surface when exposed to air or residual oxygen before and during the treatment process, it is rather difficult to facilitate nitrogen and carbon mass transfer from the treatment media to the component surface. However, during plasma processing, due to the sputtering effects of energetic ions, the oxide film can be removed easily and effective mass transfer is obtained. This makes the plasma technology unique for surface treatment of stainless steels.

An alternative is using the more conventional gaseous processes like gas nitriding and gas carburizing [21]. These have proven feasible and industrially acceptable for performing low temperature nitriding and carburizing of stainless steels, provided that the component surface is activated before the gaseous process by special chemical treatments and the oxide film formed during the gaseous process is disrupted by introducing certain special gas components [7].

It is nowadays widely accepted that hard, wear and corrosion resistant surface layers can be produced on austenitic stainless steel by means low temperature nitriding and/or carburizing in a number of different media (salt bath, gas or plasma), each medium having its own strengths and weaknesses [91]. In order to retain the corrosion resistance of austenitic stainless steel, these processes are typically conducted at temperatures below 450ºC and 500ºC, for nitriding and carburizing respectively. The result is a layer of precipitation free austenite, supersaturated with nitrogen and/or carbon, which is usually referred to as S-phase or expanded austenite [84].

Expanded austenite (EA) is a microstructural feature which responsible for the highly demanded combination of excellent corrosion and wear performances.

Expanded austenite γ_X (X = N, C) hitherto also called S-phase [68]. Expanded austenite without nitrides/carbides is obtained when high amounts of atomic nitrogen and/or carbon are dissolved in stainless steel at temperature below 450^{o}C for nitrogen and about 550ºC for carbon.

The nitrogen/carbon atoms are presumed to reside in the octahedral interstices of the f.c.c. lattice [84]. Long range order among the nitrogen/carbon atoms has so far not been confirmed with X-ray diffraction techniques. Typically, nitrogen contents in expanded austenite range from 20 to 30 at %N; carbon contents range from 5 to 12 at %C [9, 44]. In terms of N:Cr ratio the homogenity range of nitrogen-expanded austenite spans from approximately 1:1 to 3:1 [92]. Expanded austenite is meta-stable and tends to develop chromium nitrides/carbides [63, 93].

The high interstitial content of C/N is obtained because of the relatively strong affinity of Cr atoms for N and (to a lesser extent) C atoms, leading to anticipated short range ordering of Cr and N/C. Due to the low mobility of Cr atoms as compared to interstitial N/C atoms at lower treatment temperatures, chromium nitrides/carbides do not precipitate until after long exposure times and N/C is kept in solid solution by the Cr “trap sites”.

The improvement in wear resistance is perhaps the most outstanding feature of EA. The degree of improvement depends on the sliding conditions, but volume losses between one and two orders of magnitude lower than the untreated ASS are commonly reported for dry sliding [68]. This improvement is attributed to the increased surface hardness, with a typical ratio 4:1 compared to the untreated ASS [94]. The EA layer prevents the surface from undergoing plastic deformation, and changes the wear mechanism from adhesion and abrasion, to a mild oxidation wear regime. However, under heavier loads, deformation of the subsurface occurs and leads to catastrophic failure, through propagation of subsurface cracks and spallation of the EA layer [95]. In this way, the carbon EA layers, being thicker and tougher than their nitrogen counterparts, show some advantage.

With regard to corrosion, the results vary significantly depending on the testing conditions. Surprisingly, most researchers found that low temperature nitriding and/or carburizing do not harm the corrosion resistance of ASS, or even improve it. No conclusive explanation has been found for this improved corrosion behavior,

although it is clear that the benefit stands as long as nitrogen and carbon remain in solution and EA is free of precipitates [96].

In NaCl solutions, it is generally reported that EA remains passive under similar or wider range of potential compared to the untreated ASS, carbon EA showing a marginal advantage over nitrogen EA [97]. Similar or slightly higher initial current densities have usually been measured on EA, together with the absence of pitting potential, in contrast to what is usual for ASS [98]. Regarding re-passivation, the evidence indicates that the passive film heals slower on EA than on ASS [99].

2.5.1 Diffusivity of simultaneous nitrogen and carbon hybrid process on austenitic stainless steel

The hybrid process is diffusion in nature and introduces both nitrogen and carbon into the steel surface while the steel is respect to the temperature. Nitrogen is soluble in iron at the temperature range of 315^{o}C (600^{o}F) and upward. Carbon is also soluble in iron at a temperature higher than 370^{o}C (700^{o}F). These elements are soluble in a solid solution of iron [100].

From diffusion experiments performed by Million et al [101], the interesting interactions of nitrogen and carbon are known, indicating that the presence of nitrogen enhances the activity of carbon and thus, its diffusion. It should, therefore, be possible to produce expanded austenite and to enhance the layer growth by simultaneous carbon and nitrogen implantation. Treatment of austenitic stainless steel in either nitrogen or methane plasma at 400^{o}C yields the formation of expanded austenite [84]. The different amounts of nitrogen or carbon in solid solution can be explained by the strength of the interaction between nitrogen or carbon and chromium. Williamson et al [102], noted that the strong interaction of nitrogen with chromium results in the trapping of nitrogen at chromium sites. This leads to a much higher supersaturation but reduced diffusivity in comparison to a methane treatment. However, the interaction is not really strong to form CrN. Carbon has a weaker interaction with chromium, so it diffuses inwards faster and a lower supersaturation is attained under similar treatment conditions. In both cases, nitrogen and carbon remain in solid solution, presumably on interstitial sites.

Parascandola et. al. [13] went further and gives a trapping and a de-trapping model. During a hybrid treatment both carbon and nitrogen are introduced in the surface at the same time. Both carbon and nitrogen occupy the interstitial sites of the host material. A material like austenitic stainless steel has a number of interstitial sites which are considered to be trap sites due to the proximity of chromium atoms to these positions. Nitrogen has a higher affinity to chromium when compared to carbon, and therefore always fills up these trapping sites. If a carbon atom gets trapped in one of these sites it is always de-trapped and replaced by nitrogen if nitrogen is still in diffusion. Once all the trapping sites are filled up the rest of the interstitial elements diffuse more rapidly through the material. Since all the trapping sites are occupied with nitrogen, carbon moves ahead occupying new, as-yet unoccupied trapping sites. It is then de-trapped immediately as more nitrogen moves inwards. This combination of trapping and de-trapping is the reason why carbon always diffuses more rapidly and always found ahead of the nitriding front in the material.

On the other hand, the carbon species possess greater diffusivity and would penetrate further into the substrate than nitrogen [19]. Since both carbon and nitrogen occupy the same kind of interstitial sites in the fcc lattice, the arrival of the slower diffusing nitrogen atoms would force the carbon atoms (the early comer) to make available the interstitial sites. The only easy path for carbon is to diffuse further into the substrate, thus forming a push-in effect of carbon by nitrogen and a separate carbon expanded austenite layer.

2.5.2 The Influence of Process Variables and Composition of Expanded Austenite

Expanded austenite is readily obtained by gaseous treatment in various grades of stainless steels and is not restricted to austenitic stainless steel. The process parameters have a strong influence on the outcome of the surface hardening process, which provides the possibility for adjusting the case developing during gaseous treatment. The combination of treatment time and temperature should be chosen such that precipitation of chromium nitrides/carbides is effectively avoided. If precipitation does occur, Cr is removed from solid solution and the ability for passivation of the steel surface is lost (locally). As the present results show, temperatures up to 400^{o}C and 450^{o}C are readily applicable for obtaining nitrogen and carbon expanded

austenite, respectively, without the formation of undesired precipitates within the chosen treatment times [14].

This work would focus on a hybrid process which combines the nitriding and carburizing actions in a single process cycle by introducing nitrogen and carbon simultaneously into the austenite lattice to form a hardened zone comprising a nitrogen expanded austenite layer on top of a carbon expanded austenite layer [20, 70]. There exist some synergetic effects between nitrogen and carbon: under similar processing conditions, the hybrid treated layer is thicker, harder and possesses better corrosion resistance than the individual nitrided layer and carburized layer. This hybrid process is treated using nitrogen, ammonia and methane gas mixtures, which results in the formation of a uniform and carbon soot free alloyed zone with a hybrid layer structure: a nitrogen expanded austenite layer on top of a carbon expanded austenite layer, both being free from nitride and carbide precipitation. Such an alloyed zone possesses not only a very high hardness and a favorable hardness distribution, but also much enhanced corrosion resistance which is much superior to that for the untreated stainless steels and the individually low temperature nitrided and carburized layers.

Previous investigation, which regards to the influence temperature and time of thermochemical treatments using fluidized bed furnace shows that nitriding there exists an incubation time for the initiation of effective thermochemical treatment and the incubation time decreases with increasing treatment temperature. The structure of the treated layer depends on processing temperature [6]. Sun and Haruman (2008) reported that there are three most important processing parameters, i.e., gas composition, temperature and time, on the structural characteristics of the treated stainless steel in terms of layer morphology, growth kinetics and chromium compound precipitation. It was found that the development of the alloyed layers is diffusion controlled, and under proper processing conditions, a precipitate-free dual layer structure can be produced, with nitrogen and carbon dissolved in the relevant layer forming N-expanded austenite and C-expanded austenite respectively. Based on the results, a threshold temperature–time curve has been established for the investigated austenitic stainless steel [19].

The major difference between the present hybrid process and other processes lies in that no hydrogen gas is used in the hybrid process. Both nitrogen and carbon species are introduced into the conventional tube furnace and the processing temperature is sufficiently low to avoid nitride and carbide precipitation in the alloyed zone. This process has similarity with the conventional nitrocarburizing process for ferrous alloys.

However, the nature of these two processes are distinctly different in that conventional nitrocarburizing, which can be applied to most ferrous alloys, is carried out at a temperature < 590^{o}C with the purpose of producing a carbonitride compound layer at the surface [65].

Meanwhile, the present hybrid process applies to austenitic stainless steels and is carried out at much lower temperatures (400^{o}C – 500^{o}C) with the purpose of producing a hybrid structure without nitride and carbide formation. The description of diffusion process in conventional nitrocarburizing and high alloy steels was shown in Figure 2.16.

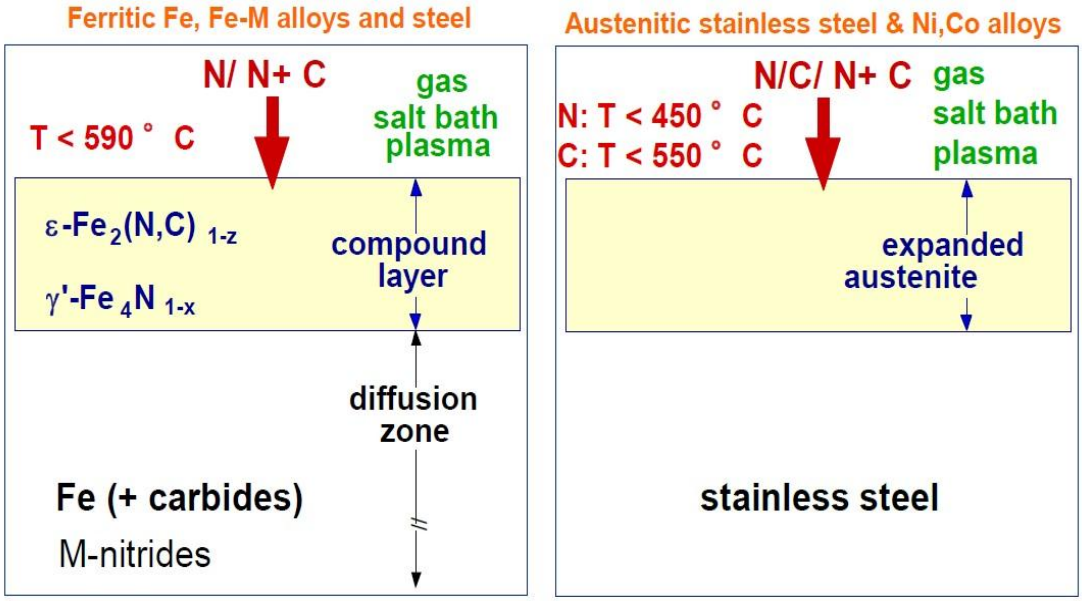

Figure 2.16. Low Temperature Surface Hardening of Fe-based Alloys [105].

CHAPTER 3

METHODOLOGY

3.1 Overview

This chapter explains the methodologies and specific procedures used to investigate the objectives set by the research. Several experiments, characterization and analytical works have been carried out in a systematic way.

The chapter is divided in to two main sections. The general steps followed are discussed in the methodology section where the steps would be outlined in detail. In the second section, the detail of the sample preparation and characterization is presented.

In this discussion the material used, techniques and equipment utilized are explained. Procedure and settings as well as the considerations in executing the experiments are also presented.

3.2 Methodology

The research work investigated a systematic development of a hybrid surface harden layer on AISI 316L and its microstructure, surface topography, elemental including structural phase analysis, near-surface mechanical properties and the corrosion resistance.

All the sample materials were prepared in the similar method, standard metallographical examination i.e. sectioning, grinding, polishing, cleaning, drying, and followed by low temperature thermochemical treatments at the appropriate parameters. The overall methodology, typical procedures, materials used and the equipments used are explained in this chapter as described in Figure 3.1.

An austenitic stainless steel AISI 316L was used throughout the experimental series with surface preparation was carried out prior to the treatment. The treatment temperatures were selected in the range of temperatures from 400 to 500^{o}C with treatment time up to 8 hours (8 h).

The present hybrid process is carried out at this temperatures with the purpose of producing a hybrid dual layer structure which comprising a nitrogen expanded austenite layer on top of a carbon expanded austenite layer without nitride and carbide formation to enhance the load bearing capacity and toughness of the alloyed surface. Hence, the case hardening process of combination carburizing-nitriding is chosen for this study.

Firstly, purging the reactor column of the conventional gas furnace by N_2 gas was carried out prior to the treatment in order to reduce abandon oxygen in the atmosphere. The treatment parameters (time, temperature, gas composition) were selected after a literature survey on similar work on austenitic stainless steels [104].

Secondly, the hybrid process involved treating the sample in an atmosphere containing both NH_3 (for nitriding) and CH_4 (for carburizing) for a total duration of 8 h. In this experiment, reactive gases were diffused from gas source as mentioned above in thermal activated environment.

The proper parameters, i.e. soaking time, treatment temperature, and gas composition were applied to obtain alloy hardened case with minimum effect to deteriorating the stainless steel substrates. Then the samples were charged to the furnace and the treatment gases were introduced and their flow rates were adjusted to meet the required composition.

Thirdly, the surface morphology of the treated specimens was characterized using Field Emission Scanning Electron Microscope (FESEM) and further collaborated with Scanning Probe Microscope (SPM) at higher re solution for the hybrid alloyed surface. Prior to this metallographic examination, the polished specimens were etched by Marbles reagent. Figure 3.1 describes the overall methodology, typical procedures, materials used and the characterization processes for resulting layers.

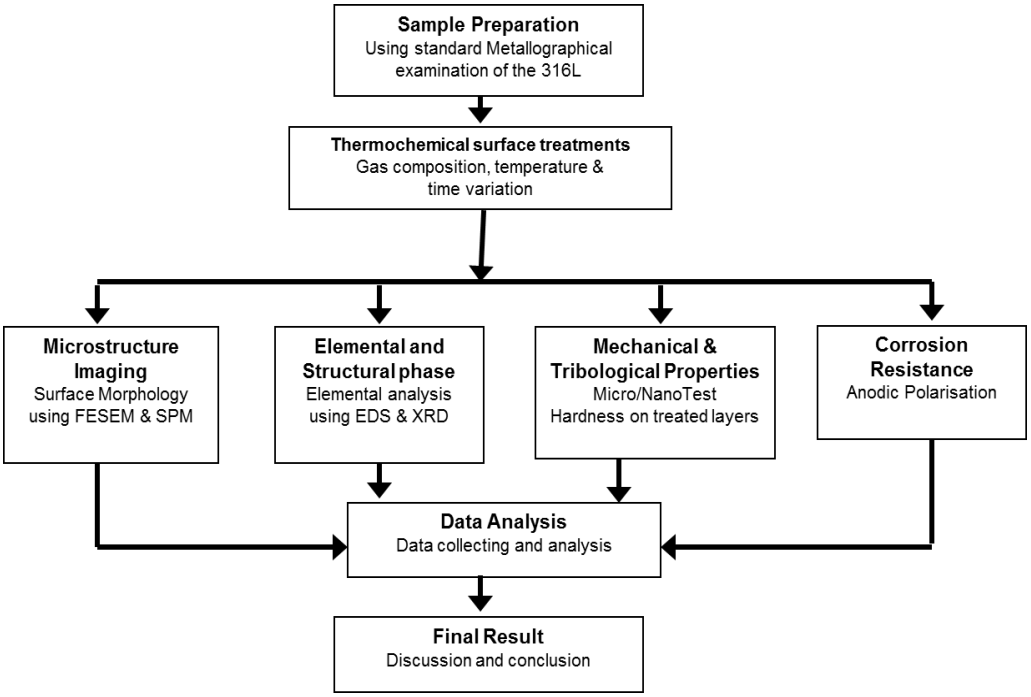

Figure 3.1. Research Methodology.

Nano-mechanical testing and microhardness profile of Vickers indentation was made across each resultant layers. The test was also performed to reveal the surface mechanical properties. X-ray diffraction (XRD) analysis using Cu-Kα radiation (40 kV, 150 mA) was employed to identify the produced phases from various process conditions. Thus, the data from the above characterization techniques, the surface characteristics of treated specimens from various treatment conditions were determined. Moreover, the specimen performance was further measured by microhardness indentation and elemental analysis by Energy dispersive Spectroscopy (EDS) and line scan mode of EDX.

Lastly, wear resistance and anodic polarization were evaluated to measure the performance improvement of hybrid treated layers.

3.3 Sample preparation and material characterization

The selection of materials and processing routes are key decisions which must be made wisely in order to obtain surface harden expanded austenite layers. Improper

material preparation may lead to the failure of obtaining expanded austenite layers, material inhomogeneity, and cracking. An optimal relationship for the treatment parameters and a proper pre-cleaning procedure were responsible for highly required better mechanical properties without impairing its corrosion resistance.

3.3.1 Experimentals

3.3.1.1 Specimen handling

In this research, the commercially available austenitic stainless steel AISI 316L from Hoto SS industries Sdn.Bhd was used. The substrate material used was AISI 316L type austenitic stainless steel, this steel was supplied in the form of 2 mm thick hot-rolled plate. Table 3.1 presents chemical compositions (in wt%) of our specimen.

Table 3.1: Chemical Compositions of Specimen.

Material	Cr	Ni	Mo	Mn	C	Si	P	S	Fe
316L	17.018	10.045	2.00	1.53	0.03	0.048	0.084	0.03	balance

Samples of 20 mm x 70 mm size rectangular coupon were cut from the plate. The sample surface was ground on 320, 600, 800, 1000, 1200 grit SiC papers, and then polished using 1 μm Al_2O_3 pastes to the mirror finish. At one end, a hole was drilled into the sample so that they can be suspended on a stainless steel wire support. This support allowed the samples to be arranged vertically inside the chamber installation, at equal distance, and this made possible for a great number of samples to be treated simultaneously in identical conditions. After all steps have been completed, the samples are kept into the dryer in order to remove unwanted contamination at the sample. Dry and clean sample were stored in closed dry cabinet to avoid environmental contamination.

3.3.1.2 Thermochemical Hybrid treatment

The thermochemical surface treatment process was performed at Nanotechnology laboratory Universiti Teknologi PETRONAS, Malaysia. The conventional tube system and schematic of hybrid thermochemical setup used in this research are shown in Figure 3.2 and Figure 3.3.

Figure 3.2. Hybrid Thermochemical Tube Furnace Setup.

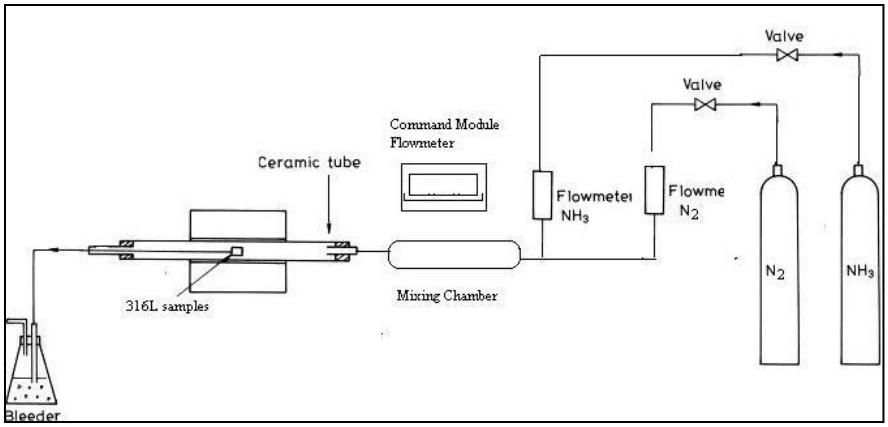

Figure 3.3. Schematic Illustration on Hybrid Thermochemical Equipment Setup.

Prior to treating, the specimens were soaked in concentrated HCl (2 M) solution for 15 minutes duration with the purpose to remove the native oxide film that commonly forms on austenitic stainless steel and protects the metal matrix from corrosion [19]. Hybrid treatments were performed at 400^{o}C, 450^{o}C and 500^{o}C in a horizontal tube furnace which involving reactive gases both NH_3 (for nitriding) and CH_4 (for carburizing) for a total duration of 8 h. The gases flows were controlled by Aalborg flow meter and the linear flow rate of gas mixture through the alumina retort were conditioned by gas mixing tank. In this system the sample were placed in the quartz boat of about 12 cm in the center of isothermal zone of electric resistance tube

furnaces. Before charging the samples, the chamber was heated to the treatment temperature of 400 and 450°C with the flow of nitrogen gas at 2.05m^3/h. Then the samples were charged to the furnace and the treatment gases were introduced and their flow rates were adjusted to meet the required composition, with the total gas flow rate maintained at 1.0 m^3 per hour as shown in Figure 3.4. Moreover, Table 3.2 summarizes the process conditions employed in this work.

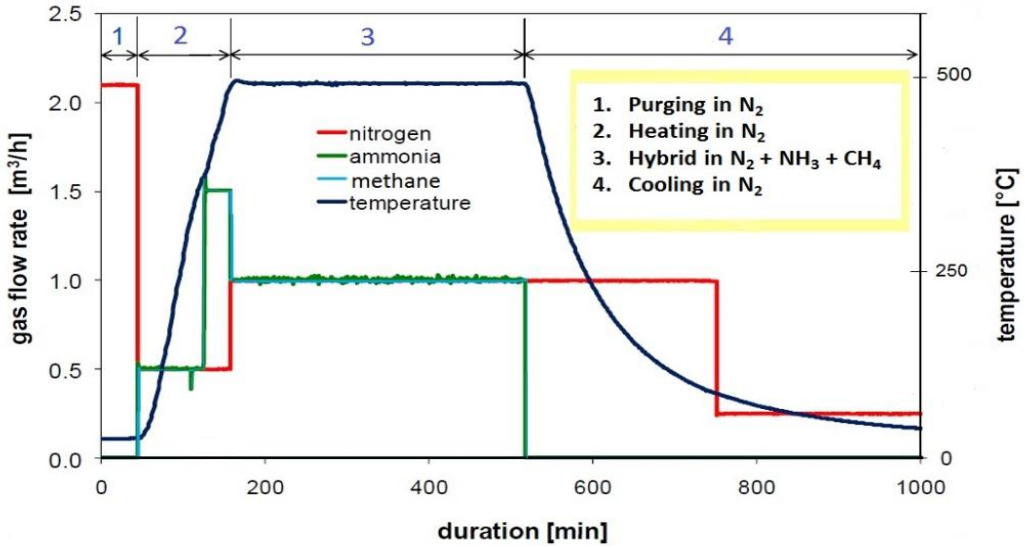

Figure 3.4. Temperature/Time Diagram of Hybrid Treatment of AISI 316L at 500°C.

The hybrid process involved treating the sample in an atmosphere containing both NH_3 (for nitriding) and CH_4 (for carburizing) for a total duration of 8 h and three different hybrid treatments were conducted. The heating rate was 5°C/min while nitrogen gas still flowing in the furnace.

Table 3.2: Treatment Conditions and Layer Thicknesses.

Treatment	Time (Hour/h)	Temperature (°C)	Gas (%)			Layer Thickness (μm)
			CH_4	NH_3	N_2	
Hybrid Process 316L	8	400	5	20	75	3.421
Hybrid Process 316L	8	450	5	20	75	6.425
Hybrid Process 316L	8	500	5	20	75	26.425

When the temperature reached 400°C, 450°C and 500°C, ammonia gas and methane gas were released and it flew into the furnace. The composition of gas that entered to the furnace chamber is 75% nitrogen, 20% ammonia and 5% methane. The duration for nitriding treatment was 8 hours. Then, the sample was cooled. The cooling rate was 30°C/min. These processes are critically controlled, low temperature, the hardening processes are occurred where nitrogen (and to a lesser extent-carbon) is introduced into the surface of substrate by holding the metal at suitable temperature of 400^{o}C, 450^{o}C and 500^{o}C in a conventional tube furnace. To achieve the correct flow of all the gases the operating pressure needs to be set. This is achieved by the adjustment of the regulators on the side of the furnace and by monitoring the pressure via the pressure gauges at the front of unit and nominal pressure was 15 kpa.

3.3.2 Characterization and Testing

This is the technique used to examine the internal structure of a material. The appearance of this "microstructure" is a significant issue to understand the properties of materials. Laboratory techniques like microscopy, spectroscopy and x-ray diffraction are combined with a thorough knowledge of thermodynamics, engineering metallurgy and applied mechanics to understand and explain the behavior of the materials. This scientific understanding is balanced by real-world understanding of manufacturing and design applications.

In present works, the samples were mirror finished ground and polished using a diamond paste and cleaned. The microstructure features and surface topography of the resulting layers were observed by Field emission scanning electron microscopy (FESEM)-Ziess Supra 55 VP with simultaneous chemical analysis by energy dispersive spectroscopy (EDS) and Universal Scanning Probe Microscopy (USPM), while phase composition and structural phase of the samples were studied by XRD (Brucker AXS D8 diffractometer) using Ni-filtered Cu Kα radiation. The surface hardness was obtained under a 1000 g load for 15 seconds by using micro Vicker's Indentation. Vickers hardness (Hv) was determined from a minimum of 10 indents, while the wear resistance was measured using Pin-on Disc Wear Test (ASTM G99-95a) method. Nanoindentation tests were conducted to quantify the mapping of mechanical properties, such as hardness and elastic modulus of the expanded

austenite. The electrochemical corrosion behavior of the hybrid treated surfaces was evaluated by measuring the anodic polarization curves in aerated 3.0 % NaCl solution at a scan rate of 1 mV/min. The tests were conducted at room temperature by using a three electrode potentiostat with a computer data logging, requisition and analysis system. Potentials were measured with reference to the standard calomel electrode (SCE). In the following subsections the details of the characterizing equipments and procedures used will be elaborated in detail.

3.3.2.1 FESEM-EDS Characterization

Surface morphology, wear tracks on treated samples were examined using a field emission Ziess Supra 55 VP scanning electron microscope (SEM) with an Energy Dispersive X-Ray (EDX) capability. The chemical compositions of elemental depth profile, wear samples were analysed using EDX during SEM examination. The analysis was carried out both qualitatively to determine the existence of certain elements and quantitatively to determine the amount of each element present. The FESEM (Zeiss Supra 55 VP) used for this research is as follows shown in Figure 3.5 (a).

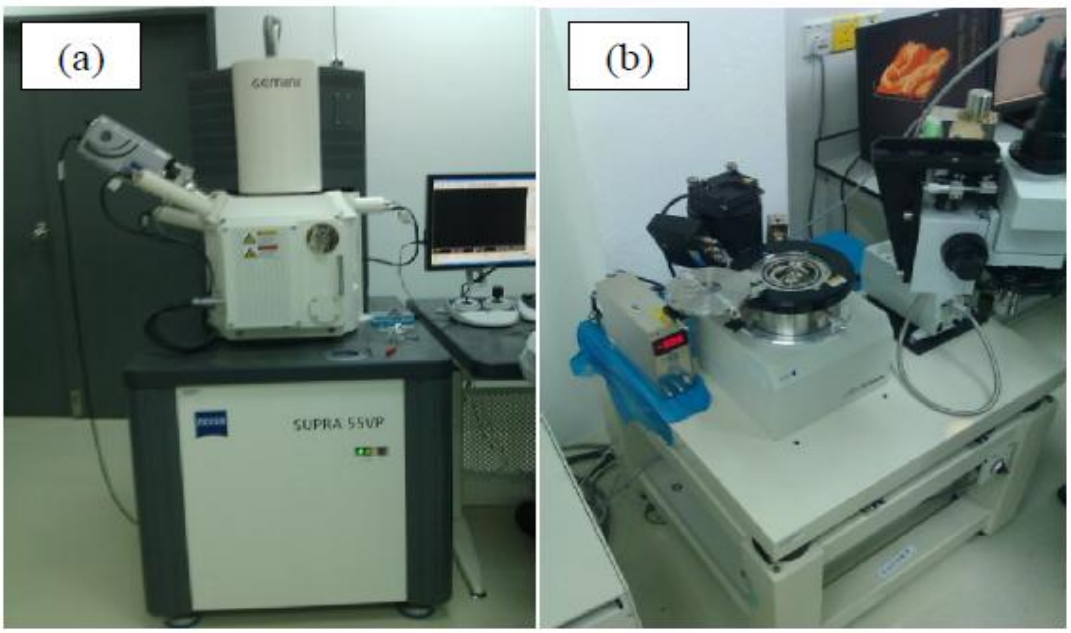

Figure 3.5. (a) Supra 55VP FESEM, (b) Nano Navi: E-sweep USPM.

FESEM was used primarily to identify the phases present and determine the morphology of treated layers. Specimens for analysis were ground flat and polished using 1µm diamond paste. It was also used to analyse the elements level at a point using the EDS system which detects X-rays emitted from the sample as a result of the high-energy electron beam penetrating into the sample. X-ray spectra can be collected and analyzed, yielding quantitative elemental information about the sample produced. Lines cans and x-ray maps can also be generated.

In this study, 6 cross section specimens from different treatments were cut from the samples with diamond cutter machine and mounted on conductive Bakelite. In order to reveal the microstructure, the polished surfaces were etched by Marble's solution (4 g CuSO4 + 20 ml HCl + 20 ml distilled water). The specimen surfaces were ground to the mirror finish and placed in the microscopes chamber which are subject to a vacuum where gas molecules interfere with the electron beam and with the emitted secondary and backscattered electrons used for imaging.

3.3.2.2 Universal Scanning Probe Microscopy (USPM)

The topography and grain sizes of the hybrid treated samples were measured using the Universal Scanning Probe Microscope (USPM) shown in Figure 3.5 (b) with type of Nano Navi (E-Sweep). It was developed to image almost any type of surface, including metals, polymers, ceramics, composites and glass samples. It can image conducting or semiconducting surfaces.

AFM or scanning force microscopy (SFM) is a very high-resolution type of scanning probe microscopy, with demonstrated resolution on the order of fractions of a nanometer, more than 1000 times better than the optical diffraction limit. This work was used a laser beam deflection system, introduced by Meyer and Amer, where a laser is reflected from the back of the reflective AFM lever and onto a position-sensitive detector. AFM tips and cantilevers are micro fabricated from Si or Si_3N_4. Typical tip radius is from a few to 10s of nm. Universal Scanning probe microscope (USPM) is the general term used to describe a microscope that allows the high-magnification observation of 3D topographic images, force modulation images, magnetic images, friction images, and electric-potential images by scanning a sample

surface with a microscopic probe. USPM can also be used to investigate on the sub-nanometer scale, in this investigation the surface topography of treated specimens from top-view and cross sectional were explored according to standard test of ANSI/ASME standard B-46.1 [105].

In this work, the hybrid treated specimen was also characterized by universal scanning probe microscope (Nano Navi E-sweep) with a probe or "tip" placed very close to the sample to reveal 3D surface topographical profile at higher resolutions. To obtain the topographical profile of the specimen, the contact mode was applied with 1.2 V constant operating force, 1 Hz scanning rate, 0.1 μm Z axis range, for both 1μm x 1μm top surface and 5μm x 5μm cross sectional cut.

3.3.2.3 X-ray Diffraction

As a means of identifying phases constituents in the treated surfaces on AISI 316L, The phase constituents in the as-received and hybrid treated surfaces were analysed with an D8 Philips X-Radiation diffractometer using Cu-Kα radiation (λ=0.154nm). The scanning step was of 0.02° per minute at a dwelling time of 3 seconds. The diffraction patterns obtained were analysed and indexed using an X'Pert High Score analytical software for automated powder diffraction. Samples were cut and surface ground and mounted using 'Blutac' adhesive. Furthermore, samples were analyzed with grains in random orientations to insure that all crystallographic directions are "sampled" by the beam. When the Bragg conditions for constructive interference are obtained, a "reflection" is produced, and the relative peak height is generally proportional to the number of grains in a preferred orientation.

The analysis is performed by comparing the diffraction pattern collected from an unknown sample with the diffraction patterns of known compounds. The experimental patterns were compared with the diffraction scans of pure compounds maintained in the ICDD Powder Diffraction File (PDF). Data reduction and S/M analysis was performed using the ANOVA software package. All scans were smoothed, theta corrected, and the background was removed. The results of Search/Match analyses are shown below each plot as a set of stick lines from the PDF. X-Ray Diffraction unit is shown in Figure 3.6.

Figure 3.6. D8 Advance XRD Machine.

3.3.2.4 Hardness measurement

In this current work, to measure the hardness of treated layers, a micro hardness test was used for indentation. The load to be tested was well polished and finished with 1200 grit paper until there is no scratch on the surface when observed under optical microscopy. The hardness measurement was obtained under a 10g load for 15 seconds by using Vicker's Indentation machine as shown in Figure 3.8. Hardness measurement was conducted based on ASTM E92 for testing Method for Vickers Hardness of Metallic Materials [106]. The Vickers hardness (Hv) was determined from a minimum of 10 indents and then it was calculated using equation 3.1 [72]. The diagonal of the indentation and crack length was measured using the optical microscopy as shown in Figure 3.7.

$$H_V = 1.85\frac{p}{D^2}. \tag{3.1}$$

where p = Load in kgf, D = arithmetic mean of the two diagonals, d1 and d2 in mm.

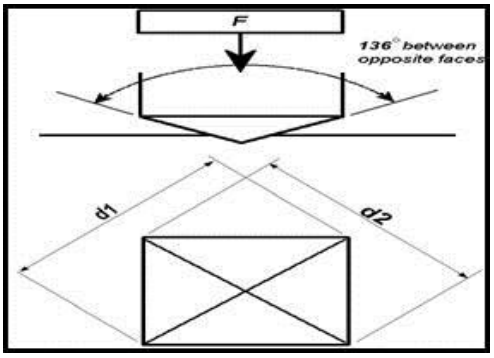

Figure 3.7. Schematic Diagram of Vickers Pyramid Indenter Pressed into Harden Layer.

Figure 3.8.Vickers Hardness Test: Model HV-1000A Microhardness Tester.

3.3.2.5 Wear test

Wear tests to the hybrid treated specimens were performed using Pin on Disk tribometer. The tests were conducted at a non-lubricated condition with an applied normal load values for the test were 17 N with the speed of 75 rpm and sliding distance of 300 m (for 30 minutes time of operation). It was conducted at room temperature and the atmosphere is set to be the laboratory air.

Figure 3.9 shows the wear test by pin on disc apparatus use to analyze the coefficient of friction of prepared samples according to the standard; ASTM G99-95a [107]. For this work, the wear test is in the dry sliding condition. Ducom TR-701-M6 Multi Specimen Tester machine used for pin-on disc wear test.

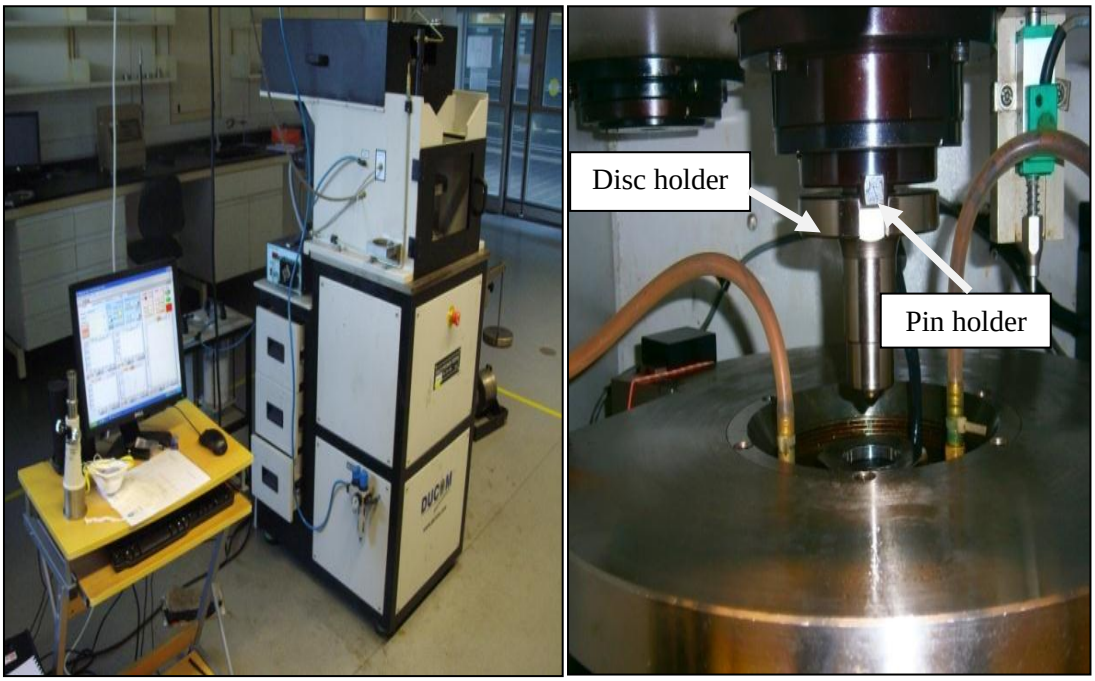

Figure 3.9. (a) Ducom TR-701-M6 Multi Specimen Tester Machine,
(b) Pin and Disc Holder.

3.3.2.6 Nanoindentation measurement

So far, the surface and near-surface mechanical properties of thin films or coatings can be related to the final performance of materials. In order to investigate the high precision measurement of mechanical properties for expanded austenite layer, nanomechanical characterizations were performed on all treated and substrate materials according to ASTM E2546 – 07 for Standard Practice for Instrumented Indentation Testing [108]. The hybrid treated specimens were fixed to the lapping fixture via polymeric adhesive. After polishing, the adhesive was dissolved with acetone, freeing the samples for bonding to the nanoindenter's sample stage.

Nanoindentation was carried out to measure continuous force and displacement as an indenter of known geometry is pressed into a sample material. The displacement is measured, in most cases, by a capacitive sensor. With instruments now having micro-Newton force and nanometer depth resolutions, it is possible to produce load-displacement curves representative of the material response in terms of hardness,

modulus and elastic recovery. The nanoindentation test were performed using Nano System 600, manufactured by Micromaterials UK, the schematic diagram for Nano System is shown in Figure 3.10 and the setting parameters to assess the mechanical properties of the outmost layer of treated samples was described in Table 3.3.

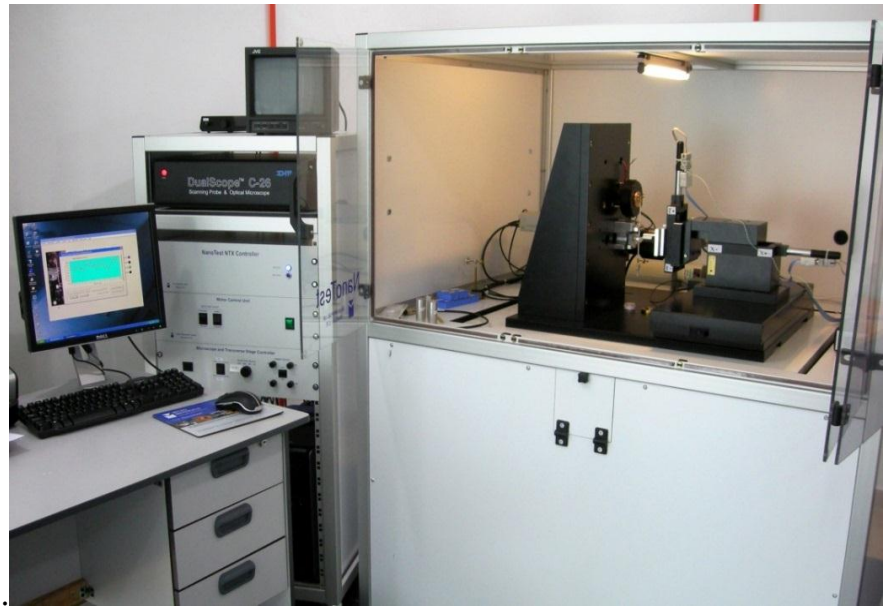

Figure 3.10. Nanoindentation Instrument at AMREC SIRIM, Sdn.Bhd. 2012, Kulim.

Table 3.3: Instrumented Hardness Settings for Nanoindentation Measurement.

Variable	Value
Type of Experiment	Depth vs. Load
Type of Indentor	Berkovich Pyramid
Maximum Load	300 mN
Maximum Depth	200 nm
Dwelling Time at Maximum Load	5 second
Loading Rate	3.99 mN/s

3.3.2.7 Corrosion test

The corrosion resistance of untreated 316L austenitic stainless steel and treated 316L austenitic stainless steels at 400°C, 450°C and 500°C in CO_2 environment was evaluated at room temperature by measuring polarization curves in 3.5% NaCl according to standard polarization test using ASTM G5 [109].

The flat cell, as schematically shown in Figure 3.11, was a three electrode set-up consisting of the specimen as the working electrode, a silver chloride (AgCl) as the reference electrode, and a platinum electrode used as the auxiliary electrode. Corrosion test was carried out by Linear Polarization Resistance (LPR) which connected to a standard three electrode cell as mentioned above.

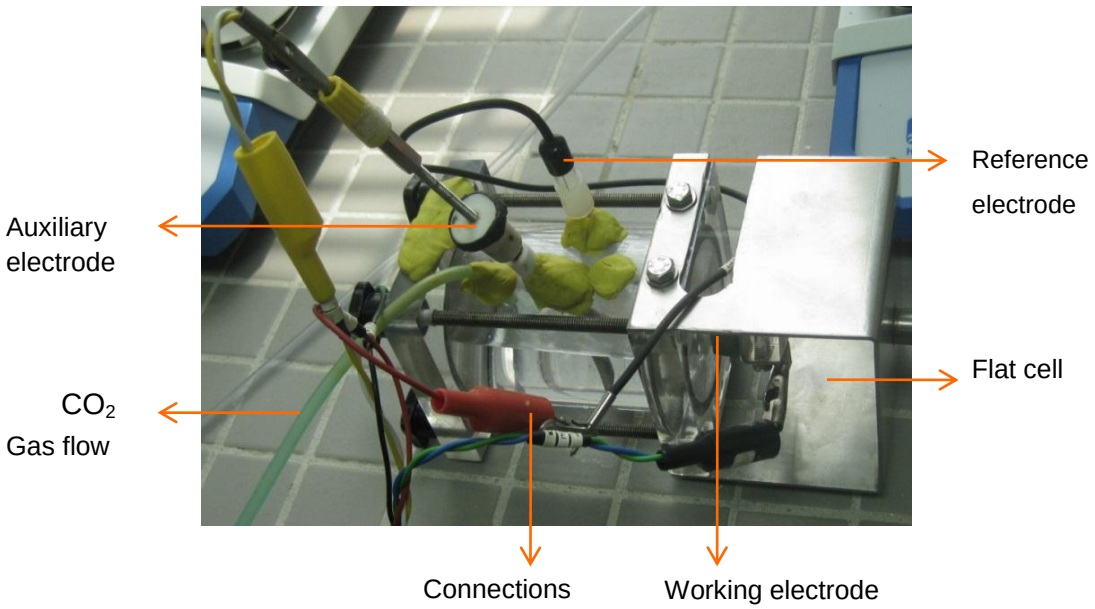

Figure 3.11. Schematic Diagram of Flat Cell used for Polarization Corrosion Test.

CO_2 gas was purged during the experiment to simulate carbon dioxide environment. It was purged into saturated solution for one hour exposure of electrode to remove all the oxygen in the water and to maintain the saturation of CO_2.

The electrochemical measurements were based on a three-electrode system, using a commercially available potentiostat with a computer control system from ACM Instruments. The working electrode was hybrid treated samples to be tested were placed against a Teflon ring at one end of the flat cell, leaving a theoretical circle area of 0.35 cm^2 on the sample surface in contact with the testing solution through a round hole in the Teflon ring. Test control, data logging and data processing was achieved by a ‘‘Sequencer’’ computer software. The scanning potential is in the range of -0.8 to + 1.2 V, and the scan rate was 1 mV/s. The ACM instruments ran and data gathered automatically into the ACM Analysis Version 4 to generate polarization curve.

CHAPTER 4

RESULTS AND DISCUSSIONS

4.1 Overview

This chapter discusses the overall results of the experimental works. The formation of expanded austenite layers by low temperature thermochemical treatments using conventional tube furnace is discussed. Reactions that may occur during thermal activated diffusion are suggested and parameters that affect the resulting layers are discussed including the mechanical properties as well as corrosion resistance.

In the first section of the chapter, the activation method for stainless steel surface, microstructure of surface hardened layer was discussed. Based on the results from the FESEM, USPM and XRD, the characteristics of the resulting layers were discussed. Moreover, an optimum processing parameters for development of novel hybrid treatments was done. In the same section, microstructure, compositional and mechanical properties were studied.

In the second section of the chapter, comparison of the mechanical properties of the expanded austenite is done in order to understand the improvements and some trends in the properties.

In the final section of chapter, the resulting layers were investigated for the corrosion resistance in corrosive environment application. The study was also focusing on the effect of temperature treatments and characteristics of surface layers temperatures on low temperature thermochemical AISI 316L. Finally a conclusion and remarks were done for the outcome of the results.

4.2 Processing

Austenitic stainless steel AISI 316L samples were treated in conventional horizontal tube furnace according to the parameters as described in Table 3.1. Different

treatment conditions were explored in this furnace, in both nitriding and carburizing atmospheres (hybrid). The hybrid treatments were performed at 400°C to 500°C in a furnace which involves reactive gases both NH_3 (for nitriding) and CH_4 (for carburizing) for a total duration of 8 h. The gases flows were controlled by Aalborg flow meter and the linear flow rate of gas mixture through the alumina retort were conditioned by gas mixing tank. In this system the sample were placed in the quartz boat about 12 cm in the center of isothermal zone of electric resistance tube furnaces.

As discussed previously in chapter 3, to overcome the problem of passive oxide film on stainless steel which acts as dense diffusion barriers for gaseous treatments, a separate HCl activation procedure is required to remove the native oxide and allow the inward diffusion of nitrogen and carbon atoms [19]. The HCl activation in recent work has been demonstrated as a successful method to remove the passivating oxide layer for gaseous hybrid treatment. Austenitic stainless steel samples were able to be hybrid treated with gas mixtures of $NH_3/CH_4/N_2$.

Besides that, the use of hydrocarbon gas in recent work by using methane addition in ammonia environment would produce transient cyanide groups that remove the Cr_2O_3 barrier film on stainless steels. This barrier film inhibits diffusion of C and N into steel surface and subsequent case hardening. This treatment is related to patent US 2007/0204934 A1 [30]. The patent claims that some additional active hydrocarbon gases in the ammonia would form HCN and would improve the uniformity of nitriding/carburizing treatment. Finally, a surface of material is able to penetrates the nitrogen/carbon. This treatment will shorten the treatment time to obtain the same case depth [110].

According to Sproge and Slycke [111], gas exchange reaction in active atmosphere containing ammonia and methane is the reaction where hydrogen cyanide is formed according to equation 4.1. This reaction can also transfer nitrogen and carbon atoms to the steel surface, as described in equation 4.2.

$$NH_3 + CH_4 \rightleftarrows HCN + 3H_2 \quad (4.1)$$

$$HCN \rightleftarrows N + C + \tfrac{1}{2}H_2 \quad (4.2)$$

The next step after exploring the possible reaction during the treatment, evaluates the hybrid layer performance of treated 316L samples in terms of weight gain as well

as average flux. The treatment condition and weight gained were achieved according to Table 4.1. The specimens were weighted before and after the treatments cycle with a conventional microbalance, accuracy of 0.1mg.

Table 4.1: Flux Values Measured from Weight Gain.

Treatment Temperature (^{o}C)	Mass before Treatment (g)	Weight Difference (g)	Percentage of Weight Difference (%)	Flux from Weight Gain (g/cm^2/s)
400	3.138	0.002	0.064	2.29 (10^{-8})
450	3.140	0.004	0.127	4.59 (10^{-8})
500	3.142	0.005	0.159	5.74 (10^{-8})

The total quantity of nitrogen and/or carbon which diffuse through the surface can be estimated by integrating the nitrogen or the carbon concentration profile over the depth of treated layer.

According to the flux balance condition at the steel interface and continuity equation of the mass accumulation within the solid [75], the rate at which the total mas of the solid changes per unit cross section area is,

$$\int_{0}^{x_{\infty}} C(x,t)dx = \int_{t_0}^{t_f} J_C dt = \frac{\Delta M}{A} \tag{4.3}$$

From the equation above, the weight gain from hybrid treating processes was calculated based on the measurement of the individual weight of each coupon before and after treatments. The importance of this nitrogen and/or carbon flux control is significant for optimizing treatment parameters. The flux values measured from the weight differences are shown in Table 4.1. Equation 4.4 is used to find *J*- flux and to find the nitrogen flux from weight gain where *A* is surface area and *t* is nitriding time.

$$J = \frac{weight.gain}{A.t} \tag{4.4}$$

From the results in Table 4.1, hybrid treated at 500°C brings about a 2.5 times higher nitrogen uptake than nitriding at 400°C. It is understood that weight difference is increased when the temperature increases in hybrid processes. Besides, it is agreed that the nitrogen flux is influenced by the temperature of the hybrid process. Based on the result, it shows that the increment of the hybrid temperature would increase the rate of nitrogen diffusion per unit area of the treatment.

Based on Figure 4.1, the graph shows that the percentage of weight difference of samples before and after hybrid increases gradually with temperature. Thus, it can be concluded that increasing the hybrid treatment temperature will increase the nitrogen and/or carbon diffusion into the sample.

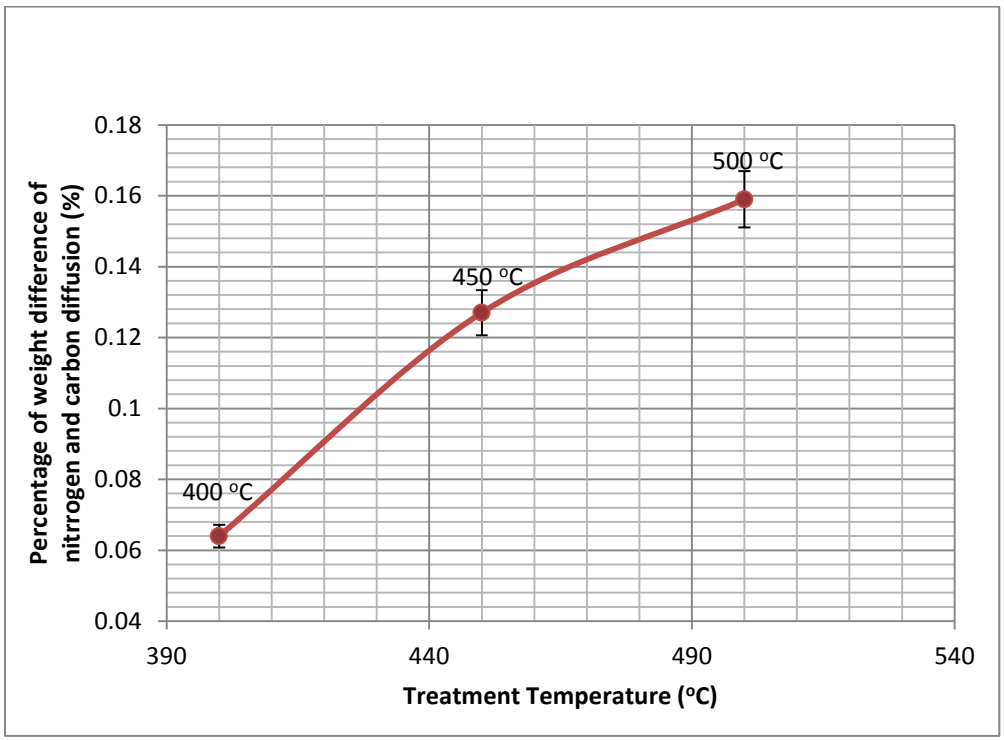

Figure 4.1. Weight Gains of Samples due to Varied Temperature Treatments.

4.2.1 Surface morphology and topography of treated layers

Different morphologies of harden layers were observed as a result of the various treatment conditions and the thicknesses of the layers produced in different specimens. According to the micrograph in Figure 4.2, expanded austenite layer is

recognized as a featureless surface layer, the featureless nature of expanded austenite compared to the clearly distinctive nature of the substrate is a result of selective etching; based on this information, expanded austenite has a higher electrochemical potential than the substrate.

For a similar treatment duration, the plasma process is reported [38, 41] to produce about 18 μm thick layer which is much higher compared to that of the present conventional hybrid treatment in horizontal tube furnace. In plasma process, the native oxide layer was removed mostly by bombardment of the plasma gas which is completely absent in conventional process.

This is one of the reasons why conventional horizontal tube furnace produced small layer thickness compared to the corresponding plasma treatments. Previous investigation revealed that nitriding at 450°C became effective after treatment for 6 h where a continuous treated layer was produced [6].

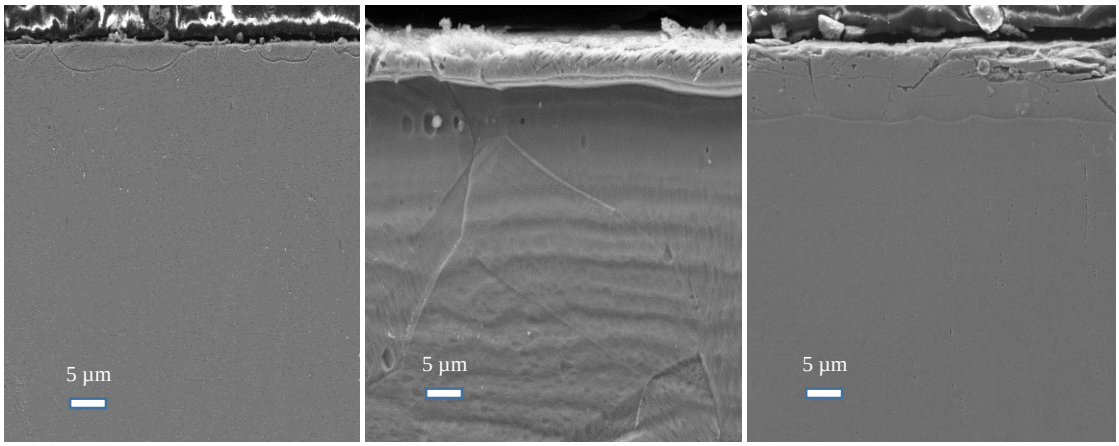

(a) (b) (c)

Figure 4.2 SEM Micrograph of the cross-sectional expanded austenite samples: (a) Hybrid 400^{o}C, (b) Hybrid 450^{o}C, and (c) Hybrid 500^{o}C

The three specimens processed under hybrid treatment conditions as shown in Figure 4.2, actually produced duplex layers although not clearly revealed in the present micrograph. These separations of dual structures were observable under SEM. The existing of small cracks (arrowed in Figure 4.2c) is believed to originate from large compressive stresses associated with the lattice expansion in γ_N. The nucleation

and growth of cracks result in a sudden release of energy within a solid have relationship with the expansion and distortion of austenite lattices result in the formation of high density dislocations and stacking faults in the hybrid layer [14].

The variations of chemical concentration in the hybrid layer were measured with EDS spectrums and line scan mode. Figure 4.3 shows the typical nitrogen and carbon profiles produced in hybrid treated 316L at different temperature. A high carbon peak was detected at the inner layer as shown Figure 4.3(b) with red colour in line analysis, thus proving the push-in effect of dissolved carbon by incoming nitrogen during the hybrid process. This argument was also related to the different diffusivity and competition of diffusion phenomena between carbon and nitrogen to occupy same interstitial sites in crystal lattices as described in the section 4.2.2.2.

Since both carbon and nitrogen occupy the same kind of interstitial sites in the fcc lattice, the arrival of the slower diffusing nitrogen atoms would force the carbon atoms (the early comer) to make available the interstitial sites. The only easy path for carbon is to diffuse further into the substrate, thus forming a push-in effect of carbon by nitrogen as shown clearly in Figure 4.3(b) and a separate carbon expanded austenite layer.

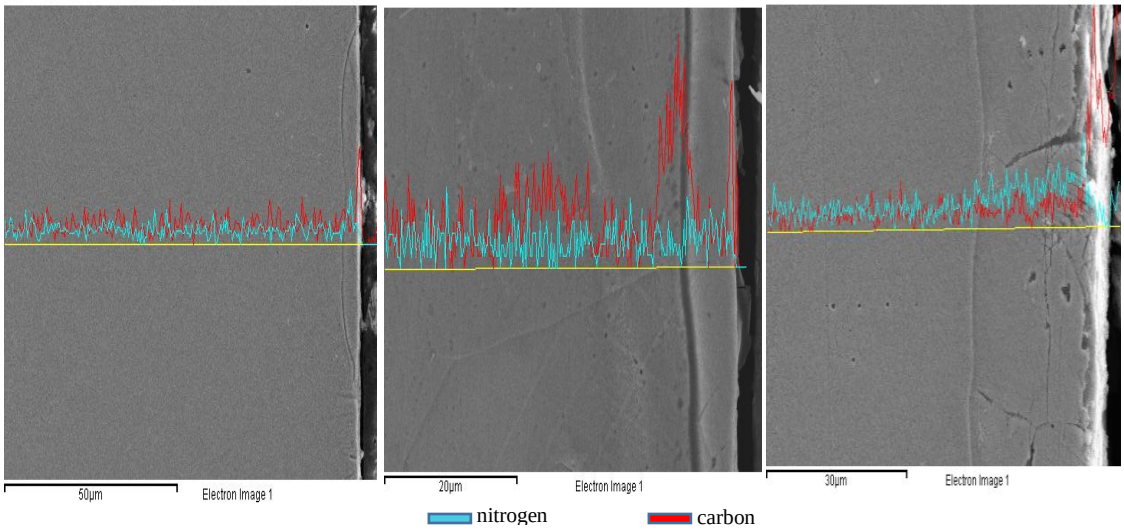

(a) (b) (c)

Figure 4.3. Elemental Analysis of Hybrid Treated Samples at Different Temperatures: (a) Hybrid 400^{o}C (b) 450^{o}C and (c) 500^{o}C.

Figure 4.4 describes the details of elemental profile of hybrid treated AISI 316L which shows the effect of thermal activated diffusion on the carbon and/or nitrogen diffusivity through surface of materials.

As shown in point (b) and (c) in the Figure 4.4, the formation of a dual layer structure is obviously the result of the simultaneous introduction of nitrogen species and carbon species in the treatment atmosphere which clearly revealed in the present micrograph. The carbon species have greater diffusivity and would penetrate further into the substrate than nitrogen [19].

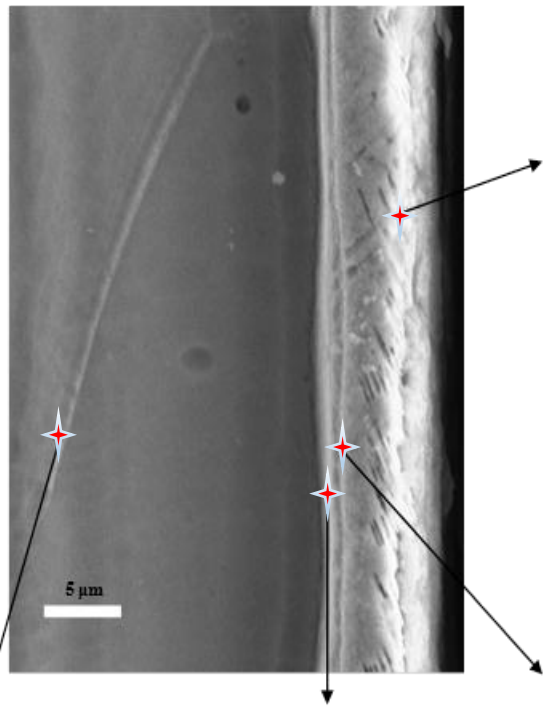

(d) Top Layer

Element	Weight%
N	4.76
C	7.87
Cr	13.82
Fe	57.82
Ni	8.66
Mo	0.85
Balance	6.22

(a) Substrate

Element	Weight%
N	-
C	0.76
Cr	17.13
Fe	67.71
Ni	9.96
Mo	1.36
Balance	3.08

(b) Bottom Layer

Element	Weight%
N	0.12
C	0.64
Cr	17.19
Fe	67.19
Ni	10.19
Mo	1.45
Balance	3.22

(c) Intermediate Layer

Element	Weight%
N	0.97
C	2.21
Cr	15.24
Fe	57.73
Ni	8.14
Mo	2.41
Balance	13.3

Figure 4.4. Details of Elemental Profile of Hybrid Treated AISI 316L at 450^{o}C.

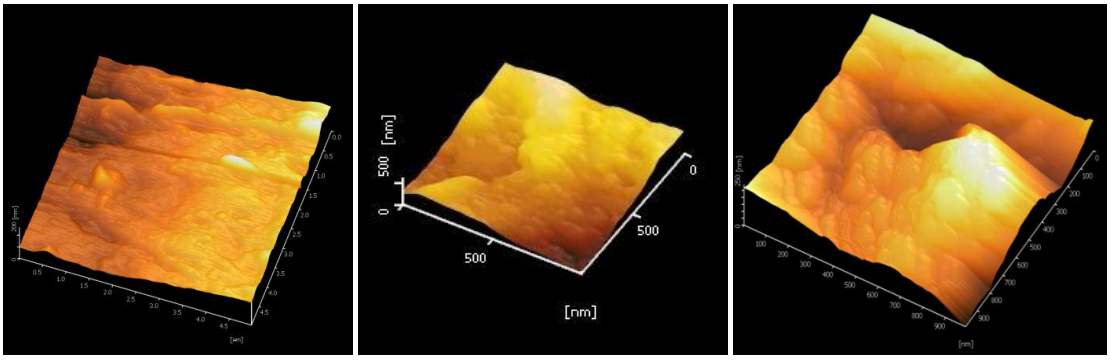

(a) (b) (c)

Figure 4.5. 3D Surface Topography resulting from USPM: (a) Hybrid 400^{o}C, (b) Hybrid 450^{o}C and (c) Hybrid 500^{o}C.

Surface topography of hybrid treated specimens from top view and cross sectional of expanded austenite were also investigated by a scanning probe microscope. The USPM observation at higher resolution of all treated surfaces shows a higher surface roughness after treatments. Meanwhile, Figure. 4.5 (a), (b), and (c) shows the 3D surface topography of the treated specimens as determined by USPM which describe high resolution image of typical grain structure.

As confirmed by cross section FESEM micrograph, it is observed that the granular structure growth of the two sub-layers as a result of nitrogen and carbon diffusion which shows the results of deposition process. The densely packed columnar structure of the two expanded austenite layers in Figure 4.5(c) correlates well with the globular surface structure observed in Figure 4.6. The presence of CrN in treated samples 316L at 500^{o}C is confirmed by XRD as in Figure 4.8.

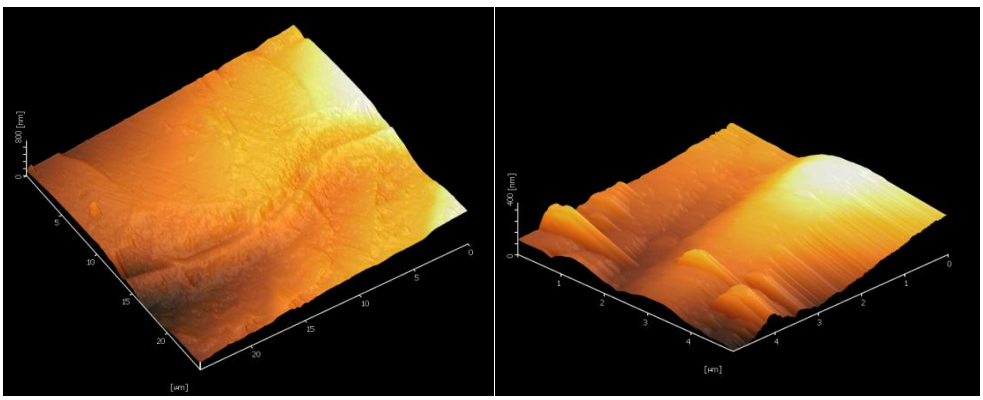

Figure 4.6. Cross-Sectioned Hybrid Treated USPM Topography.

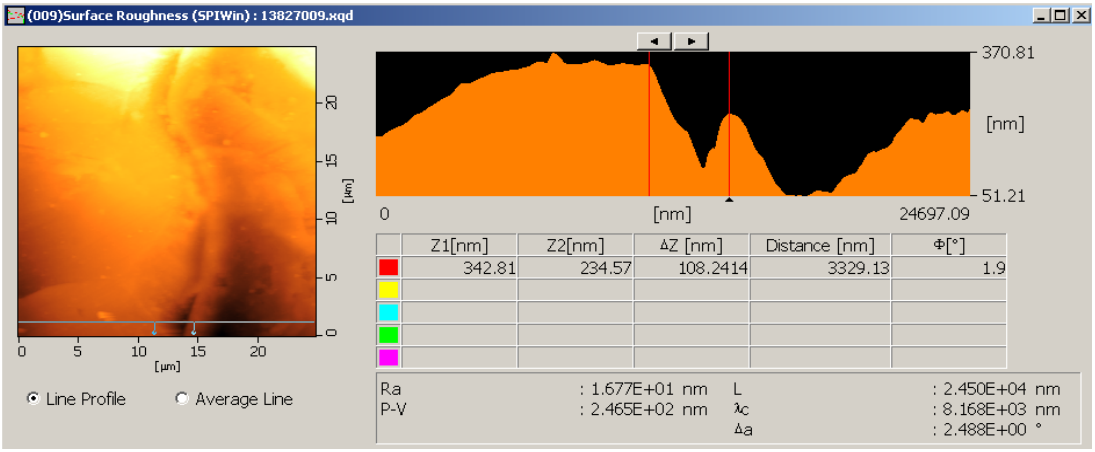

Figure 4.7. (a).

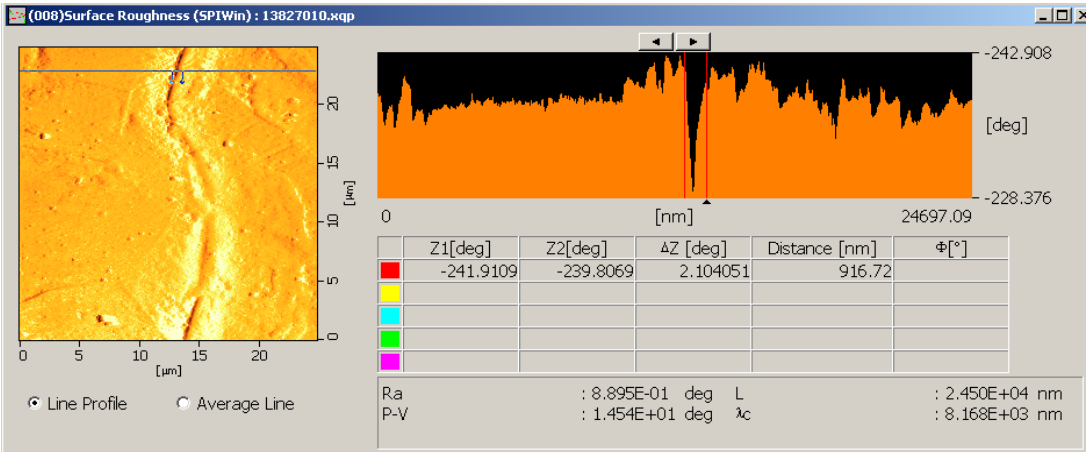

Figure 4.7. (b)

Figure 4.7. (a) and (b). Cross-Sectioned Surface Roughness of Hybrid Treated USPM Topography.

USPM examination of the cross-section reveals further details that have not been noticed before (Figure 4.7). The dual layer structure is clearly seen in Figure 4.6, which also exposes the columnar growth of the two sub-layers as a result of nitrogen and carbon diffusion. The densely packed columnar structure of the two expanded austenite layers correlates well with the globular surface structure observed in Figure 4.5. However, using the Scanning Probe Microscopy, the presence of these dual structures can be clearly seen in 3D picture, as depicted in Figure 4.6 which shows that the bottom layer consisting of γ_C structure is more deeply attacked by the Marble etchant as compared to γ_N structure of the top layer, and thus it appears darker as indicated in the picture.

4.2.2 Phase Composition and mechanical properties of expanded austenite layer

In this subsection, the phase composition of expanded austenite layers has been investigated at room temperature by X-ray diffraction method. The effect of temperature treatment on the mechanical properties of the resulting layers was also calculated to determine the optimum treatment parameters for these low temperature thermochemical treatments.

4.2.2.1 X-Ray diffraction of hybrid treated 316L

Figure 4.8 summarizes the phase compositions of the treated specimens as determined by XRD from the specimen hybrid treated at 400°C, 450°C and 500°C for 8h. As confirmed by XRD analysis in Figure 4.8, the hybrid treated surface layer comprises mainly the expanded austenite. For the hybrid process, consisting of dual layers (Figure 4.3b and Figure 4.4), reveals another thin interfacial layer. This interfacial layer is believed to be due to the accumulation of carbon as confirmed by the line scan elemental analysis. This finding is also in agreement with the literature [5].

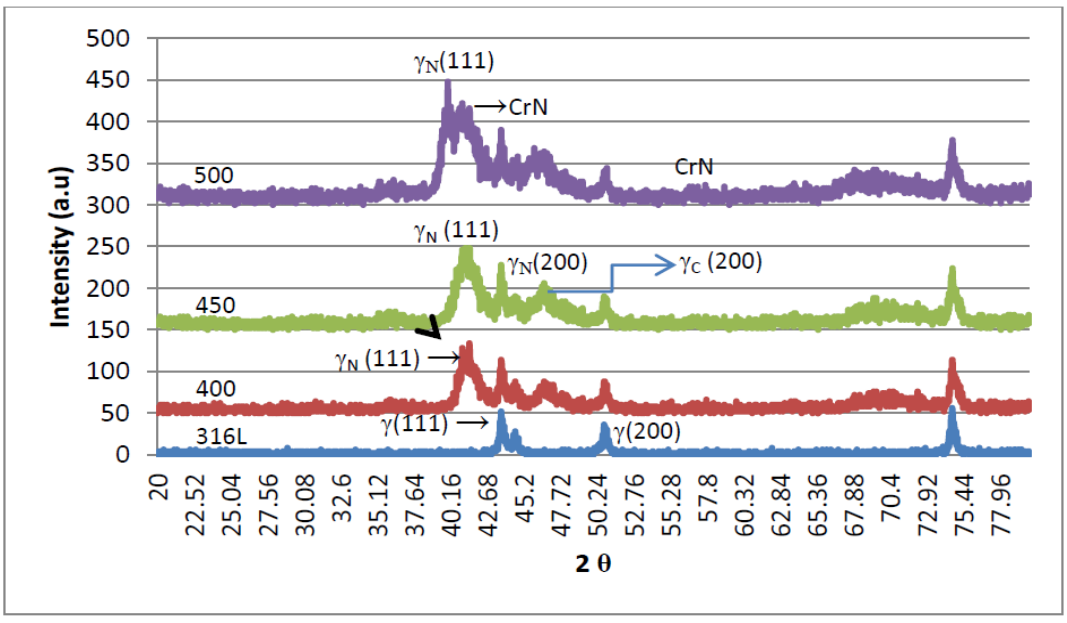

Figure 4.8. Comparison of XRD Patterns of Specimens at 400°C, 450 °C and 500°C.

One interesting aspect of the diffraction displayed in Figure 4.8 regards the variation of the (200) diffraction line width in relation with 2θ angle. This behavior can be explained by the lattice distortion caused by the greater amount of nitrogen in the interstitial sites and/or only by crystallographic orientation present in this expanded austenite [9, 112]. The XRD analysis for sample 400 and 450^{o}C does not show any peak from nitride or carbide phase.

The XRD analysis of hybrid treated layers confirmed the phase composition and layer structure as discussed in section 3.1 for various resultant layers. In the resultant layers of 500^{o}C samples, there were nitride and carbide precipitates were detectable by XRD. These results are in agreement with previous works [113-115] on individual plasma nitriding and carburizing which conclude that the formation of nitride and carbide precipitates require a higher temperature, and the temperature of 450°C does not favour the formation of these precipitates. Thermodynamically, chromium nitrides and carbides could form under this process condition. However, at this relatively low processing temperature, the rate of precipitation is sluggish such that for a short treatment period, the results of nitrided and carburized layers are precipitation-free. The significant amount of carbon or nitrogen dissolved in the layer obviously leads to the supersaturation of the austenite lattices [91].

The austenite lattice in the surface alloyed layer is expanded as evidence from the shift of the XRD peaks to lower diffraction angles as compared to the corresponding peaks from the un-treated substrate. Beside the shiftment of peaks to the lower 2θ angle, there was an anomalous phenomena due to the cubic lattice parameter calculated on γ_N(200) reflection. This reflection was significantly larger than those obtained from other reflection. This behavior was not completely understood but it was certainly related to the introduction of a massive amount of nitrogen and carbon in the austenite as investigated by previous works [20].

Based on the XRD results, a lattice expansion by 6.7% was found for the γ_N phase and 3% for the γ_C phase in the present work. The position of the peaks depends on the temperature of the treatment and a slight shift towards lower 2θ angles observed for the samples of thermochemical treatments in comparison with untreated sample. The

larger amount of nitrogen incorporated in this layer is dissolved in the austenite lattice, causing lattice expansion.

The lattice constant calculated from the *d*-spacing for the (200) plane is higher than the lattice constant calculated by the *d*-spacing of the (111) plane. The lattice parameter of the γ_N phase increases with nitrogen concentration and can be as large as 0.390 nm, as compared to 0.358 nm for face-centre cubic austenite of the substrate. This registers a lattice expansion by nearly 7%, which causes significant hardening effect and induces many structural disorders in the treated layer as describes in Table 4.2, such as stacking faults, dislocations and residual stresses as reported by previous investigators [6].

Table 4.2: Lattice Expansion Measured on Expanded Austenite from XRD Peak Shift for Hybrid Specimens at 400^{o}C, 450^{o}C and 500^{o}C.

Treatment	**Expanded austenite lattice expansion**
Substrate 316L	-
Hybrid 400	4.8%
Hybrid 450	5.4%
Hybrid 500	6.7%

The equation $\Delta a/a$ refers to the relative difference in lattice spacing as well as lattice expansion which is derived by O. Öztürk [116].

$$\Delta a/a = [\{a(\gamma_N) - a(\gamma)\}/a(\gamma)]. \quad (4.5)$$

or

$$\%\exp = \left(\frac{a(hkl) - 3.5911}{3.5911}\right) x100 \quad (4.6)$$

where 3.5911 is the standard austenite lattice parameter according to JCPDS 33-0397.

The interplanar spacing *d(hkl)* was calculated by Bragg's law. The lattice parameter calculation of the new phase γ_N and γ_C could be detimined. As described in Table 4.2, the lattice expansion in hybrid layers at 400°C is about 5%, as compared to 5.4 % at 450°C. On the other hand, the lattice expansion in hybrid 500°C is 6.7%.

4.2.2.2 Interstitial Diffusion

The nitrogen and/or carbon diffusion in austenitic steels occurs by a trapping and de-trapping mechanism driven by chromium sites in the austenitic structure. As a shown in Figure 4.4, it presents the separation of the nitrogen and carbon in the chemical profiles as discussed previously is due to a phenomenon in diffusion called trapping and de-trapping explained by Parascandola et al. [117].

During a hybrid treatment, both carbon and nitrogen are introduced in the surface at the same time. Both carbon and nitrogen, occupy the interstitial sites of the host material. A material like austenitic stainless steel has a number of interstitial sites which are considered to be trap sites due to the proximity of chromium atoms to these positions. Nitrogen has a higher affinity to chromium when compared to carbon, and therefore nitrogen always fills up these trapping sites. If a carbon atom gets trapped in one of these sites, it is always de-trapped and is replaced by nitrogen if nitrogen is still in diffusion. Once all the trapping sites are filled up, the rest of the interstitial elements diffuse more rapidly through the material. Since all the trapping sites are occupied with nitrogen, the carbon moves ahead occupying new, as-yet unoccupied trapping sites. It is then de-trapped immediately as more nitrogen moves inwards. This combination of trapping and de-trapping is the reason why carbon always diffuses more rapidly and always found ahead of the nitriding front in the material.

According to the results in Figure 4.3, it describes that elemental profile of carbon across the hybrid treated layer was obtained by EDS-SEM to reveal the push-in effect of dissolved carbon by nitrogen. As expected, the hybrid treatment resulted in the formation of a dual layer structure with a thick nitrogen expanded austenite (γ_N) occupying the outer layer zone and a thinner carbon expanded austenite (γ_C) occupying the inner layer zone. Although not clearly revealed in the present micrograph, this separation of dual structure is observable under optical microscope. The carbon profile across the hybrid dual layer is given in Figure 4.3.

A high carbon peak was detected at the inner layer, thus proving the push-in effect of dissolved carbon by nitrogen during the hybrid process. The only easy path for carbon is to diffuse further into the substrate, thus forming a push-in effect of carbon by nitrogen and a separate carbon expanded austenite layer. The push-in effect still

prevailed, which would lead to the formation of a dual layer structure. But since there was no more carbon supply during the nitriding cycle, the carbon atoms which are pushed to the nitriding front still continued to diffuse into the substrate, leading to the gradual leveling off of the carbon concentration and thus the diminish of the carburized layer. This condition agrees with previous woks in [5]. Other possibility could be due to the decarburization of the carburized layer during the early stage of the subsequent nitriding cycle, which would lead to a reduction in the carbon expanded austenite (γ_C) layer thickness.

As described in section 4.2.2.1, the XRD patterns for the treated and untreated materials are very similar except the reflection peaks from the expanded austenite layer shifted to lower angles when compared to the corresponding austenite FCC peaks. The peak shifting is an indication that the lattice of FCC austenite was expanded and thus, it is stressed. The larger the peak shifting the more the layer is expanded and stressed. The peaks of the 450°C hybrid layers are at a point between the corresponding peaks for both 400°C and 500°C samples. It seems that the diffusion of nitrogen was probably hindered by carbon atoms which are already occupied interstitial sites.

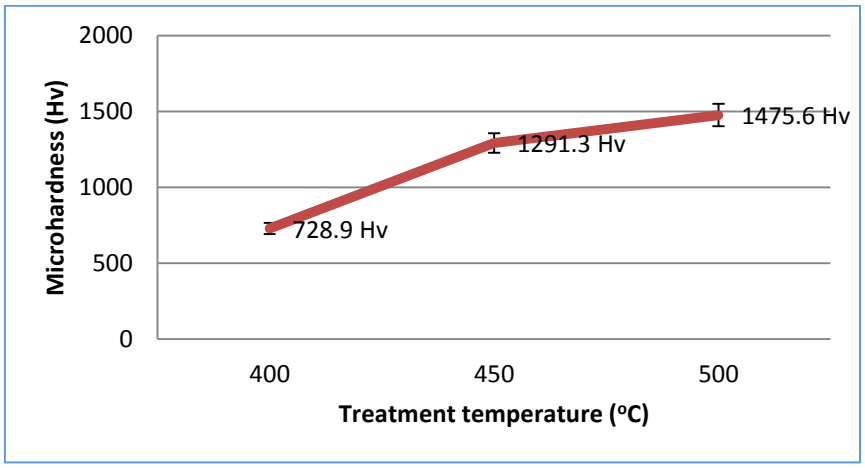

Figure 4.9. Micro Hardness Data as Function of Hybrid Treated Temperature.

4.2.2.3 Hardness measurements

Figure 4.9 shows the depth profiles for hybrid thermochemically hardened stainless steel which typically give a trend of increasing depth with higher temperatures and

longer process variations. Microhardness test was performed to determine the characteristics of each specimen under the influence of the treatment. The tests were conducted to the samples start from the surface and along on the cross section of the treated samples (400^{o}C, 450^{o}C and 500^{o}C). The load used was 10 gf and the dwell time was 15s. Therefore, the data collected for the un-treated and treated samples was tabulated in Table 4.3. Moreover, the surface microhardness of treated layers as a function of temperature is shown in Figure 4.9. The surface micro hardness value of the sample hybrid at 400^{o}C was 728.9 HV showing 3.3 times as the surface microhardness of the untreated sample (220.0 HV). For the sample nitrided at 450^{o}C, the surface microhardness value was 1291.3 HV, which was about 5.9 times harder than that of the untreated sample.

Table 4.3: Microhardness Data of Untreated Sample and Hybrid Treated Samples.

Distance of indentations from the surface (µm)	**Vickers Hardness (HV)**			
	Untreated	400^{o}C	450^{o}C	500^{o}C
2	220.0	728.9	1291.3	1475.6
4	200.7	721.2	1225.9	1453.7
6	190.5	700.4	1255.4	1469.3
8	180.7	301.4	892.2	1458.1
10	198.1	220.02	620.2	1442.2
12	215.1	321.3	300.3	1288.1
14	198.9	220.6	290.1	1072.6
16	212.8	215.3	238.6	819.8
18	182.0	208.8	254.1	744.7
20	204.8	198.1	250.6	692.7
25	185.0	209.03	253.5	407
30	220.0	211.4	239.7	367.5
35	210.1	206.7	228.9	254.8
40	216.0	208.6	236.5	253.6
45	224.4	211.7	227.1	260.7
50	204.4	203.2	226.06	225.3

The result from Table 4.3 is agreed with previous work [14] where the hardness depth profile is related to the carbon content in intermediate range which effectively bridges the mismatch between high nitrogen surface and the austenite substrate.

The transition from a very hard surface which has high interstitial contents/lattice dilatation to soft substrate occurs smoothly. Finally, the hybrid layer possesses the most favorable hardness distribution: the surface hardness is as high as that of the hybrid treated layer, and the hardness decreases gradually towards the layer/core interface. Such a gentle hardness gradient in the dual layer from hybrid process is expected to be beneficial in achieving enhanced tribological and load bearing properties [10, 114].

The highest hardness value (1475.6 HV) for this investigation is obtained in the sample hybrid at 500^{o}C. This high surface microhardness value on 500^{o}C may be related to the presence of hard chromium nitride/carbide precipitates in the hybrid layer [20]. The microhardness profiles of the samples untreated and hybrid at 400^{o}C, 450^{o}C, and 500°C are shown in Figure 4.10.

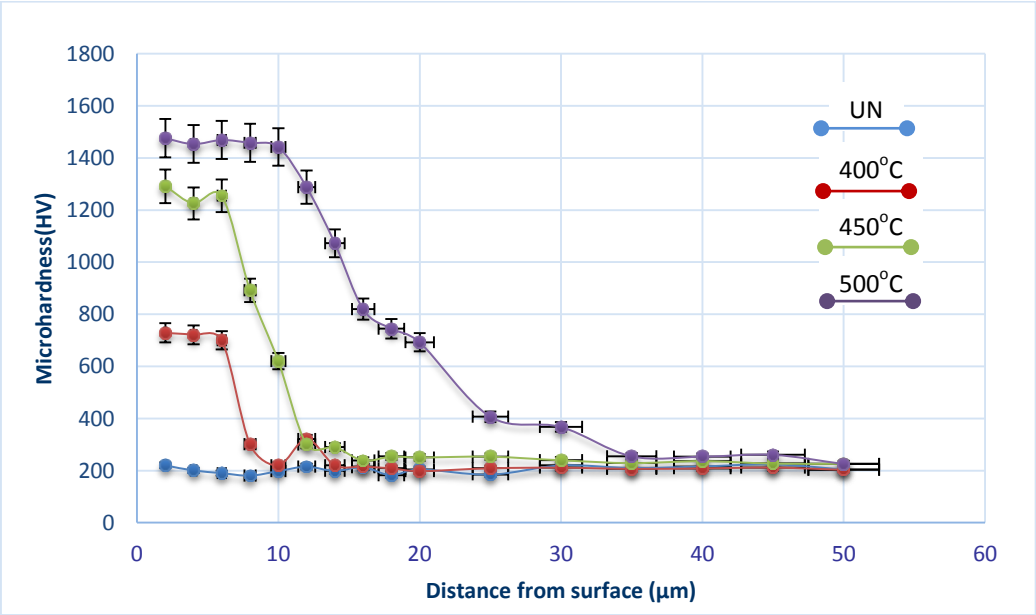

Figure 4.10. Microhardness Profiles of Untreated−Treated Samples vs Temperature.

All the hybrid samples were found to be harder that the untreated samples. A 6µm hardened layer with hardness around 720 HV was achieved on the sample treated at 400°C. As hybrid temperature increased, higher hardness values and thicker hardened layers were obtained. For the sample hybrid at 500°C, the microhardness value (400-1500 HV) remained higher than the untreated sample throughout the thicker hardened layer (about 30µm). The microhardness profile shows that the treatment temperature influences the hardness of the hybrid samples. The effectiveness of the treatment to increase the hardness of the steel was verified. On the other hand, the hardness of the hybrid samples maintained at a high level and at a certain distance, it decreased gradually from modified layer to the metal core.

The type of indentation marks was shown in Figure 4.11 (a) and (b) which describes the size of indentation at different layers using different hardness test equipment.

Based on the hardness level that achieved, treated samples at 400^{o}C, 450^{o}C and 500^{o}C were increased respectively, but only treated at 450^{o}C is preferable in corrosive media as described in the next section.

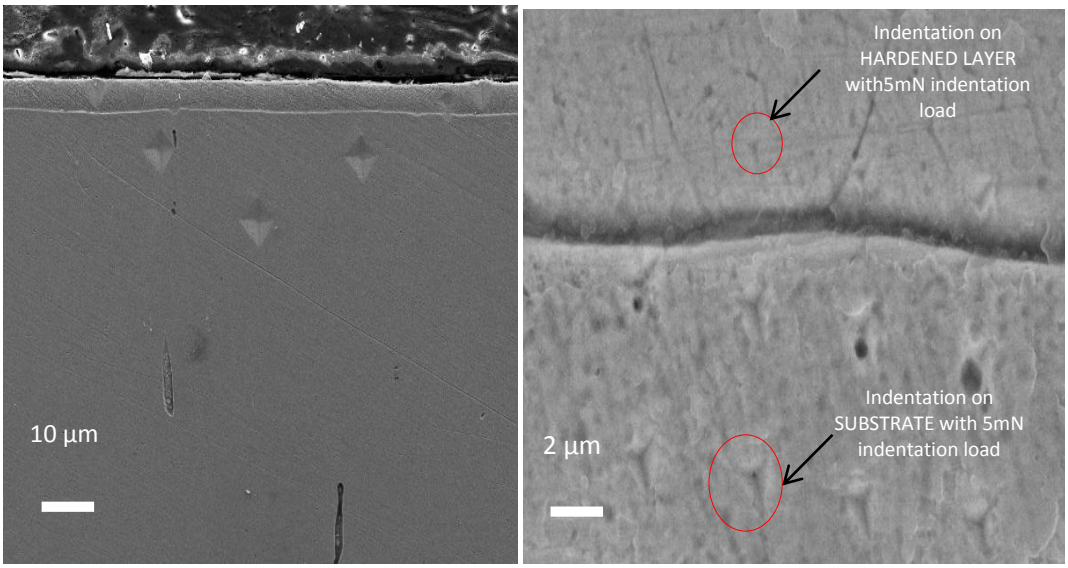

(a) (b)

Figure 4.11. Microhardness Indentation of hybrid treated sample
(a) Vickers and (b) Nanoindentation.

4.2.2.4 Effect of treatment temperature on the wear resistance of hybrid treated layer

For UN sample, the large plastic deformation is obviously observed on the worn region which is shown in Figure 4.12 (a) and (b). The morphology of the worn region for UN sample also showed suffered heavy scars and plate-like wear debris which identified as galling. These were occurs due to tearing and local plastic deformation. The thick and continuous debris layer were explain that the wear severely occurred on the sample by abrasive mechanism, while the plate-like wear debris are due to the adhesion wear mechanism, where the material or wear debris (particles) transferred on the surface and would then be plastically deformed and compacted by the rubbing action between the slider and the disc [63].

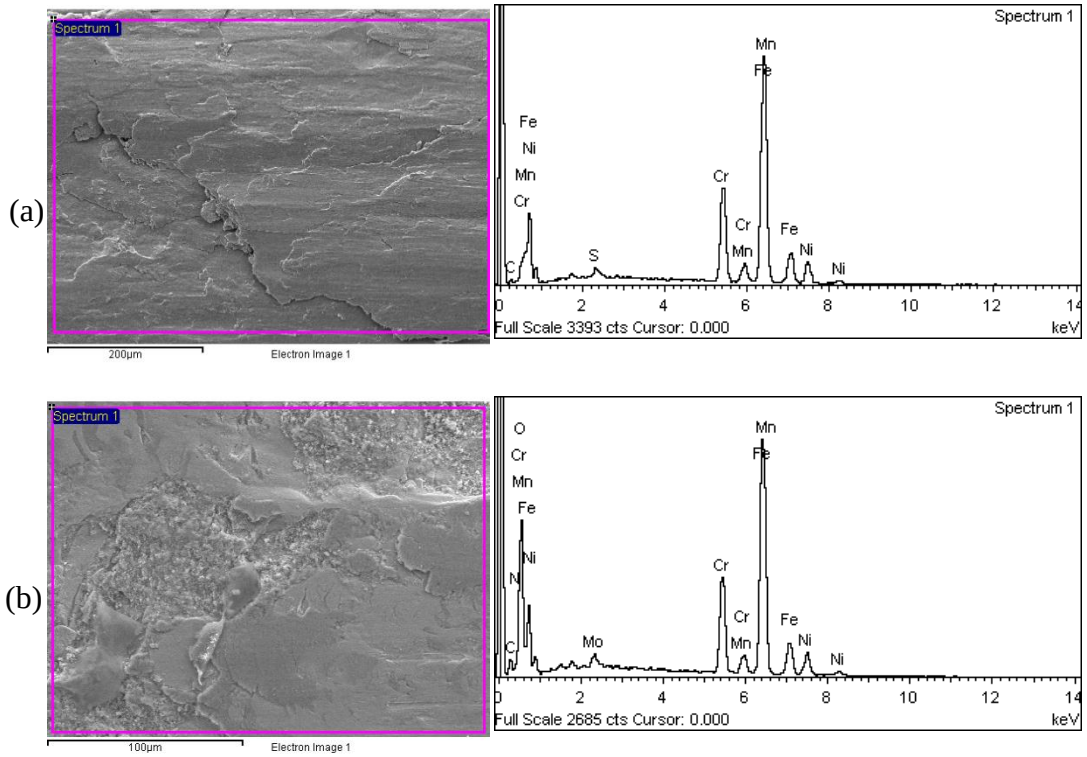

Figure 4.12 (a) Worn Morphology Untreated 316L,
(b) Worn Morphology for 400^{o}C Sample

The morphology characteristic of sample 400 could be obviously seen to be less worn and the shallow plow built up on the surface. This indicates that abrasive wear also experienced on the sample but not severely compared to untreated sample.

The structure seems that the mechanism occurred is slight abrasive wear. The spot taken on the surface digging clearly had shown the abrasion of the samples. This is the characteristic of treated steel where only abrasive mechanism dominates the wear process [118, 119].

The thicker continuous debris layer formed on this sample combining with protective oxide layer prevent from intimate contact and adhesion on the surface. This is why only abrasive mechanism took place. From the image of wear track obtained on these sample show that there was some crack occurred on the worn region. However, as shown in the Figure 4.12 (a) and 4.12 (b) the mechanism of the abrasive and adhesive wear still took place on the sample slightly compared to untreated sample.

In Figure 4.13 (a), the worn region morphology for 450^{o}C sample is observable with several surface digging and also with narrower and superficial wear track [63, 120].

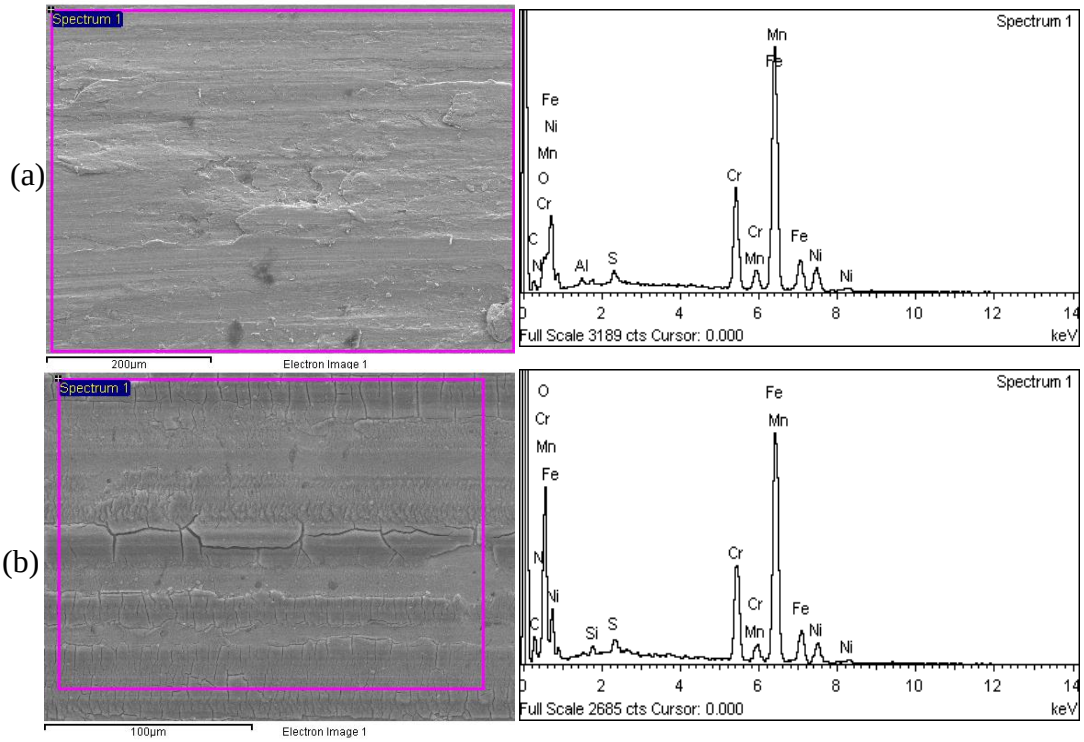

Figure 4.13. (a) Worn Morphology for 450^{o}C Sample,
(b) Worn Morphology for 500^{o}C Sample.

Table 4.4 shows the element compositions analysis using EDX method for worn surfaces on flat specimens. For comparison purposes, the unworn surface was used accordingly.

Table 4.4: EDX Analysis (Mass%) of Worn Surface for Three Test Temperatures.

Temp (^{o}C)	O	Mn	Cr	Ni	N	Mo	S	Si	C	Al	Fe
(Unworn)	-	1.53	17.02	10.05	0.94	2.00	0.03	0.048	0.03	0.75	50.82
Untreated	11.66	1.49	16.94	10.01	0.94	1.98	0.55	0.21	4.84	0.81	50.57
400	18.45	1.17	12.81	6.96	0.94	1.95	0.53	0.19	4.17	0.76	50.82
450	9.89	1.60	15.26	8.62	0.81	1.93	0.83	0.32	8.79	0.70	51.21
500	14.91	1.06	10.52	9.90	0.39	1.97	0.66	0.37	9.46	0.85	49.81

Based on the analysis, the oxide was always presence on all of the specimens. As shown in Figure 4.12 (a), the thick continuous debris layers which represent low wear resistance were found on untreated samples where highest chromium content exist. Besides that, the Iron and chromium elements were also identified within the oxide.

The rise of carbon content from EDX data of unworn to 500^{o}C samples as well as Molybdenum for 400^{o}C may come from the material transfer of pin to the sample. For treated samples, the compacted wear debris was also found with high oxide content which represent higher wear resistance as shown in SEM micrograph Figure 4.13 (a) and 4.13 (b).

The indication of material transfer was related to the increase of specific element from wear debris production which controls the wear condition as well as the debris morphology on load-bearing wear. However, EDX does not reveal the type of oxides present within the oxide of the wear debris. The interchanging the alloying elements mechanism need further studies

Relation of the coefficient of friction vs time was shown in Figure 4.14. This figure shows the comparison results of coefficient of friction vs. time profile, untreated 316L sample yield the highest coefficient of friction, which averagely ranging from 1.4-2.0. Then, the coefficient of friction followed by the sample of 400 with 0.8-1.4, 450 with 0.6-0.8 and 500 0.3-0.5 hybrid treated steel.

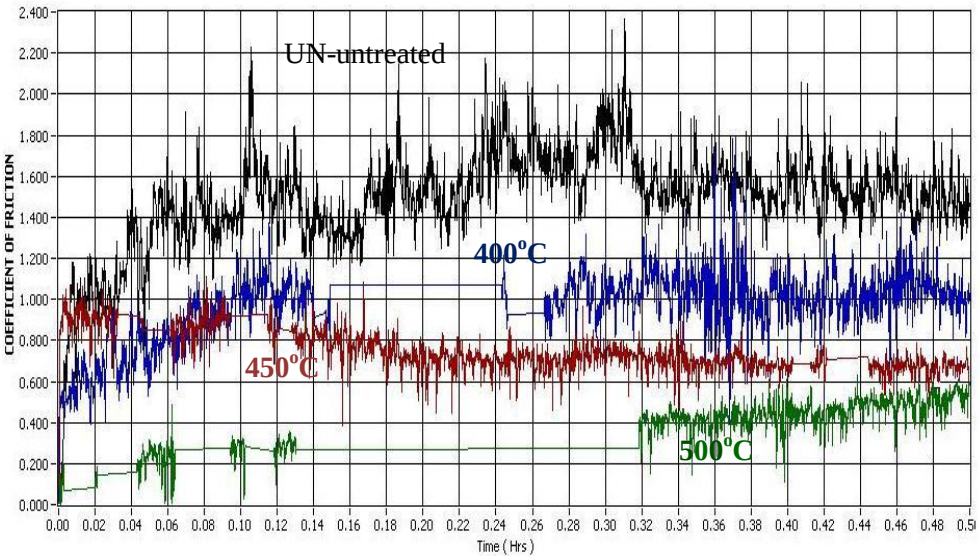

Figure 4.14. Coefficient of Friction vs. Time Profile for Untreated, 400°C to 500°C.

Theoretically, lowest coefficient of friction gives highest wear resistance during wear mechanism on the surface. The presence of hybrid treated layer on the samples of 400, 450 and 500 could be explained that the formation of hybrid layer provide a convenient support to the substrate, which may introduce an increasing of wear resistance [115]. According to investigation by [117] formation of nitrided layer on steels is increased in thickness as the time of nitriding treatment is extended. This is the reason why the sample of 500 achieved high wear resistance.

4.2.2.5 Effect of treatment temperature on nanoindentation results

The NanoTest 600 instrument was used to perform continuous depth vs. load measurements on a treated specimen. The surface treated layers thickness was approximately 5 µm and the substrate material was austenitic stainless steel AISI 316L. Experimental parameters were controlled, loading rate 3.99 mN/s, maximum load 300 mN, maximum depth 200 nm, dwelling time at maximum load 5 second. Maximum load of 300 mN used to demonstrate the necessity of using shallow indentations. To preclude substrate influences with a hard layer on softer substrate, the indentation depth should not exceed approximately 10% of the film thickness.

Figure 4.15 shows the areas which consist of substrate, interface and harden layer respectively after measured by Depth-Sensing Indentations with maximum loads 300 mN and maximum depth was 200 nm.

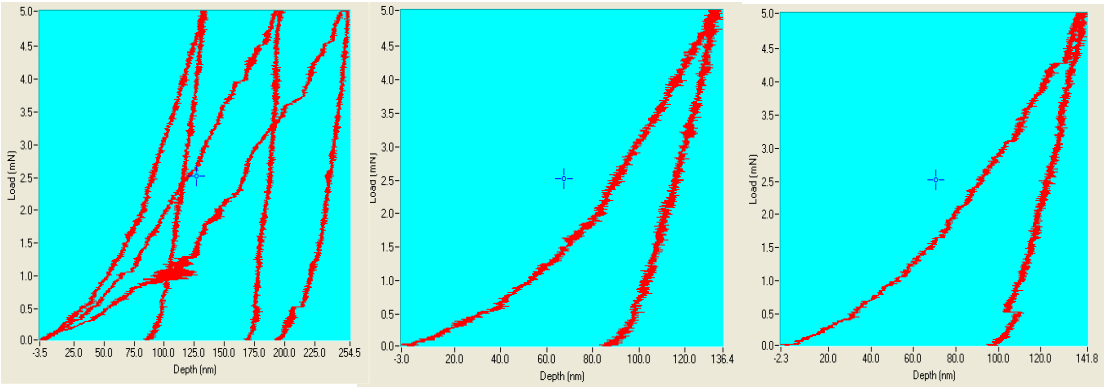

(a) (b) (c)

Figure 4.15. Depth-Sensing Indentations Performed on: a) Hybrid Treated Layer, b) Hybrid 500^{o}C, (c) Hybrid 400^{o}C.

The hardness and elastic modulus values have been extracted from the elastic unloading curves according to the equivalent indenter method. Performed in the same conditions, regular arrays of 6 x 6 indentations covering a 24.32 x 21.89 μm^2 area were realized in order to probe about three different areas as described in Figure 4.17 from different samples which consist of substrate, interface and harden layer. Depth sensing indentations curves from different hybrid treated layer is shown in Figure 4.15.

The nanoindentation tests on AISI 316L untreated and hybrid treated samples has confirmed a considerable increase in hardness 4 to 5 order and a small rise in the elastic modulus of the material after the hybrid thermochemical treatments as describe in Table 4.5.

The curves in Figure 4.15 has shown that there was an agreement with previous investigation which explained the resilience and toughness of the material are of significant importance, and the ratio of hardness to elastic modulus has been reported to be a more appropriate index than the mere hardness, to rank the wear resistance [67, 89].

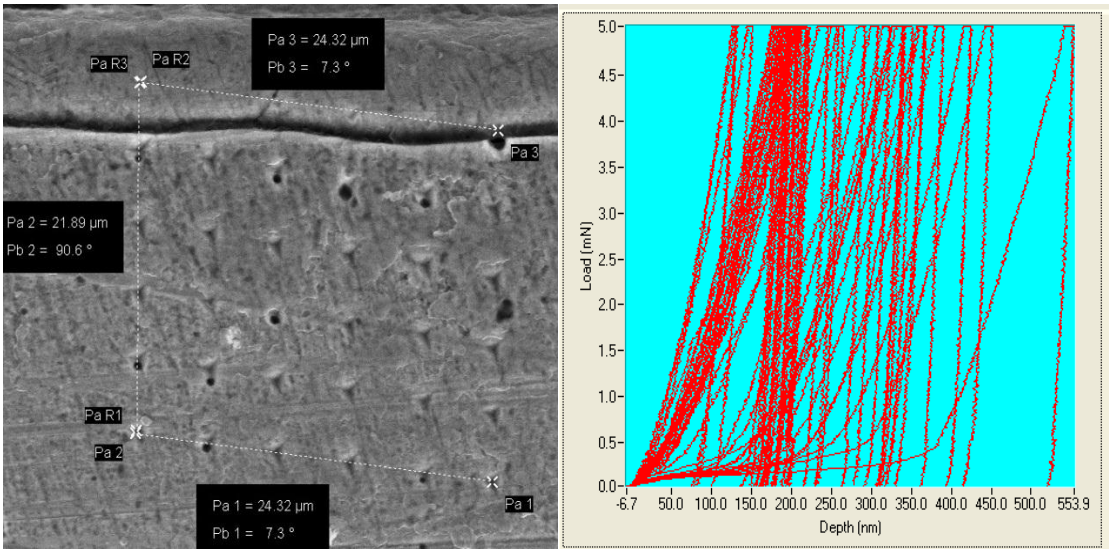

Figure 4.16. Hardness Mapping for Regular Arrays of 6 × 6 Indentations on 450^{o}C Sample.

Additional quantitative information concerning microstructure can be achieved by hardness mapping presented by Figure 4.16. The harden layer of the expanded austenite around the site of the local hardness was substantially higher than the surrounding matrix based on the grid of nanoindents. The curve of hardness maps indicates that some grain boundaries also confirm signs of local hardening [123].

Figure 4.16 determines the two phases with different hardness trend which is resulting from nanoindentation measurement between substrate and hardened layer. The hardness changes vs. depth within a grain is related to the nitrogen/carbon concentration and the large hardness distribution observed at a depth about 25 µm is the consequence of the orientation-dependent nitrogen/carbon diffusion which has an agreement with previous work with respect to the changes of compressive stress, lattice expansion and elemental profiles resulting from interstitial diffusion and topography analysis [124].

Moreover, Figure 4.3 and Figure 4.4 show that the hybrid treated layer are not homogeneous and the elastic modulus evolutions against the depth in Figure 4.16 may be related to the nitrogen concentration profile. Further interpretation would thus require a better knowledge of local nitrogen and/or carbon profiles within the grains.

Table 4.5: Roughness, Indentation Hardness and Elastic Modulus for Each Hybrid Treatment.

Treatment (^{o}C)	Roughness, Ra (µm)	Layer thickness (µm)	Hardness (GPa)	Elastic Modulus (GPa)	E/H
Untreated	0.12	-	2 ± 0.2	210 ± 2	97.22
Hybrid 400^{o}C	0.22	3.421	7.892 ± 0.7	167.518 ± 4.2	21.226
Hybrid 450^{o}C	0.28	6.425	8.471 ± 0.5	173.64 ± 3.1	20.50
Hybrid 500^{o}C	0.36	26.425	13 ± 0.5	220 ± 5	16.26

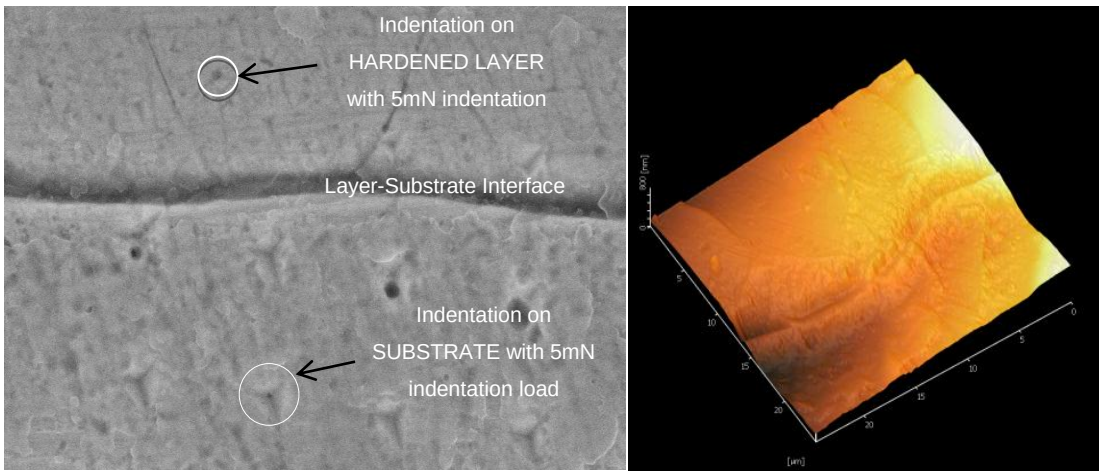

(a) (b)

Figure 4.17. (a) Depth-sensing Indentations on Hardened Layer of 450^{o}C sample and (b) its cross sectional topography

Furthermore, USPM and SEM micrograph in Figure 4.17 has shown the measurement on the surface roughness which is defined in Table 4.5. The table has describes the effect of temperature and the level of surface roughness of treated materials. The hybrid treated surfaces became rougher with respect to the treatment temperature. Comparing to as-polished 316L surface, the average roughness of the hybrid treated surfaces increased about 3 times with the increasing treatment temperature. The main reason for the roughness development is due to the different expansions rates of differently oriented grains during the treatment, which is agree with previous investigation [95]. Also, it is believed that the compressive stresses might contribute to the roughness increase of the treated surfaces. Observation with

higher magnification on Figure 4.17 shows that indentation size on substrate is bigger than indentation on hardened layer which indicating that the hardened layer has higher hardness level than substrate which shows an agreement with previous work [70, 125].

Recent findings as shown in Table 4.5 describes that the high nitrogen and/or carbon contents in the layers resulting from deposition process was related to the increase of the surface roughness. Based on the investigation by Randall et al, the high surface roughness is comparable with the best tribological performances where it attributable to the combinations of high surface hardness and relatively low elastic modulus [89]. As a result, this argument was confirmed the reduction of tendency to plastic deformation and also reduces the mismatch of properties and keeping deformation within the elastic range.

4.2.3. Corrosion resistance performance of expanded austenite layers

Thermochemical treatment as a class of processes when performed above the nitride/carbide formation temperatures generally decreases the corrosion resistance of stainless steels. Hybrid treatment of austenitic stainless steel at elevated temperatures, typically above 450^{o}C, increased the surface hardness of the steel, but led to significant loss of its corrosion resistance due to the sensitization effect [119].

Thus, an experiment has been performed by the author to investigate and analyze this problem. The corrosion resistance of un-treated 316L austenitic stainless steel and treated 316L austenitic stainless steels at 400^{o}C, 450^{o}C and 500^{o}C was evaluated by measuring polarization curves in 3.5% NaCl solution as shown in Figure 4.18. The flat cell which is a three-electrode set-up consists of the specimen as the working electrode, a silver chloride (AgCl) as the reference electrode, and a platinum electrode used as the auxiliary electrode. The area exposed to the solution was 0.35 cm^{2}. The scanning potential was in the range of −0.8 to 1.2 V, and the scan rate was 1 mV/s.

The potentiodynamic curves of anodic polarization of samples un-treated and hybrid treated at 400^{o}C, 450^{o}C and 500^{o}C in 3.5% NaCl solution were presented in Figure 4.18. It can be seen that the current density for the untreated 316L steel initially is low, but it rapidly increases to high values at a potential of around -0.45 V.

It is well known that this sudden increase in current density is caused by the ‘‘break-through’’ of the passive film on stainless steel surface.

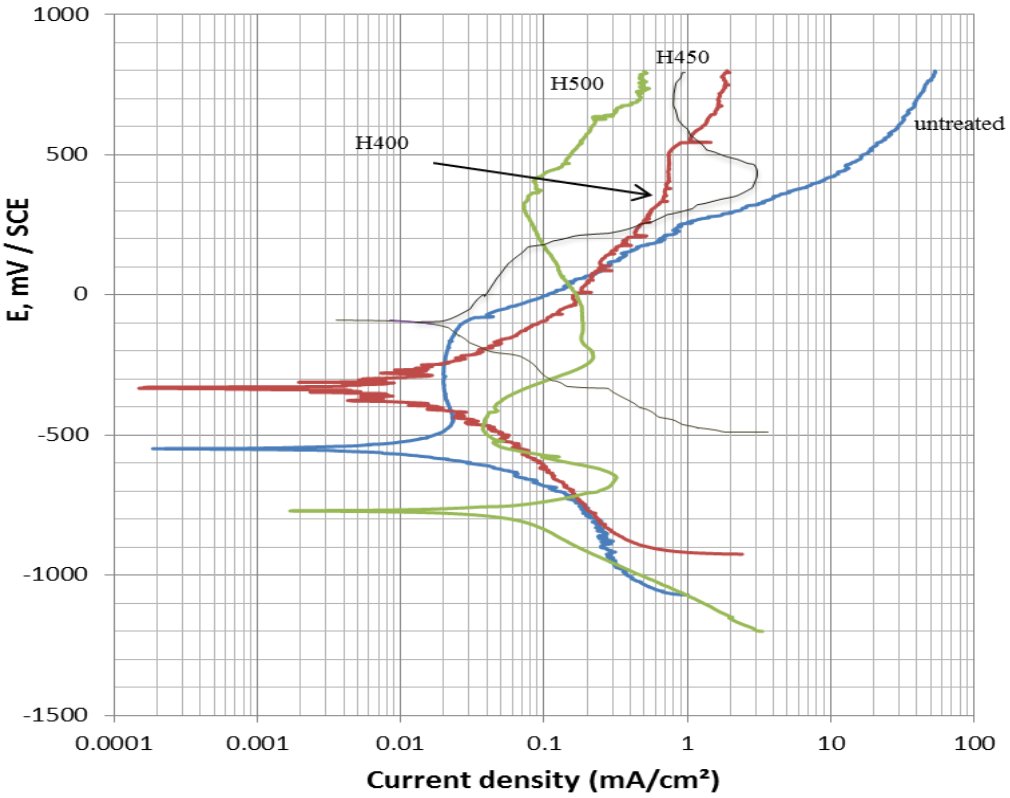

Figure 4.18. Polarization Curve for Hybrid Treated compared to Untreated 316L.

Table 4.6: Results of Corrosion Resistance Test on treated AISI 316L Stainless Steel in 3.5% wt.% NaCl Solution.

	Untreated	Hybrid 400°C	Hybrid 450°C	Hybrid 500°C
E_{corr}(mV)	-544.34	-330.22	-99.42	-775.01
I_{corr} (mA/cm^2)	0.022	0.009	0.014	0.068

From Figure 4.18 and Table 4.6, hybrid treating at a low temperature (400°C) has changed the polarization properties of the 316L steel and also, shifted the corrosion potential (Ecorr) to a higher value, from -544.34 mV (for untreated) to -330.22 mV (for treated at 400°C). Besides, the current density of the steel is reduced, from 0.022

mA/cm^2 (for untreated) to 0.009 mA/cm^2 (for hybrid at 400^oC), demonstrated an improvement in corrosion resistance.

This result displays an enhancement in corrosion resistance by several orders of magnitude and indicates the excellent corrosion resistance of the hybrid sample at 400^oC as compared to that for the untreated sample. The much enhanced corrosion resistance observed for the hybrid sample at 450^oC may be attributed to the supersaturation of the upper part of the nitrogen and/or carbon-enriched layer without precipitation of chromium nitride/carbide. Thus, chromium is retained in solid solution for corrosion protection [8, 120]. Moreover, the enhancement of its corrosion resistance may be related with the layer formed at 450^oC has new phase composition, containing a new type of expanded austenite. This layer would contribute to the observed higher hardness and better corrosion resistance as compared to untreated sample [126].

It is generally believed that hybrid at such a high temperature of 500^oC would adversely affect the corrosion resistance of austenitic stainless steel, so that after hybrid treating, the steel will lose its ‘‘stainless’’ feature. Based on the results in Figure 4.16 and Table 4.6, the corrosion potential (Ecorr) of treated sample at 500^oC was moved to -775.01 mV, and the corrosion density (Icorr), 0.068 mA/cm^2, obviously higher than the untreated sample.

These results indicated that the corrosion resistance of the hybrid sample at 500^oC is reduced as compared with the untreated sample. This behavior was mainly due to the formation of CrN in the compound layer. This effect leads to depletion of chromium from the adjacent matrix and consequently unable to produce Cr_2O_3 passive layer to make stainless feature. Therefore, the corrosion resistance property of the stainless steel is reduced [119].

For all the treated steels, anodic currents after hybrid treatments were higher than those for untreated steels (disregarding currents above E_{corr}), except for treated at 500^oC. This may suggest that the high resistance to pitting of low-temperature hybrid treated steels might be in some way associated with their increased general reactivity which is agree with previous investigation [127].

CHAPTER 5

CONCLUSIONS

5.1 Conclusions

The main objective of this experimental research was to develop a novel hybrid surface harden layer on AISI 316L using conventional tube furnace at low temperature, which have improved hardness as well as wear resistance without impairing its corrosion resistance even improving it.

This objective was achieved by determining the optimum hybrid treatment parameters to produce surface harden expanded austenite layers. The near-surface region characteristics were systematically studied. The anodic polarization was investigated to determine the effect of temperatures to the corrosion resistance performance of expanded austenite in corrosive environment. Nanoindentation and wear tests were conducted to quantify the mapping of mechanical properties, such as hardness and elastic modulus of the expanded austenite. The microstructure and topography of hybrid treated layers were also investigated using FESEM and USPM.

The following conclusions were derived based on the objectives set for this research:

- Appropriate and optimized treatment parameters for hybrid hence microstructural tailoring, improved mechanical properties in AISI 316L were achieved. Systematically, the result showed a composition of expanded austenite which responsible for highly required better mechanical properties without impairing its corrosion resistance. The HCl activation in recent work has been demonstrated as a successful method to remove the passivating oxide layer for gaseous hybrid treatment. Besides that, the use of hydrocarbon gas in recent work by using methane addition in ammonia atmosphere would produce transient cyanide groups that remove the Cr_2O_3 barrier film on stainless steels.
- The investigation of surface characteristics of harden layer show that

Metallographic examination revealed that treatment at 400°C for times up to 8h could not produce a continuous expanded austenite layer on the specimen surface. When temperature was to 450°C, a uniform layer was formed on the surface. Increasing the temperature to 500°C resulted in the formation of a relatively thick treated layer after 8 h treatment. Some dark phases were formed in the layers, particularly in the upper part of the layer can be attributed to the formation of chromium nitrides/carbides. In terms of Microhardness measurements on the as-treated surfaces as a function of processing of the three temperatures. Nanoindentation tests reveal a lower elastic modulus and hardness for untreated compared to the treated samples where the later have enhance E/H ratio exhibit the decreasing tendency to plastic deformation, while keeping deformation within the elastic range. With regards structural/elemental analysis and, hardness measurement indicate that under the present treatment conditions, there exists a good correlation of treating reactions with the improvement of hardness level from 200 from untreated sample to 1475 Hv. As confirmed by XRD, this treated layer comprises mainly the expanded austenite. Below this main layer, a thin interfacial layer is evident, which is believed to be due to the accumulation of carbon in this interfacial region.

- The performance assessments were generally fulfilled with hybrid treatments. Wear test results correlate well with the hardness test results and confirm the improvement in wear resistance of the specimens after the treatments. The poor wear resistance of lowest temperature treatment seems to be correlated with its thin layer formation and its ragged surface morphology. The polarization curves measured for selected specimens. The polarization behavior of the untreated AISI 316L steel is as expected, and is characterized by a well-defined passive region from the corrosion potential to +40 mV (SCE). Some film breakdown occurs at this potential followed by partial reformation. From all these treatments, the best corrosion resistance was achieved by treatment at 450^{o}C. Therefore, the sample treated at 450^{o}C was the best corrosion resistance for corrosive environments. In term of hardness and wear resistance, treated samples at 400^{o}C and 500^{o}C can be considered but it is not preferable in corrosive media.

5.2 Recommendations for future works

For future consideration and following up of this research, additional work should be done to further investigate and improve the mechanical properties of the composite.

- A separate work for the modeling or analysis or prediction of performance of the hybrid treated produced in service may be proposed to compare the results with the experimental work here in this research.
- The identification to obtain optimum parameter for generating expanded austenite on 316L in this investigation was achieved at 450^{o}C, where the high level hardness and wear resistance were achieved without impairing its corrosion resistance. On the other hand, the hard-thick layer of the hybrid treatment at 500^{o}C has higher level of load bearing capacity and toughness but it impairing the corrosion resistance. Further improvement and more inderstanding of process design on heat treatment of stainless steels to achieve hard-thick precipitation free would give significant contribution with accurate and easy method for monitoring the microstructure evolution as demanded in industrial application.
- Recently, the use of surface treated AISI 316L is getting in demand not only in friction materials parts but also in medical applications and electronic consuming devices such as housing for Iphone5. With this observation, further study may be done in testing the expanded austenite layers for the application in many other fields.

REFERENCES

[1] Hsu, K.-L., Ahn, T. M. and Rigney, D. A.: *Friction, wear and microstructure of unlubricated austenitic stainless steels*, Wear (1980) **60**, *1*, 13-27

[2] K. Ichii, K. Fujimura and T. Takase, Structure of the Ion-nitrided Layer of 18-8 Stainless Steel, in *Stainless Steel 2000*, p13-22, Ed. Tom Bell and Katsuya Akamatsu, Maney Publishing, Leeds, 2001.

[3] D. B. Lewis, A. Leyland, P. R. Stevenson, J.Cawley and A. Matthews, Metallurgical study of low-temperature plasma carbon diffusion treatments for stainless steels, *Surf. Coat. Tech*. 60 (1993) 416-423.

[4] Wei, R., Wilbur, P. J., Sampath, W.S., Williamson, D.L, Wang, L., (1991) Sliding wear of nitrogen ion-implanted stainless steels. *J. Lubrication Engineering*, 47 4, 326-334.

[5] Williamson, D.L., Wang, L, Wei, R., Wilbur, P. J., (1990) Solid solution strengthening of stainless steel surface layers by rapid, high dose, elevated temperature nitrogen ion implantation. *J. Materials Letters,* vol. 9, Number 9, May, 302-308.

[6] Haruman, E. et al., Low temperature fluidized bed nitriding of austenitic stainless steel, *Solid State Phenomena, Trans Tech Publication*, Vol. 118, (2006) p. 125-130.

[7] K. Gemma, T. Obtruka, T. Fujiwara, M. Kwakami, Prospects for rapid nitriding in high Cr austenitic alloys, in *Stainless Steel 2000*, p159-166, Ed. Tom Bell and Katsuya Akamatsu, Maney Publishing, Leeds, 2001.

[8] Sun, Y., Li, X.Y., Bell, T., Low temperature plasma carburizing of austenitic stainless steels for improved wear and corrosion resistance, *J. Surf. Eng*. 15, p. 49-54, 1999.

[9] Sun, Y., Bell, T., Kolosvary, Z., and Flis ., The Response of austenitic stainless steels to low temperature plasma nitriding, *J. Heat Treatment of Metals*, 1, 9-16, 1999.

[10] Y. Sun. E. Haruman, Influence of processing conditions on structural characteristics of hybrid plasma surface alloyed austenitic stainless steel, Surf. Coat. Tech. 202 (2008) 4069-4075.

[11] Buhagiar, J., Li, X. and Dong, H., "Formation and microstructural characterisation of S-phase layers in Ni-free austenitic stainless steels by low-temperature plasma surface alloying", Surface and Coatings Technology, Volume 204, Issue 3, Pages 330-335, October 2009.

[12] Agren, J., Du, Hong., Theoretical treatment of nitriding and nitrocarburizing of Iron. Metallurgical and Materials Transactions A. April 1996, V. 27A. p. 1073-1080.

[13] Parascandola, S., Moller, W., and Williamson, D. L., (2000), Successful nitriding of austenitic stainless steel: the diffusion mechanism of nitrogen and the role of the surface oxide layer, *Stainless Steel 2000*, Maney – IoM–IFHTSE – JSHT, 201-214.

[14] T. Christiansen, and M. A.J. Somers, "Low temperature gaseous nitriding and carburising of stainless steel", Surface Engineering, Volume 21, Numbers 5–6, pp. 445-455(11), October 2005.

[15] K.-T. Rie, E. Broszeit, Plasma diffusion treatment and duplex treatment — recent development and new applications, *Surf. Coat. Tech*. 76–77 (1995) 425-436.

[16] J.C. Stinville, P. Villechaise, C. Templier, J.P. Riviere, M. Drouet, Plasma nitriding of 316L austenitic stainless steel: Experimental investigation of fatigue life and surface evolution, Surf. Coat. Tech. 204 (2010) 1947-1951.

[17] Y. Sun, Kinetics of low temperature plasma carburizing of austenitic stainless steels, J. Mater. Proc. Tech. 168 (2005) 189-194.

[18] M. Tsujikawa, S. Noguchi, N. Yamauchi, N. Ueda and T. Sone, Effect of molybdenum on hardness of low-temperature plasma carburized austenitic stainless steel, Surf. Coat. Tech. 201 (2007) 5102-5107.

[19] P. Kochmanski and J. Nowacki, "Influence of initial heat treatment of 17-4 PH stainless steel on gas nitriding kinetics", Surface and Coatings Technology, Volume 202, Issue 19, 25 June 2008, pp. 4834-4838.

[20] X.Y. Li, J. Buhagiar, H. Dong, Characterisation of dual S-phase layer on plasma carbonitrided biomedical austenitic stainless steels, *Surf. Eng*. 26 (2010) 67-73.

[21] F. Ernst, Y. Cao, G.M. Michal, A.H. Heuer, Carbide precipitation in austenitic stainless steel carburized at low temperature, *Acta Mater*. 55 (2007) 1895-1906.

[22] N. Shohoji, T. Marcelo and M. Katsura, "Influence of metastable species (non-graphitic carbon and ammonia gas) in the reactants on the composition of the reaction product (carbide, carbonitride and nitride)", Solid State Ionics, Volume 38, Issues 3-4, Pages 187-194, 1990.

[23] Honeycombe, R. W. K., and Bhadeshia, H. K. D. H., (1995) Steels Microstructure and Properties (2nd edn.), Edward Arnold, p. 330.

[24] Davis, J.R., (eds.) (1992) ASM Handbook (10th edn.), vol. 3, ASM International, Materials Park, Ohio.

[25] Davis, J.R., (eds.) (January 1994) Stainless Steels, ASM Specialty Handbook, ASM International, Ohio (USA); p.205-228.

[26] Farrar, J.C.M, Marshal, A.W., Zhang, Z., (1997) A comparison of predicted and measured ferrite levels in duplex and super-duplex weld metal, duplex stainless steels 97-5th World Conference proceedings, Stainless steel world, 997, KCI Publishing, p. 4.

[27] Ronald Lesley Plaut, Clara Herrera, Doris Maribel, Escriba, Paulo Rangel Rios, Angelo Fernando Padilha., (2007), A short review on wrought austenitic stainless steels at high temperatures: processing, microstructure, properties and performance. Materials Research, Vol. 10, No. 4, 453-460, 2007.

[28] George, G. and H. Shaikh, Introduction to austenitic stainless steels, in Corrosion of Austenitic Stainless Steels - Mechanisms, Mitigations and Monitoring H.S. Khatak and B. Raj, Editors. 2002, Alpha Science International Ltd.: Pangbourne, UK. p. 1-36.

[29] T. Sourmail, Review: Precipitation in Creep-Resistant Austenitic Stainless Steels, Mater. Sci. Techn. 2001:17, p. 1-14.

[30] P.N. Kogyo K.K., Method for activating surface of metal member, Patent 2007/0204934 A1, 2007.

[31] E. Ranjbarnodeh, H. Pouraliakbar, A. H. Kokabi, Finite Element Simulation of Carbide Precipitation in Austenitic Stainless Steel 304, International Journal of Mechanics and Applications 2012, 2(6): 117-123.

[32] Marshall, P., Austenitic Stainless Steels: Microstructure and Mechanical Properties. 1984, Essex: Elsevier Applied Science Publishers Ltd.

[33] Parvathavarthini, N., Sensitization and testing for intergranular corrosion, in Corrosion of Austenitic Stainless Steels - Mechanisms, Mitigations and Monitoring H.S. Khatak and B. Raj, Editors. 2002, Alpha Science International Ltd.: Pangbourne, UK. p. 117-138.

[34] Dillon, C. P., (1995) Corrosion Resistance of Stainless Steels. New York: Marcel Dekker, Inc.

[35] Wallinder, D., et al., EIS and XPS study of surface modification of 316LVM stainless steel after passivation. Corros. Sci., 1999. 41: p. 275-289.

[36] Shahryari, A. and S. Omanovic, Improvement of pitting corrosion resistance of a biomedical grade 316LVM stainless steel by electrochemical modification of the passive film semiconducting properties. Electrochem. Commun., 2007. Vol. 9, pp. 76-82.

[37] Kamachi Mudali, U. and M.G. Pujar, Pitting corrosion of austenitic stainless steels and their weldments, in Corrosion of Austenitic Stainless Steels - Mechanisms, Mitigations and Monitoring H.S. Khatak and B. Raj, Editors. 2002, Alpha Science International Ltd., Pangbourne, UK. p. 74-105.

[38] Haraldsson, C. and S. Cowen, Characterization of Sandvik Bioline High-N – A comparison of standard grades F1314 and F1586, in Stainless Steels for Medical and Surgical Applications, G.L. Winters and M.J. Nutt, Editors. 2003, ASTM International: Pittsburg, PA, USA p. 3-12.

[39] Windler, M., R. Steger, and G.L. Winters, Quality aspects of high-nitrogen stainless steel for surgical implants, in Stainless Steels for Medical and Surgical Applications, G.L. Winters and M.J. Nutt, Editors. 2003, ASTM International, Pittsburg, PA, USA p. 72-81.

[40] J. Janovec et al, Phases in Austenitic Stainless Steels, Journal of Materiali in Tehnologije 37 (2003) 6 307. Slovenija.

[41] Davis, J.R., ed. Corrosion: Understanding the basics. 2000, ASM International, Ohio.

[42] R.T. Loto, Pitting corrosion evaluation of austenitic stainless steel type 304 in acid chloride media, J. Mater. Environ. Sci. 4 (4) (2013) 448-459.

[43] Baba, H., T. Kodama, and Y. Katada, Role of nitrogen on the corrosion behavior of austenitic stainless steels Corros. Sci., 2002. 44: p. 2393-2407.

[44] Blawert, C., et al., Characterisation of duplex layer structures produced by simultaneous implantation of nitrogen and carbon into austenitic stainless steel X5CrNi189. Surf. Coat Technol., 2000. 128-129: p. 219-225.

[45] Bayoumi, F. and W.A. Ghanem, Effect of nitrogen on the corrosion behavior of austenitic stainless steel in chloride solutions Mater. Lett., 2005. 59: p. 3311-3314.

[46] Dayal, R.K., Crevice corrosion of stainless steels in Corrosion of Austenitic Stainless Steels - Mechanisms, Mitigations and Monitoring H.S. Khatak and B. Raj, Editors. 2002, Alpha Science International Ltd.: Pangbourne, UK. p. 106-116.

[47] Pan, J., C. Karlén, and C. Ulfvin, Electrochemical study of resistance to localized corrosion of stainless steels for biomaterial applications J. Electrochem. Soc., 2000. 147(3), pp. 1021-1025.

[48] M. Shimada et al., Optimization of grain boundary character distribution for intergranular corrosion resistant 304 stainless steel by twin-induced grain boundary enngineering, Acta Materialia, 2002:50, pp. 2331-2341.

[49] Muraleedharan, P., Metallurgical influences on stress corrosion cracking, in Corrosion of Austenitic Stainless Steels - Mechanisms, Mitigations and Monitoring H.S. Khatak and B. Raj, Editors. 2002, Alpha Science International Ltd.: Pangbourne, UK. p. 139-165.

[50] Wood, R.J.K., Tribo-corrosion of coatings: a review. J. Phys. D: Appl. Phys., 2007. 40: p. 5502-5521.

[51] Annual Book of ASTM Standards, Standard terminology relating to wear and erosion, in ASTM Standard G 40-02. 2002, West Conshohocken, PA, USA. p. 165-172.

[52] Ludema, K.C., Friction, Wear, Lubrication A Textbook in Tribology 1996, Washington DC: CRC Press. 257.

[53] Dearnley, P.A. and G. Aldrich-Smith, Corrosion-wear mechanisms of hard coated austenitic 316L stainless steels. Wear, 2004. 256: p. 491-499.

[54] Watson, S.W., et al., Methods of measuring wear-corrosion synergism. Wear, 1995. 181-183(Part 2): p. 476-484.

[55] Ju, X., The ceramic conversion treatment and tribological characterizations of NiTi shape memory alloys, PhD ThesisThe University of Birmingham, 2007.

[56] Hoeppner, D.W. and V. Chandrasekaran, Fretting in orthopaedic implants: a review. Wear, 1994. 173: p. 189-197.

[57] Zhou, Z.R. and L. Vincent, Mixed fretting regime. Wear, 1995. 181-183: p. 531-536.

[58] Hallab, N.J. and J.J. Jacobs, Orthopedic implant fretting corrosion. Corros. Reviews, 2003. 21(2-3): p. 183-213.

[59] Torsten Holm, Furnace Atmospheres No. 3 – Nitriding and Nitrocarburising, Linde Gas Division, Germany, 2009.

[60] T. Czerwiec, Presentation in International Symposium on Surface Hardening Corrosion Resistant Alloys – ASM, Case Reserve Western University, Cleveland, Ohio USA, May, 2010.

[61] Clark, D.S. and Varney. W.R., 1962. Physical Metallurgy for Engineers, Litton Educational Publishers.

[62] Bell, T., and Sun, Y., (2001) Stainless Steel 2000, Proc. Int. Current status seminar on thermochemical Surf. Eng., Maney Publishing, Osaka, p. 275.

[63] Li, X. Y., and Bell, T., (2004) Sliding wear properties of active screen plasma nitrided 316 austenitic stainless steels, J. Wear. Vol. 256, Issues 11–12, pp. 1144–1152.

[64] F. Borgioli, A. Fossati, E. Galvanetto and T. Bacci, “Glow-discharge nitriding of AISI 316L austenitic stainless steel: influence of treatment temperature”,

Surfaces and Coatings Technology, 200, 2474 - 2480, (2005).

[65] T. Christiansen and MAJ. Somers, Presentation in International Symposium on Nitriding 3, Nitrex Metal, Las Vegas, NV, USA, Nov., 2013.

[66] British Standard EN 10052:1994. (2014, May 10). Vocabulary of heat treatment terms for ferrous products, pp. 14.
Available: http://sanyosteel.com/files/EN/EN%2010052.pdf (URL).

[67] Leyland, A. and Matthews, A, 2000: 'On the significance of the H/E ratio in wear control: a nanocomposite coating approach to optimised tribological behaviour', Wear, 246, 1-2, 1-11.

[68] Thaiwatthana, S., Li, X. Y., Dong, H. and Bell, T., (2002) Comparison Studies on Properties of Nitrogen and Carbon S-phase on Low Temperature Plasma Alloyed AISI 316 Stainless Steel, J. Surface Engineering, 18(6), 433-437.

[69] T. Bell et al., Controlled Nitriding in Ammonia-Hydrogen Mixtures, Source Book on Nitriding (American Society for Metals, 1977), pp. 259-265.

[70] Shahjahan Mridha, 2007, 'Gas nitriding of En40B steel with highest growth rate of the case and reduced white layer formation', Intl. J. of Microstructure and Materials Properties, Vol.2, No 1, pp. 54-63.

[71] Sun, Y., and Bell, T., (1997), A numerical model of plasma nitriding of low alloy steels. J. Mater. Sci Eng. A, vol. 224, 33-47.

[72] L. B. Garrido, E. F. Aglietti, L. Martorello, M. A. Camerucci, and A. L. Cavalieri, "Hardness and fracture toughness of mullite-zirconia composites

obtained by slip casting," Materials Science and Engineering: A, vol. 419, pp. 290-296, 2006.

[73] Ratajski, J., 2004, "Model of Growth Kinetics of Nitrided Layer in the Binary Fe-N System," International Journal of Materials Research and Advanced Techniques (Z. Metallkd.), 95(9) pp. 823-828.

[74] Somers, M. A. J., and Christiansen, T., 2005, "Kinetics of Microstructure Evolution during Gaseous Thermochemical Surface Treatment," Journal of Phase Equilibria and Diffusion, 26(5) pp. 520-528.

[75] Karabelchtchikova, O., 2007, "Fundamentals of Mass Transfer in Gas Carburizing," PhD Dissertation, Worcester Polytechnic Institute.

[76] Michalski, J., 2011, "Characteristics and calculations of atmospheres for controlled gas nitriding of steel," Instytut Mechaniki Precyzyjnej, Warszawa.

[77] Wei, Y., Zurecki, Z., and Sisson Jr., R. D., 2012, "Thermodynamic model-assisted evaluation of phase transformations in subcritical austenitic nitriding," Materials Science and Technology (MS&T) 2012. Pittsburgh, PA, pp. 180.

[78] F.E. Harris, “Case Depth - an Attempt at a Practical Definition,” Metal Progress, 44 (1943), 265-272.

[79] Parrish, G. and Harper, G. S.: Production gas carburizing, 1st Ed. (1985) Oxford, Pergamon.

[80] Hurricks, P. L.: Some aspects of the metallurgy and wear resistance of surface coatings, Wear (1972) 22, 3, 291-319.

[81] Bell, T., and Sun, Y., (1998) Process for the treatment of austenitic stainless steel. (UK patent 9715180.7 UK).

[82] Yingying Wei, Simulation, optimization and development of thermo-chemical diffusion processes, PhD dissertation Worcester Polytechnic Institute, 2013.

[83] Hertz, et al., (2008) Technologies for low temperature carburising and nitriding of austenitic stainless steel, International Heat Treatment and Surface Engineering, vol. 2, No. 1.

[84] Christiansen, T.L., Somers, M.A.J., (2006) Characterisation of Low Temperature Surface Hardened Stainless Steel, Struers Journal of Materialography 9/2006.

[85] Yin, R., (2005) Carburization of 310 stainless steel exposed at 800-1100oC in 2% CH4/H2 gas mixture, J. Corrosion Science 47, 1896-1910.

[86] Ueda, Y., Kanayama, N., Ichii, K., Oishi, T. and Miyake, H. (2005) Effect of nitrogen on the plasma(ion)-carburized layer of high nitrogen austenitic stainless steel, J. Surface and Coatings Technology 200, 1-4, 521-524.

[87] Parascandola, S., Moller, W., and Williamson, D. L., (2001), Successful nitriding of austenitic stainless steel: the diffusion mechanism of nitrogen and the role of the surface oxide layer, Stainless Steel 2000, Proc. Int. Current status seminar on thermochemical Surf. Eng., Maney Publishing, Osaka, p. 201-214.

[88] Zhang, Z.L., Bell T., Structure and Corrosion Resistance of Plasma Nitrided Stainless Steel, J. Surf. Eng. 1 (2) (1985) 131.

[89] Leyland, A. and Matthews, A, 2004.: 'Design criteria for wear-resistant nanostructured and glassy metal coatings', Surface and Coatings Technology, 177-178, 317-324.

[90] J.C. Stinville, P. Villechaise, C. Templier, J.P. Riviere, M. Drouet, Plasma nitriding of 316L austenitic stainless steel: Experimental investigation of fatigue life and surface evolution, Surf. Coat. Tech. 204 (2010) 1947-1951.

[91] Bell, T.: Surface engineering of austenitic stainless steel, Surface Engineering (2002) 18, 6, 415-422.

[92] T. Christiansen and M Somers, Controlled Dissolution of Colossal Quantities of Nitrogen in Stainless Steel, Metallurgical and Materials Transaction A Vol. 37A, March 2006—675.

[93] Y. Jiraskova, O. Schneeweiss, S. Havlcaek, C. Blawert, H. Kalvelag, Surface modification of stainless steels by carbon/nitrogen implantation* Czechoslovak Journal of Physics, Vol. 51 (2001). No. 7, 693-701.

[94] Qu, J., Blau, P. J., and Jolly, B. C., (2007) Tribological properties of stainless steel treated by colossal carbon supersaturation, J. Wear, 263, 1-6, 719-726.

[95] Sun, Y. and Bell, T.: Dry sliding wear resistance of low temperature plasma carburized austenitic stainless steel, Wear (2002) 253, 5-6, 689-693.

[96] Li, X. Y. and Dong, H.: Effect of annealing on corrosion behaviour of nitrogen S-phase in austenitic stainless steel, Materials Science and Technology (2003) 19, 10, 1427-1434.

[97] Martin, W. C. and Wiese, W. L.: Atomic, molecular, and optical physics handbook in 2.1st Ed. (2002) Gaithersburg, NIST.

[98] Aoki, K. and Kitano, K.: Surface hardening for austenitic stainless steels based on carbon solid solution, Surface Engineering (2002) 18, 6, 462-464.

[99] Dong, H., Qi, P.-Y., Li, X. Y. and Llewellyn, R. J.: Improving the erosion-corrosion resistance of AISI 316 austenitic stainless steel by low-temperature plasma surface alloying with N and C, Materials Science and Engineering A: Structural Materials: Properties, Microstructure and Processing (2006) 431, 137-145.

[100] David Pye, Nitriding Techniques, Ferritic Nitrocarburizing, and Austenitic Nitrocarburizing Techniques and Methods, Sub chapter 8.19 Steel Heat treatment : Metallurgy and Technologies, @2006 by Taylor & Francis Group, LLC.

[101] B. Million, J. Kucera, A. Rek, K. Stransky, and M. Hajduga: Metallography (1995), 362.

[102] D. L. Williamson, O. Ozturk, R. Wei and P. J. Wilbur, "Metastable Phase Formation and Enhanced Diffusion in Fcc Alloys under High-Dose, High-Flux Nitrogen Implantation at High and Low Ion Energies," Surface and Coatings Technology. 65 (1994) 15.

[103] T. Bell: Current status of supersaturated surface engineered s-phase materials, Key Eng. Mater., 2008, 373, 289–295.

[104] T. Christiansen, M.A.J Somers, Low temperature gaseous surface hardening of stainless steel: the current status, Int. J. Mat. Res 100 (2009) 10, pp. 1361-1377.

[105] ANSI/ASME B46.1-2009 Surface Texture, Surface Roughness, Waviness and Lay.

[106] ASTM E92-82(2003) Test Method for Vickers Hardness of Metallic Materials

[107] ASTM G99-05(2010), Standard Test Method For Wear Testing With A Pin-On-Disk Apparatus.

[108] ASTM E2546–07 for Standard Practice For Instrumented Indentation Testing.

[109] ASTM G5-94(2011)e1 Standard Reference Test Method for Making Potentiostatic and Potentiodynamic Anodic Polarization Measurements.

[110] Xiaolan Wang, Activated Atmosphere Case Hardening of Steels,PhD dissertation, Worcester Polytechnic Institute 2011.

[111] L Sproge and J Slycke, Control of the compound layer structure in gaseous nitrocarburising, Materials Science Forum Vols. 102-104 (1992) pp. 229-242.

[112] Fewell, M.P., et al., The nature of expanded austenite. Surf. Coat Technol., 2000. 131 (1-3): p. 300-306.

[113] Y. Sun, X.Y. Li and T. Bell, X-ray diffraction characterisation of low temperature plasma nitrided austenitic stainless steels, J. Mater. Sci. 34 (1999) 4793-4802.

[114] S. Thaiwatthana, X.Y. Li, H. Dong and T. Bell, Mechanical and chemical properties of low temperature plasma surface alloyed 316 austenitic stainless steel, Surf. Eng. 18 (2002) 140-144.

[115] F. Ernst, Y. Cao, G.M. Michal, A.H. Heuer, Carbide precipitation in austenitic stainless steel carburized at low temperature, Acta Mater. 55 (2007) 1895-1906.

[116] Ozturk, O. and D.L. Williamson, Thermal stability of the high-N solid-solution layer on stainless steel Surf. Coat Technol., 2002. 158-159: p. 288 - 294.

[117] Y. Li et al, Plasma Nitriding of AISI 316L Austenitic Stainless Steels at Anodic Potential, J. of Surface and Coating Technology, Vol. 206, 8-9, 2430-2437, 2012.

[118] Wang Liang, Xu Bin, Yu Zhiwei, Shi Yaqin, The Wear and Corrosion Properties of Stainless Steel Nitrided By Low-Pressure Plasma-Arc Source Ion Nitriding at Low Temperatures, Surface and Coatings Technology 130, p. 304-308, 2000.

[119] Y. Li, L. Wang, J. Xu, D. Zhang, Plasma Nitriding of AISI 316L Austenitic Stainless Steels at Anodic Potential, Surface and Coatings Technology 30 October 2011.

[120] B. Hashemi , M. Rezaee Yazdi, V. Azar, The Wear and Corrosion Resistance of Shot Peened–Nitrided 316L Austenitic Stainless Steel, Vol. 32, Issue 6, 2011, 3287-3292.

[121] S.C. Gallo, Active Screen Plasma Surface Engineering of Austenitic Stainless Steel for Enchanced Tribological and Corrosion Properties, PhD thesis University of Birmingham, 2009.

[122] RAM. Subbiah, D R. Rajavel, Dry Sliding Wear Behaviour Analysis of Nitrided 316LN Grade Austenitic Stainless Steels Using Gas Nitriding Process, p. 98-101, 2005.

[123] C. Tromas, J.C. Stinville, C. Templier, P. Villechaise, 2012, Hardness and elastic modulus gradients in plasma-nitrided 316L polycrystalline stainless steel investigated by nanoindentation tomography. J.of Acta Materialia, Vol. 60, Issue 5, pp. 1965–1973.

[124] Randall, Nicholas X., Matthieu Vandamme, and Franz-Josef Ulm. (2009), "Nanoindentation analysis as a two-dimensional tool for mapping the mechanical properties of complex surfaces." Journal of Materials Research< Vol. 24, pp. 679-690.

[125] N. Oumarou, J-Ph. Jehl, R. Kouitat, Ph. Stempfle, 2010, 'On the variation of mechanical parameters obtained from spherical depth sensing indentation', Int.J. of Surface Science and Engineering, Vol.4, No.4/5/6, pp.416 – 428.

[126] Thaiwatthana, S., Li, X. Y., Dong, H. and Bell, T.: Corrosion wear behaviour of low temperature plasma alloyed 316 austenitic stainless steel, Surface Engineering (2003) 19, 3, 211-216.

[127] Flis, Corrosion and passivation of plasma nitride stainless steels, Surface Engineering 2010 Vol. 26, No. 1–2, pp. 103-113.

PUBLICATIONS DURING THE RESEARCH WORK

1. A. Triwiyanto, E. Haruman, M.B. Sudin, S. Mridha and P. Hussain,, 2011. Structural and properties development of expanded austenite layers on AISI 316L after low temperature thermochemical treatments.. J. Applied Sci., 11: 1536-1543.

2. A**.** Triwiyanto, Patthi Hussain, M. Che Ismail, 2011, Behavior of Carbon and Nitrogen after Low Temperature Thermochemical Treatment on Austenitic and Duplex Stainless Steel, J. of Applied Mechanics and Materials, 110-116, 621

3. A. Triwiyanto, Patthi Hussain, M. Che Ismail, 2011, Elemental analysis of treated layers on stainless steel after low temperature hybrid thermochemical treatments, 978-1-4577-1882-3 ©2011 IEEE.

4. A. Triwiyanto, P. Hussain, A. Rahman, M.C Ismail, 2013, The Influence of Nitriding Time of AISI 316L Stainless Steel on Microstructure and Tribological Properties. Asian Journal of Scientific Research, 6: 323-330.

5. Askar Triwiyanto, Patthi Hussain, Mokhtar Che Ismail, 2013, Microstructure and Nanoindentation Characterization of Low Temperature Hybrid Treated layer on Austenitic Stainless Steel, IOP Conf. Series: Materials Science and Engineering 46 (2013) 012043.

6. Askar Triwiyanto, Patthi Hussain, Mokhtar Che Ismail, Nanoindentation and Microstructure of Hybrid treated of AISI 316L at Low Temperature, Int. J. of Materials Engineering Innovation, Vol. 5, No. 1, 2014.

BOOK CHAPTER:

7. Askar Triwiyanto, Patthi Hussain, Esa Haruman and Mokhtar Ismail, 2012 Low Temperature Thermochemical Treatments of Austenitic Stainless Steel Without Impairing Its Corrosion Resistance, in "Corrosion Resistance", book edited by Hong Shih, ISBN 978-953-51-0467-4. DOI: 10.5772/32893.

8. Askar Triwiyanto, Patthi Hussain, Silvia Anggraeni, and Mokhtar Ismail, 2013, Surface Morphology and Nanoindentation of Low Temperature Hybrid Treated of AISI 316L, book Chapter in “Recent Trends in Nanotechnology and Materials Science, Engineering Materials”, ISBN 978-3-319-04515-3 DOI: 10.1007/978-3-319-04516-0_8, Springer International Publishing Switzerland 2014.

CONFERENCES

1. A. Triwiyanto, A., E. Haruman, M.B. Sudin, S. Mridha and P. Hussain,, 2011. Structural and properties development of expanded austenite layers on AISI 316L after low temperature thermochemical treatments;, International Conference on Plan Equipment and Reliability (ICPER), June 2010, Kuala Lumpur, Malaysia.

2. A. Triwiyanto, Patthi Hussain, M. Che Ismail, 2011, 'Behavior of Carbon and Nitrogen after Low Temperature Thermochemical Treatment on Austenitic and Duplex Stainless Steel', International Conference on Mechanical and Aerospace Engineering (ICMAE), 2011, Bangkok, Thailand.

3. A. Triwiyanto, Patthi Hussain, M. Che Ismail, 2011, Elemental analysis of treated layers on stainless steel after low temperature hybrid thermochemical treatments, National Postgraduate Conference (NPC), September 2011, Seri Iskandar, Perak, Malaysia.

4. A. Triwiyanto, P. Hussain, A. Rahman, M.C Ismail, 2012, The Influence of Treatment Time of Nitrided AISI 316L Stainless Steel on Microstructure and Tribological Properties, 3rd International Conference on Production, Energy and Reliability (ICPER 2012), Kuala Lumpur, Malaysia.

5. Askar Triwiyanto, Patthi Hussain, Mokhtar Che Ismail, 2012, 'Empirical Modeling for Diffusion of Nitrogen Into AISI430 Ferritic Stainless Steel', 3rd International Conference on Production, Energy and Reliability (ICPER 2012), Kuala Lumpur, Malaysia.

6. Askar Triwiyanto, Patthi Hussain, Mokhtar Che Ismail, 2012, 'Characterization of Surface Treated Layers Austenitic Stainless Steel and 9.3Cr Ferritic Steel Resulting from High Temperature Nitriding', 3rd International Conference on Production, Energy and Reliability (ICPER 2012), Kuala Lumpur, Malaysia.

7. Askar Triwiyanto, Esa Haruman, Patthi Hussain, Mokhtar Che Ismail, 2012, Characterization of Hybrid Treatments Product of Low Temperature Thermochenical Treatments of Austenitic Stainless Steel at Different Temperature, 21st Scientific Conference of the Microscopy Society Malaysia (EMSM 2012)

8. Askar Triwiyanto, Patthi Hussain, Mokhtar Che Ismail, 2013, Microstructure and Nanoindentation Characterization of Low Temperature Hybrid Treated layer on Austenitic Stainless Steel, International Conference on Manufacturing, Optimization, Industrial and Material Engineering (MOIME 2013) Bandung, Indonesia, 09 - 10 March 2013.

9. Askar Triwiyanto, Patthi Hussain, Mokhtar Che Ismail, 'Nanoindentation Analysis of Low Temperature Hybrid Treated AISI 316L', 2013 Annual Postgraduate Conference (APC 2013), Seri Iskandar, Perak, Malaysia.

10. Askar Triwiyanto, Azman Zainuddin, Kamarul Abidin, M.Ariff Billah and Patthi Hussain, 2014, 'Mathematical Modelling of Nitride Layer Growth for Low Temperature Gas and Plasma Nitriding of Austenitic Stainless Steel' (3-4 June, ICPER 2014), Kuala Lumpur, Malaysia.

APPENDIX

A. Table I: Typical Compositions of Austenitic Stainless Steels [27].

Type	UNS designation	C	Mn	Si	Cr	Ni	Mo	N	Others
AISI 201	S20100	≤0.15	5.50-7.50	≤1.00	16.00-18.00	3.50-5.50	-	0.25	-
AISI 202	S20200	≤0.15	7.50-10.0	≤1.00	17.00-19.00	4.0-6.0	-	0.25	-
AISI 205	S20500	0.12-0.25	14.0-15.5	≤1.00	16.50-18.00	1.0-1.75	-	0.32-0.40	-
AISI 301	S30100	≤0.15	≤2.00	≤1.00	16.00-18.00	6.0-8.0	-	-	-
AISI 302	S30200	≤0.15	≤2.00	≤1.00	17.00-19.00	8.0-10.0	-	-	-
AISI 303	S30300	≤0.15	≤2.00	≤1.00	17.00-19.00	8.0-10.0	0.6	-	-
AISI 304	S30400	≤0.08	≤2.00	≤1.00	18.00-20.00	8.0-10.5	-	-	-
AISI 304H	S30409	0.04-0.10	≤2.00	≤1.00	18.00-20.00	8.0-10.5	-	-	-
AISI 304L	S30403	≤0.03	≤2.00	≤1.00	18.00-20.00	8.0-12.0	-	-	-
AISI 304N	S30400	≤0.08	≤2.00	≤1.00	18.00-20.00	8.0-10.5	-	0.10-0.16	-
AISI 304LN	S30451	≤0.03	≤2.00	≤1.00	18.00-20.00	8.0-12.0	-	0.10-0.16	-
AISI 308	S30800	≤0.08	≤2.00	≤1.00	19.00-21.00	10.0-12.0	-	-	-
AISI 309	S30900	≤0.20	≤2.00	≤1.00	22.00-24.00	12.0-15.0	-	-	-
AISI 310	S31000	≤0.25	≤2.00	≤1.00	24.00-26.00	19.0-22.0	-	-	-
AISI 316	S31600	≤0.08	≤2.00	≤1.00	16.00-18.00	10.0-14.0	2.0-3.0	-	-
AISI 316H	S31609	≤0.08	≤2.00	≤1.00	16.00-18.00	10.0-14.0	2.0-3.0	-	-
AISI 316L	S31603	≤0.03	≤2.00	≤1.00	16.00-18.00	10.0-14.0	2.0-3.0	-	-
AISI 316LN	S31653	≤0.03	≤2.00	≤1.00	16.00-18.00	10.0-14.0	2.0-3.0	0.10-0.16	-
AISI 316N	S31651	≤0.08	≤2.00	≤1.00	16.00-18.00	10.0-14.0	2.0-3.0	0.10-0.16	-
AISI 317	S31700	≤0.08	≤2.00	≤1.00	18.00-20.00	11.0-15.0	3.0-4.0	-	-
AISI 317L	S31703	≤0.03	≤2.00	≤1.00	18.00-20.00	11.0-15.0	3.0-4.0	-	-
AISI 321	S32100	≤0.08	≤2.00	≤1.00	17.00-19.00	9.0-12.0	-	-	Ti≥5 x %C
AISI 321H	S32109	0.04-0.10	≤2.00	≤1.00	17.00-19.00	9.0-12.0	-	-	Ti≥5 x %C
AISI 347	S34700	≤0.08	≤2.00	≤1.00	17.00-19.00	9.0-13.0	-	-	Nb≥10 x %C
AISI 347H	S34709	0.04-0.10	≤2.00	≤1.00	17.00-19.00	9.0-13.0	-	-	1.0≥Nb≥10 x %C
654 SMO®	S32654	≤0.02	2.00-4.00	≤0.50	24.0-25.0	21.0-23.0	7.0-8.0	0.45-0.55	Cu = 0.30-0.60

(AISI = american iron and steel institute; UNS = unified numbering system).

B. Table II: Secondary Phases in Austenitic Stainless Steels without Concentrations of Non-Metallic Elements [40].

Phase, crystal lattice	Lattice param. (nm)	Fe (%)	Cr (%)	Ni (%)	Mo (%)	Si (%)	Steel
σ-phase, tetrag.	$a = 0.883$ $c = 0.461$	49-52	32-34	4-7	8-11	1	AISI 316
		52	38	5	–	4	19Cr-12Ni-0.02C
	$a = 0.883$ $c = 0.460$	55	29	5	11	–	AISI 316
		19	44-48	2-6	17-19	3	20Cr-25Ni-4Mo
Laves, hexag.	$a = 0.475$ $c = 0.779$	37	11	4	42	5-6	AISI 316
	$a = 0.473$ $c = 0.772$	38	11	6	45	–	AISI 316
		35	13	3	43-47	2	316-LN-3
	$a = 0.473$ $c = 0.772$						
χ-phase, b.c.c.	$a = 0.890$	51-53	23-24	4	18	1	AISI 316
	$a = 0.888$	52	21	5	22	–	AISI 316
		51	23	3	21	1	316 LN-3
		48	27	3	22	–	UNS 31803
M_6C f.c.c.	$a = 1.082$	11-12	29-33	21-26	24-26	6-8	AISI 316
		9-12	33-48	21-33	24-26	6-9	AISI 316A30X
		8	48	37	-	9	19Cr-12Ni-2Si-0.02C
	$a = 1.095$						
$M_{23}C_6$, f.c.c.	$a = 1.063$	14	72	3	10	–	AISI 316
	$a = 1.067$	17	78	4	–	–	19Cr-12Ni-2Si-0.02C
	$a = 1.064$	21-23	62-72	1	1-5	–	20Cr-25Ni-4Mo
	$a = 1.057$	17	63	2	11-13	-	316LN
MX, f.c.c.	$a = 0.422$	–	1	–	–	Ti = 99	AISI 321
Cr_2N, hexag.	$a = 0.476$ $c = 0.442$	–	100	–	–	–	AISI 316
		1	82	–	4	–	316 LN-3
		2-4	83	2-4	7-11	1	20Cr-25Ni-4Mo
Z-phase, tetrag.	$a = 0.286$ $c = 0.739$	32	43	1	21	1	316 LN-3
π-phase, cub. pr.	$a = 0.647$	28	35	3	30-37	–	UNS 31803
		24-26	55-58	12	–	6-7	20Cr-25Ni-4Mo
R-phase, hexag.	$a = 1.093$ $c = 1.934$	32	25	5	33-35	4	20Cr-25Ni-4Mo
		24	23-27	5	46-44	5	